Schweizerische Eidgenossenschaft
Confédération suisse
Confederazione Svizzera
Confederaziun svizra

Department of the Environment,
Transport, Energy and Communication DETEC

Swiss Federal Office of Energy SFOE
Energy Research and Cleantech

Final report

ACSICON

Novel Analysis and Control Solutions for Dynamic Security Issues in the future ENTSO-E network with high Converter-Based Generation

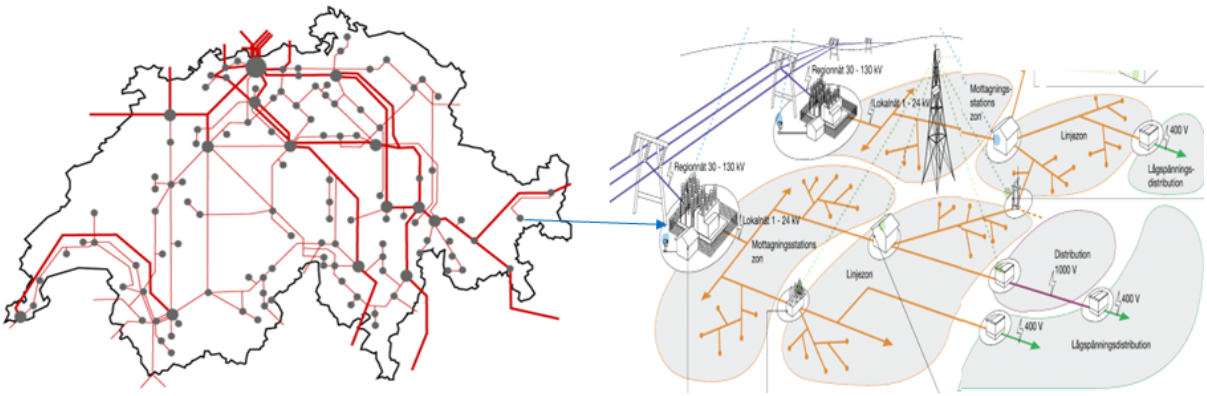

HITACHI ABB

Date: May 31, 2021

Location: Bern

Subsidiser:
Swiss Federal Office of Energy SFOE
Research Programme Grids
CH-3003 Bern
www.bfe.admin.ch
energieforschung@bfe.admin.ch

Subsidy recipients:
ETH Zürich, Forschungsstelle Energienetze
Sonneggstrasse 28, CH-8092 Zürich
www.fen.ethz.ch

ABB Power Grids Switzerland Ltd
Power Grids Research
Segelhofstrasse 1A
CH-5405 Baden 5 Dättwil
www.hitachiabb-powergrids.com

Author:
Mats Larsson (Hitachi ABB Power Grids Ltd.), mats.larsson@hitachi-powergrids.com
Alexander Fuchs (Forschungsstelle Energienetze - ETH Zürich), fuchs@fen.ethz.ch
Turhan Demiray (Forschungsstelle Energienetze - ETH Zürich), demirayt@fen.ethz.ch

SFOE head of domain: Dr. Michael Moser, michael.moser@bfe.admin.ch
SFOE programme manager: Dr. Michael Moser, michael.moser@bfe.admin.ch
SFOE contract number: SI/501728-01

Summary

The energy transition is expected to lead to an increased generation from converter-connected distributed energy resources (DER) like photovoltaic and wind. At the same time, some traditional synchronous machine based generation is being decommissioned, for instance due to cost reasons or the nuclear phase-out, leading to new dynamic stability challenges. Recent developments have resulted in so-called grid-forming converter control architectures that also enable the provision of grid services such as frequency and voltage control, for which grid operation has traditionally relied on synchronous machine based generation.

The project has investigated the potential of grid support from converters as well as the necessary practical considerations regarding controller tuning to allow penetration levels of grid-forming DERs upwards of 100% of the distribution grid load. Furthermore, model aggregation procedures have been developed to allow an adequate dynamic modelling of DER based grid support in large scale transmission grid studies. A large disturbance in form of a system split of the continental ENTSO-E system has been studied for multiple development paths of converters replacing synchronous machines. It has been found that equipping a small share of the new converters (5%-10%) with grid support capabilities is sufficient to maintain the dynamic power system performance at today's level, even if more than 50% of the synchronous generation is otherwise replaced by static converters without grid support.

Zusammenfassung

Es wird erwartet, dass die Energiewende zu einer erhöhten Erzeugung aus Konverter-gekoppelten dezentralen Energiequellen (DER) wie Photovoltaik und Wind führt. Gleichzeitig wird ein Teil der traditionellen Produktion aus Synchronmaschinen reduziert, beispielsweise aus Kostengründen oder durch den Ausstieg aus der Kernenergie, was zu neuen Herausforderungen für die dynamische Netzstabilität führt. Neue Entwicklungen sogenannter netzbildender Regelungsarchitekturen für Konverter, ermöglichen auch die Bereitstellung von Netzdienstleistungen wie Frequenz- und Spannungsregelung, für die der Netzbetrieb traditionell auf Synchronmaschinen zurückgreift.

Das Projekt untersuchte das Potenzial der Netzunterstützung durch Konverter sowie die notwendigen praktischen Überlegungen zur Reglereinstellung, um einen Anteil von netzbildenden DERs von über 100% der Verteilnetzlast zu ermöglichen. Darüber hinaus wurden Modellaggregationsverfahren entwickelt, die eine hinreichend genaue dynamische Modellierung der DER-basierten Netzunterstützung für grosse und komplexe Simulationen auf Übertragungsnetzebene ermöglichen. Eine grosse Störung in Form eines Systemsplits des kontinentalen ENTSO-E-Systems wurde für mehrere Entwicklungspfade untersucht, bei denen Konverter Synchronmaschinen ersetzen. Es wurde festgestellt, dass die Ausstattung eines kleinen Anteil der neuen Umrichter (5%-10%) mit Netzunterstützung ausreicht, die dynamische Stabilität des Netzes auf dem heutigen Niveau zu halten, selbst wenn ansonsten mehr als 50% der synchronen Erzeugung durch statische Umrichter ohne Netzunterstützung ersetzt wird.

Résumé

La transition énergétique devrait entraîner une augmentation de la production à partir de ressources énergétiques distribuées (RED) connectées au réseau par convertisseur, comme le photovoltaïque et l'éolien. Dans le même temps, une partie de la production traditionnelle basée sur des machines synchrones est mise hors service, par exemple pour des raisons de coût ou à cause de la sortie du nucléaire, ce qui entraîne de nouveaux défis en matière de stabilité dynamique. Des développements récents ont donné lieu à des architectures de contrôle de convertisseurs dites "formatrices de réseau" qui permettent également de fournir des services de réseau tels que le contrôle de la fréquence et de la tension, pour lesquels l'exploitation du réseau reposait traditionnellement sur la production par machines synchrones.

Le projet a étudié le potentiel de soutien du réseau par les convertisseurs ainsi que les considérations

pratiques nécessaires concernant le réglage des contrôleurs pour permettre des niveaux de pénétration des RED formant le réseau supérieurs à 100% de la charge du réseau de distribution. En outre, des procédures d'agrégation de modèles ont été développées pour permettre une modélisation dynamique adéquate du soutien au réseau basé sur les RED dans les études de réseaux de transmission à grande échelle. Une grande perturbation sous la forme d'une scission du système continental ENTSO-E a été étudiée pour plusieurs voies de développement des convertisseurs remplaçant les machines synchrones. Il a été constaté qu'il suffisait d'équiper une petite partie des nouveaux convertisseurs (5 à 10%) de capacités de soutien du réseau pour maintenir les performances dynamiques du système électrique au niveau actuel, même si plus de 50% de la production synchrone est remplacée par des convertisseurs statiques sans soutien du réseau.

Contents

Glossary

ADN active distribution grid 9, 15, 54, 60, 71, 72, 77, 113

APC active power controller 17

CCC current controlled converter 18

CER centralized energy resource 16

DER distributed energy resource 9, 16, 19, 54, 60, 112, 113

EMT electromagnetic transient 9, 36

FEN Forschungstelle Netze, ETH Zürich 15

HAPG Hitachi ABB Power Grids 16

PCC Short for point-of-common-coupling, which is the network node where an asset e.g. a wind generation plant or HVDC transmission system connected to the bulk power grid. In this report, it is also used to describe the connection point between transmission and distribution. type 17, 53, 120

PLL phase locked loop 17, 18, 120

PV photovoltaic 16, 17

RMS root-mean-square 9, 36

RPC reactive power controller 17

SCADA Short for supervisory control and data acquisition systems, which are control systems used to coordinate the operation of several georaphically dispersed assets. Used for example in power grid operation to coordinate the power flow on the network through switching of transmission lines and dispatching of generators. Often also used in wind and power plants to coordinate the operation of each individual wind turbine or photovoltaic unit to make the plant dispatchable as seen from the point of common coupling. type 16

VSM virtual synchronous machine 121

Management summary

The ACSICON project was executed in 3 main work packages, focusing on the dynamic modeling of the distribution grids, the creation of reduced dynamic distribution grid models for the use at the transmission grid level and the transmission grid investigation. A specific project goal was, to interpret the results and insights from the Swiss perspective.

In **WP1**, the monitoring of trends in the renewables identified the need for grid support through distributed energy resource (DER)s. Representative control structures for grid forming as well as grid following control systems were reviewed and typical candidates were adopted from scientific literature.

Simulation models of DER were constructed as electromagnetic transient (EMT) models and subsequently reduced to allow faster simulation through root-mean-square (RMS) simulation. The models for distribution grid components, and in particular grid-following and grid-forming converters were validated in both the simulation tools (DYMOLA and FLEXDYN) of the two project partners. They produce very similar results, which ensures that the findings from all work packages are consistent, irrespective of which simulation was used. As testbed for the DER implementations a reference distribution grid topology defined in a previous CIGRE working group was adopted. Based on the original implementation this was then parameterized to allow simulation of the distribution grid under varying penetration levels of DER generation of 5-100 %. It was found that default tuning parameters recommended by the original authors for grid forming control were not adequate for deployment in a realistic distribution grid, particularly with high penetration levels.

To allow operation of the reference grid with up 100 % of potential renewable production, detailed analysis and adaption control parameters are necessary. The workpackage demonstrated the use of modal analysis to ensure stable and robust operation.

In **WP2** methods to extract the aggregated dynamic characteristics of active distribution grids were developed. A linear aggregation procedure that can be used to generate low order equivalents of active distribution grid (ADN)s to be used as load models in large-scale RMS simulations. The models are of low order, and can accurately reproduce the small-signal behaviour of the ADN in terms of its active and reactive power response to voltage and frequency disturbances in the transmission grid. The procedure has been tested on a realistic grid model under penetration levels ranging from 5-100 %. The main limitation of the model, is that it is linearized and thus ignores capacity constraints of DERs. Thus, the model makes the implicit assumption that sufficient headroom is available in each DER.

Furthermore, an aggregation procedure to allow reduced order modelling of the ADNs was developed and implemented in the two simulation environments. The accuracy of the reduced order linear models has been investigated for a frequency range of several hundred mHz and found adequate. Under worst-case conditions of a penetration level of 100 % the reduced model can be used to predict the nadir frequency following a generation loss of 6.25 % within an accuracy of 3 mHz.

For comparison, a nonlinear aggregation with 3 components reduces the model complexity while maintaining the key constraint, the headroom of the DERs. It has been compared through simulation to the detailed Cigre grid model. It also allows a validation of the linear aggregation results performed by HAPG.

WP3 studies the dynamic challenges and opportunities of the energy transition through distributed converter-based generation with and without grid-supporting functionality, aggregated at the transmission grid level. To this end, two independent trends with opposite impact on the global power system stability were investigated. First, synchronous machines and their inherent grid control mechanisms are replaced by static converter-based generation with grid-following characteristics, like common PV and wind power generation. Secondly, distribution grids are increasingly penetrated by distributed energy resources, some of which can be chosen to have grid-forming characteristics to support the global grid control functionality. The combination of both trends were applied to a detailed dynamic model of the continental ENTSO-E power system with 10'000 buses and loads, 30'000 branches and 1'000 synchronous machines. The model was imported and validated with the high-performance power system simulator FLEXDYN. The model was then adapted to different load flow scenarios, synchronous

generation was partly replaced with static generator models, and loads were equipped with grid-control functionality, scaling and applying the aggregated distribution grid models developed in WP2 more than 7'000 times. The benchmark disturbance scenario simulated a system split into three asynchronous regions, leading to strong oscillations in each zone.

Based on performance measures of the time-domain simulation results, including nadir, ROCOF and relative frequency deviation, conclusions were drawn on the impact of the two types of DER (grid-following and grid-forming) has been drawn. It has been found, that if a small share of the new converters (5%-10%) is equipped with grid-forming capabilities (such as the VSM control scheme) the dynamic performance can be maintained at today's level, even if more than 50% of the synchronous generation is otherwise replaced by static (grid-following) converters. The effect is particularly strong for the frequency nadir and low levels of grid-forming DER penetration, with diminishing returns for higher levels of grid-forming DER. For ROCOF and relative frequency deviation the effect is still present, but less pronounced.

The results also confirm the frequency support capability of the active distribution networks studied in WP1, on the transmission grid level.

Finally, a roadmap has been proposed for Switzerland, proposing a step-wise introduction of grid-forming DERs, preferably first using existing utility size batteries. A penetration level of grid-forming DERs in Switzerland of up to about 1% (100 MW) will represent an important Swiss pioneering contribution towards the future dynamic security of the ENTSO-E power grid.

1 Introduction

1.1 Project background and objectives

Power system dynamic stability is a key requirement for the secure and reliable operation of the power grid. The replacement of conventional power sources from synchronous generation with distributed renewable energy resources (DRES) like photovoltaic and wind causes dynamic stability challenges. Frequency stability challenges due to a decrease of inertia have also been identified in a survey of European TSOs as the number one stability challenge for future system operation [3]. These challenges are caused by the loss of rotational inertia, reduced passive damping torque and stabilizing generation controls, leading to an increase in system-wide frequency violations, local transient voltage angle violations and the overall system fragility after disturbances. In a business as usual scenario, the new renewable generation will be equipped with a simple converter current controller with the single objective of supplying power to the grid. Newer types of DRES converter controls include different forms of synchronous machine emulation to provide inertia, damping and other types of dynamic stability enhancing actions to the grid. At the moment, there is no industry consensus on what control structures should be used and how to tune and configure such controllers for maximum benefit to the overall stability of the grid. Furthermore, a large share of the DRES will be installed at the distribution level where their effect on overall system stability is not well understood. Since the changes of the relevant power system infrastructure is taking place now, it is desirable to obtain a better understanding of these issues and potential future policy changes. The robust solution to these challenges is a prerequisite for the successful European energy transition, as formulated for Switzerland by the Energy Strategy 2050, and is the focus of this project report.

The project follows a dual approach in three steps to develop a roadmap for the transition of the dynamic characteristics of the Swiss energy system. On the one hand, a dynamic performance analysis toolbox (developed at HAPG) for power system components and small benchmark systems is used of to model and investigate the impact of converter-based generation under state-of-the art and more advanced control paradigms. The tool allows to detect local and external dynamic interactions between the converters of the distribution grids and with external dynamic power system components, mostly for small benchmark systems on the distribution grid level. On the other hand, a high-performance real-time simulation tool (developed at FEN) is used for the assessment of a detailed dynamic transmission grid model of Switzerland and the ENTSO-E continental Europe synchronous area (CESA). An integrated assessment of the future global dynamic power system performance with a substantial part of the generation harvested from the distribution grids can be achieved using a combination of these two tools, resulting in a hybrid approach of top-down and bottom-up power system modeling. This way, novel local converter control schemes and global power system dynamic challenges are evaluated jointly, as opposed to using isolated models of benchmark networks or a too simplified representation of the lower network levels.

A key challenge towards a successful integrated large-scale power system dynamic performance evaluation is the representation of the distribution grid level behaviour from the point of view of the transmission grid. The goal is to obtain a model that is sufficiently simple for large-scale simulations but still captures all relevant dynamic characteristics and limitations of the underlying distribution grid. The different approaches to perform this distribution grid aggregation are a central step of this project. Linearization based models combined with standard model reduction techniques may suffice for minor disturbances and an overall modal analysis of the global power system model. Larger disturbances may require a full nonlinear modeling approach and the incorporation of constraints, e.g. related to energy storage capacity and current limits. For both approaches it is desirable to preserve the physical interpretation of the variables involved, in particular when the selected converter control scheme involves an interface with global power system variables. In this context, it is also required to appropriately model the aggregated impact of dynamic converter control schemes from DRES, such as inertia emulation and damping, that are embedded in the distribution grids to enhance the surrounding transmission grid.

The subsequent analysis using the large-scale power system simulation tool shall determine the vul-

nerability and potential dynamic power system breakdown point for different expected scenarios of the energy transition.

1.2 State-of-the-art

Current studies on dynamic stability of low-inertia power grids can broadly be split into two categories. On the one hand, theoretical control concepts and stability proofs are developing new control approaches with small to mediums size test systems, often missing an accurate representation of today's power system and a characterisation of other related dynamic stability challenges beyond reduced inertia. While it is appropriate to use small benchmark systems for the development of novel control techniques, the effects on a large-scale network need to be studied using large-scale models in order to incorporate the global power system topology, operation conditions and complex interactions between multiple dynamic power system components.

On the other hand, an approach closer to the large-scale power system application consists of studies on large-scale power system models that investigate the theoretical impact of simplified dynamic control schemes. However, these often miss an accurate representation of the control implementation, realistic measurements and the actual converter behaviour. This project bridges this gap between theoretical low-inertia control concepts and practical power system implications in a realistic setting.

The tool used in this project enable the investigation of large networks such as the future ENTSO-E network with thousands of buses, generators and converters using a detailed modelling of all related physical and control components [13, 11, 6]. Furthermore, an analysis toolbox is used for the model-based estimation of grid stability metrics and the identification of potential dynamic stability issues and potential adverse interactions between power system components [21]. The project combines these tools, resulting in an integrated scheme for the allocation, design and tuning of converter-based dynamic control approaches. The tools are also be instrumental in creating novel low order equivalents to represent the aggregate impact of stability enhancing control in low and medium voltage grids.

1.2.1 Approach and research method

Based on the expertise from the previous investigations with the simulation-based and the analytical software tool, the project identifies the relevant simulation scenarios of the future ENTSO-E power system. This goes hand in hand with the analytical results of individual power system components in small benchmark systems to identify how to best trigger the adverse dynamic behaviour. The result is a set of relevant power system benchmark cases of the ENTSO-E CESA grid. Depending on the selected components, the potential Swiss deployment scenarios include a broad deployment of distributed converter-based control schemes, such as coupled PV-battery sources or large concentrated actuators such as FACTS and HVDC-based injections at certain locations within Switzerland. The distribution grid aggregation starts with an existing linear analysis tool that is combined with linear model reduction techniques. In addition, a benchmark network is selected and appropriately parameterized to capture the aggregated behaviour of nonlinear constrained distribution grid and converter models. In the development process, both tools are validated with the linearized power system model and low-level component models. Stability metrics are computed by fusing the results of the two individual tools. The outcome is a powerful tool to investigate global power sytem stability and develop the large-scale deployment of novel dynamic control approaches in a scenario with high converter-based generation. The final recommendation for the Swiss power system relies on initial practical insights (such as dominant oscillatory modes within Europe), analytical results of current and future state-of-the-art models (such as adverse interactions between converters resulting in harmonic instabilities) as well as systematic parameter sweeps of the selected approach to converter-based control for dynamic grid support.

In the initial phase of the work (WP1), typically proposed control structures to provide grid support in converter based generation and energy storage are reviewed. This includes so called virtual synchronous machines, that are already today used by equipment vendors, but also newer control structures pro-

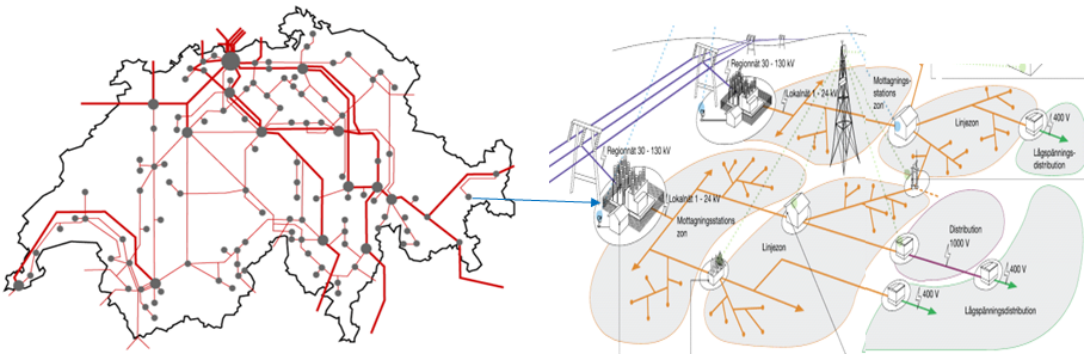

Figure 1: Hierarchical structure of the power system.

posed by academia. Models of these were implemented in the HAPG analysis toolbox. These models are then combined with models of representative distribution grids and scenarios with various penetration levels of converter based generation are constructed. Through simulation or analytical techniques, the behavior of the distribution grid including its grid supporting distributed energy resources, can be described as seen from the interconnection between the HV transmission grid and the MV distribution grid (indicated by the blue arrow in Figure 1) using aggregate simulation models.

Since the simulation models include every component in the distribution grid, they are typically of too high complexity for use in the ENTSO-E system level analysis.

Therefore, in WP2, both linear and nonlinear model reduction techniques are applied to reduce these models into forms simple enough to incorporate in system level simulation and analysis. For small disturbances, the distribution grid models developed in WP1 can be abstracted into a frequency dependent impedance of the distribution grid seen from its connection point to the transmission grid. This results in a linear transfer function matrix modeling the small disturbance behavior that can be reduced to accurate low order equivalents, suitable for the system level analysis planned in WP3.

However, it is assumed that distributed grid supporting generation is behaving in a coherent way as seen from the transmission grid interface. To ensure this, the investigation of local dynamic phenomena within the distribution grid is necessary. To this end, the project also identifies potential of harmful interaction between grid-supporting controllers in a distribution grid and demonstrates tuning techniques to ensure stable and coherent behavior of the distributed grid supporting resources.

In parallel with the linear analysis track where an appropriate and applicable theoretical framework is available, model reduction using heuristic or simulation based nonlinear techniques will be investigated. While less straightforward and associated with higher risk than the linear techniques previously discussed, nonlinear techniques are useful to better capture the system behavior during large disturbances. Examples include the modeling of constraints of the converter systems and the distribution grid as well as islanding conditions.

The ultimate goal of the project is, to assess the impact of grid support from converter based generation on the transmission grid level and to investigate, how grid support functionality today provided by large synchronous machines can be replaced with distributed grid support at lower voltage levels. First, this encompasses the construction of appropriate software interfaces such that the aggregate models from WP2 can be used in the transmission grid simulation tool, to be applied for system level analysis. Furthermore, a number of reference scenarios based on the ENTSO-E grid under varying levels of decommissioning of large synchronous machines will be constructed along with performance metrics to capture e.g. the quality of frequency control and inter-area oscillation mode damping. The role of grid support functionality from generation at distribution level in ensuring that the aforementioned performance metrics do not significantly deteriorate as large synchronous machine based generation is replaced with distributed generation at lower voltage levels.

1.2.2 Targeted outcomes

In essence, the project answers, how Switzerland can contribute to the solve the global dynamic stability challenge in the future ENTSO-E system. The specific outcomes provided by the project include:

- Selection of a benchmark network model, benchmark models for aggregated decentralized and isolated control components as well as a set of benchmark scenarios capturing the dynamic stability challenge in Europe due to increased converter-based generation.
- Low order equivalent linear and nonlinear models of distribution systems accurately representing the effect of distribution grid support by converter based generation and storage. Evaluation of the effectiveness and reliability of the proposed method.
- Implementation of an integrated power system simulation tool based on an iterative procedure between simulation-based performance measures, analytical power system characteristics and the power system component selection, tuning and placement.
- Identification of critical future scenarios leading to system breakdown when no additional stability measures are taken.
- Investigation of how the deployment of new components and/or new dynamic grid-supporting converter control schemes can broadly enhance the dynamic power system performance.
- Validation of the findings for the global power system with low-level distribution grid models.
- Concrete policy recommendations, how Switzerland can contribute to address the future global dynamic stability issues using existing and new components and/or control schemes. Comparison with the potential Swiss contribution with that of other European regions based on the central location in the electrical network

2 Dynamic modeling of distribution grids (WP1)

2.1 Introduction

2.1.1 Objective

The overall objective of workpackage 1 is to provide modelling basis for the development of the distribution grid scenarios in WP2. An environment where ADN can be simulated under varying levels of penetration of grid supporting is required for WP2 and WP3. This involves selection of DER models as well as a benchmark distribution grid. Furthermore, the interoperability of multiple DERs and adjustmentment for the grid environment are necessary.

2.1.2 Approach

This Work Package sets the basis for how distributed converter-based generation are modeled in the later parts of the project.

First a review of the emerging need for grid support by converter based resources is made indicating that due to the foreseen intertia and short-circuit power reduction as a result of increased penetration of centralized and distributed renewable is likely necessary in the future.

Representative grid following and grid forming control schemes are selected based on available scientific literature and implemented in two simulation frameworks. Firstly, an implementation in Modelica using the ConverterStab toolbox [22] was made. These models are used for the analytical tuning studies that are necessary to adapt them to the distribution grid, as well as the linear model aggregation task in WP2. Furthermore they are used as basis for the generation of ADN models necessary for the system studies in WP3. Secondly, an implementation has been made for the simulation tool used at Forschungstelle Netze, ETH Zürich (FEN). These models serve as the basis for the nonlinear model aggregation in WP2.

A representative benchmark distribution grid model model was selected based on the work in a previous CIGRE working group [4]. This benchmark network was parametrized such that distribution grids with varying penetration levels of grid supporting converter based resources can be simulated.

Finally, to ensure stable operation under large penetration of grid supporting DERs, also local network phenomena like interactions between different converter-based sources and overall stability is studied in the same distribution grid. The tuning of the converter control was adapted to grid environment and varying levels of penetration.

2.2 Dynamic converter modeling

This section describes the dynamic converter modeling relevant to the following investigations. It includes selection of dynamic models and control methods for distribution grids with converter-based generation and storage. Within the workpackage, basic current control of the converters for power tracking as well as newer types of converter controllers such as virtual synchronous machine approaches have been reviewed and implemented in a RMS and EMT simulation and stability analysis frameworks available at Hitachi ABB Power Grids (HAPG) [22].

2.2.1 Problem description

In many countries the energy transition has led to a widespread reduction in the number of synchronous machines connected to the power grids. The main driver of this is the, sometimes subsidized, widespread deployment of wind and photovoltaic generation units which depending on market conditions, may render the classical large-scale synchronous machine based generation no longer profitable.

Figure 2 shows a forecasted scenario of 2050 from DNV-GLs Energy transition outlook 2020 [7] where it is clearly seen that the dominant growth of new generation is expected to be in the form of solar photovoltaic (PV) as well as onshore and offshore wind installations, while traditional generation sources such as coal-fired thermal plants will be on the decline.

This development is carried out in primarily two dimensions: centralized energy resource (CER)s are typically medium- to large-scale wind placed offshore or onshore. Whereas the scale of these installations in the past have been relatively modest compared to conventional thermal generation with the largest having af a total generation capacity of a few hundred MWs, the largest plants in operation today have ratings of around 1 GW making their size comparable to classical thermal generation. Several projects already under construction have total rating of 2-3 GW. In most cases the individual solar and wind units are converter interfaced with grid-following control systems but the plant is equipped with SCADA system to allow the plant to behave more or less like a conventional plant except for the variability of production. Some projects also plan the combination with energy storage enabling these plants to balance the production variability and the possibility of treating these plants in the market and grid operation in the same way as conventional generation. Energy storage systems may also be deployed standalone for the purpose of relieving congestion on the transmission grid, energy arbitrage or to enhance the stability of the grid.

DERs are most often very small to medium scale installations with ratings of a few hundred kWs up to several MWs. The small scale units are typically connected on the low voltage grid behind the meter and are a rule not dispatchable by the DSOs. Very small- to medium-scale solar energy installations, most commonly PV, are designed to generate moderate amounts of electricity to be placed onto the local electrical distribution system at the point of both generation and used. They are designed as stand-alone facilities or could be used to generate greater electrical energy in conjunction with other similar nearby installations. Another type of DER is energy storage systems installed by distribution grid operators or behind the meter energy storage system used to store e.g. solar energy or to ensure continued power supply in case of grid outages. The number of all types of DER is rapidly growing.

The rapidly growing penetration of both CER and DER poses a challenge to grid operation as synchronous machine based conventional generation are being phased out or may no longer be grid connected due to high fuel cost. Moreover, the power system relies on a number of key properties of the synchronous machines for stable operation such as:

Self-synchronization that ensures that multiple synchronous machines operating in parallel align to a uniform frequency without supervisory control.

Inertia support that ensures that synchronous machines automatically respond to frequency deviations with a power injection proportional to the rate-of-change of frequency.

Frequency response that ensures that the generation unit can participate in frequency control by ad-

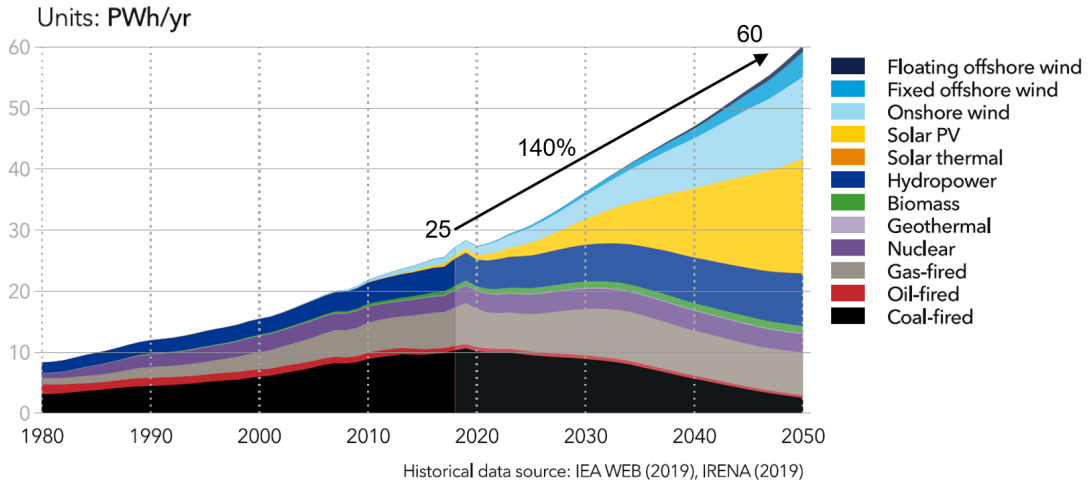

Figure 2: World installed electricity generation capacity scenario from DNV-GLs Energy transition outlook 2020 [7]

justing its output power with a factor proportional to the absolute frequency deviation.

Fault current injection Due to the inertia of the rotor and thereby the angle of the internal EMF in the machine, a generator response to a very low grid voltage by injection a large current. This property enables the fast detection of faults and proper operation of protection systems in the grid.

To meet the requirements of the future grid, new solutions need to be found to provide these features as the amount of grid connected synchronous machine capacity is decreasing.

2.2.2 Grid following vs Grid Forming Converter Control

Traditional converter based energy sources with traditional control schemes respond to grid voltage and frequency changes with the objective of supplying a constant current to the grid. This current is determined by the generation of the primary energy source and is determined with the sole purpose of evacuating the generated power onto the grid. A control system ensures the energy balance between produced energy and that put onto the grid. These control systems are referred to as grid following (non-grid supporting), and do not provide the services of voltage and frequency support. Therefore it is of interest to consider alternative and improved control structures.

On the other hand, a grid forming converter operates in voltage control mode and receives a reference voltage in terms of voltage magnitude from the reactive power controller (RPC) which typically operates with a voltage magnitude reference value for the PCC. The angle reference is obtained from the active power controller (APC) which typically operates with a frequency reference. This angle reference is generated by an internal oscillator operating either with fixed frequency given by the frequency reference, or compensated with a droop term to allow synchronization with other grid forming converters or existing grids. In this way they provide support in case of freqeuncy variations on the grid.

Figure 3 shows principal overviews of representative control schemes for grid-following (left) and grid-forming (right) converters. The principal difference is that the grid forming control relies on a phase locked loop (PLL) grid to synchronize to the grid. This requires a sufficiently stable grid voltage and therefore places requirements on the short-circuit power for the control to function. The APC of a grid following converters typically regulates the DC link voltage which fluctuates due to varying power production of the primary generation source behind, for example a PV panel, and thus determines the active power injection into the grid. The RPC typically regulates the reactive power injection into the grid. Together the APC and RPC generates the active and reactive current references to the converter which operates in current control mode. The voltage and angle reference for the voltage source converter

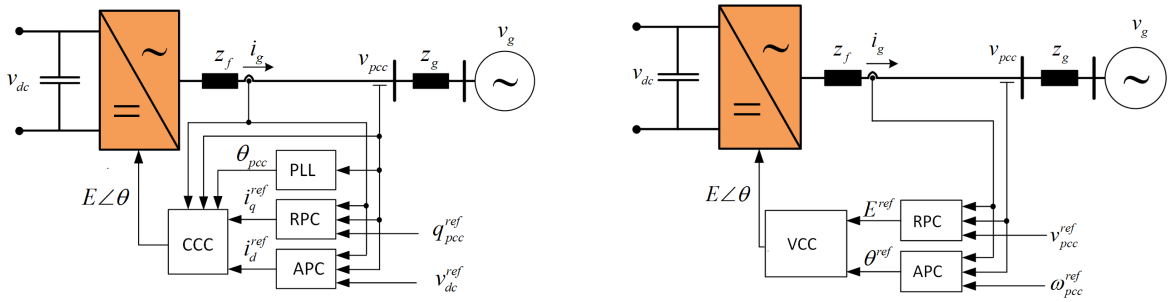

Figure 3: Simplified schematics of grid-following (left) and grid-forming (right) converter control schemes.

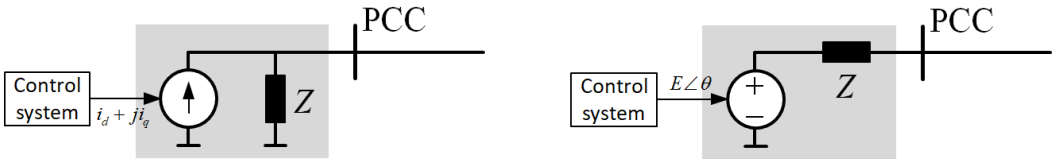

Figure 4: Equivalent circuit of grid-following (left) and grid-forming (right) converter control schemes.

comes from an embedded current controller that tracks the current references in a current controlled converter (CCC). The differentiation of active and reactive current relies on an estimate of the grid phase angle estimate from the PLL.

From an analytical and modelling perspective, the grid following converter can be represented as a controlled current source driven by the control system in parallel with an equivalent admittance and the voltage controlled converter as a controlled voltage source in series with an equivalent impedance. Due to the frequency dependency of the passive components as well as the driving control system, the equivalent impedance and admittance are also frequency dependent. See corresponding equivalent circuits in Figure 4. A key property of a grid forming converter is that it exhibits low output impedance in the low frequency range, and thus the terminal voltage remains stiff under varying load. Correspondingly, grid following converters exhibit a high output impedance in the low frequency range such that the current remains stiff as the PCC voltage changes.

2.2.3 Key results and connection to other tasks

This task has discussed the emerging need for grid supporting converters and discussed representative converter control structures for later use in the benchmark system modelling in Section 2.3. Detailed implementation will be described in Section 2.3.2.

- Electricity is expected to be the fastest growning energy carrier in the next decades
- A significant share of the growth will come in the form of distributed renewables, embedded in the distribution grid.
- The power systems currently relies on having a sufficient amount of synchronous machine based generation for sufficient equivalent inertia to respond to frequency changes, frequency control capability to correct short term frequency deviations and short-circuit strength to keep the operational voltage stable and provide sufficient fault current to activate protection systems in case of fault.
- In some countries, the shift towards renewable energy results in decommissioning of synchronous machine based generation.

- A significant share of the DERs will be non-dispatchable from the point of transmission grid operator, and thus it is necessary to rely on the local control to ensure a good behviour towards grid, and any frequency and voltage support must be triggered on local criteria.
- There are principal difference between grid-forming and grid following converter control architectures. The provision of voltage and frequency requires a change in philosophy, as most DER today rely on grid following control architectures.
- Use of grid forming or grid supporting control architectures, allow converter based DERs to contribute freqeuncy and voltage support services to the grid.

2.3 Distribution grid scenarios

2.3.1 Problem description

This section describes the selection and investigation of a benchmark network representative of a European distribution grid. This task also includes the selection of representative control architectures for grid following and grid forming DERs. The goal is to create a model that generates distribution grid cases based on a set of given parameters like the overall system loading and the share of RES generation to be used as a testbed for generating simplified, aggregated models, suitable for use in large-scale scenario studies in WP2.

2.3.2 CIGRE Medium Voltage Benchmark System

A detailed reference grid model is to be used as benchmark model in the project. For this purpose the CIGRE medium voltage benchmark system from [4] was adapted and simulation models capable of EMT as well as RMS simulation constructed. Generic models of common distributed renewable energy resources (DERs) and grid forming converter systems have been included based on the structures discussed in qualitative terms in Section 2.2.2. These include fuel cells, photovoltaic generation, wind and diesel generators and battery energy storage systems. Currently the wind generators and battery energy storage systems in the model are equipped with converter control system with so-called virtual synchronous machine (VSM) functionality as described by [5]. This is one example of a grid-forming control strategy. In all cases, the grid side converters are represented using detailed models. The machine or generator side converter have been omitted and replaced by constant current injectors on the DC side. Future work may consider a more detailed representation of the primary energy sources, but as the work in this project focuses on the behaviour of the DER towards the grid, this simplification is adequate considering the purpose of the study.

Figure 5 shows the single line diagram of the network and Table 1 shows the types and rating of the various DER units. The grid model assumes a connection point to a 220 kV level transmission grid and includes modelling of the medium voltage grid at 20 kV. The low voltage grids are represented by impedance loads initialized based on power flow data of the original source [4]. There are two distribution feeders, one of which is modelled in detail including DER units as tabulated in Table 1. This feeder is connected by several cable sections. The second feeder is modelled with two load buses connected via overhead lines. In the base case considered here, the sum of the load is around 44 MW and the total DER capacity about 3.4 MW. This results in a relatively low penetration level of DER of 8% in terms of the ratio between converter system rating and the total active power load. All loads in the system are modelled with resitive-inductive behaviour and tuned according to the power factor and load power given in the original source [4].

The CIGRE MV benchmark has been implemented in Modelica using the ConverterStab toolbox [22]. The graphical representation of the model is shown in Figure 6. As shown in the figure, this is a one to one mapping of the original single line diagram in Figure 5.

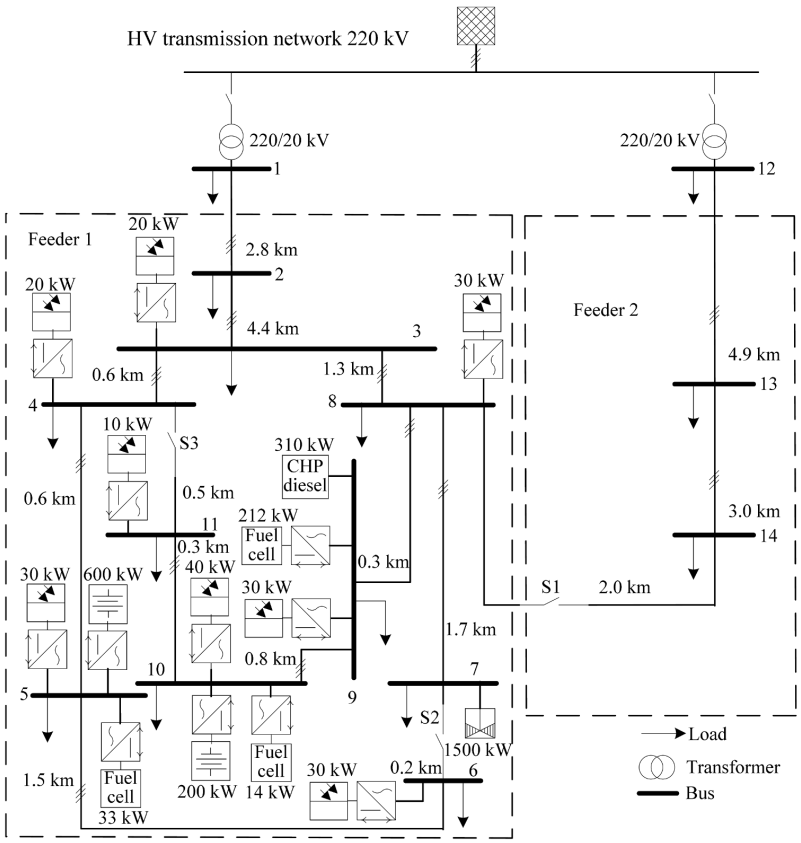

Figure 5: Single line diagram of CIGRE medium voltage distribution network benchmark system [4].

Node	Name	DER type	Pmax (kW)
3	PV3	Photovoltaic	20
4	PV4	Photovoltaic	20
5	PV5	Photovoltaic	30
5	Bat5	Battery	600
5	FC5	Residential fuel cell	33
6	PV6	Photovoltaic	30
7	WT7	Wind turbine	1500
8	PV8	Photovoltaic	30
9	PV9	Photovoltaic	30
9	CHPD9	CHP diesel	2*310 [1]
9	CHPFC9	CHP fuel cell	212
10	PV10	Photovoltaic	40
10	Bat10	Battery	200
10	FC10	Residential fuel cell	14
11	PV11	Photovoltaic	10

Table 1: Types and ratings of DER units.

Node	Apparent Power, S (kVA)		Power Factor	
	Residential	Industrial	Residential	Industrial
1	15300	5100	0.98	0.95
2				
3	285	265	0.97	0.85
4	445		0.97	
5	750		0.97	
6	565		0.97	
7		90		0.85
8	605		0.97	
9		675		0.85
10	490	80	0.97	0.85
11	340		0.97	
12	15300	5280	0.98	0.95
13		40		0.85
14	215	390	0.97	0.85

Table 2: Load parameters.

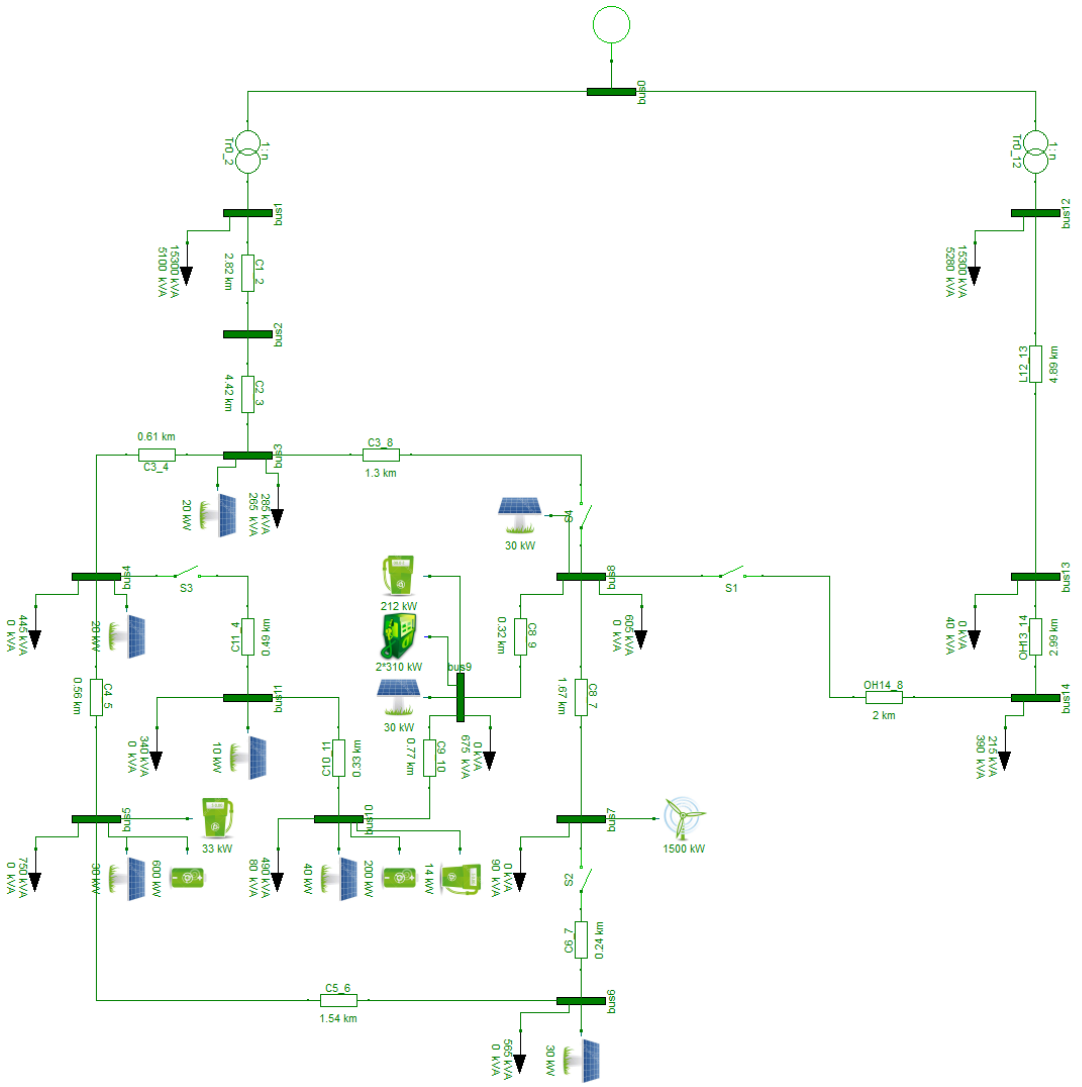

Figure 6: Modelica implementation of CIGRE MV benchmark model using ConverterStab.

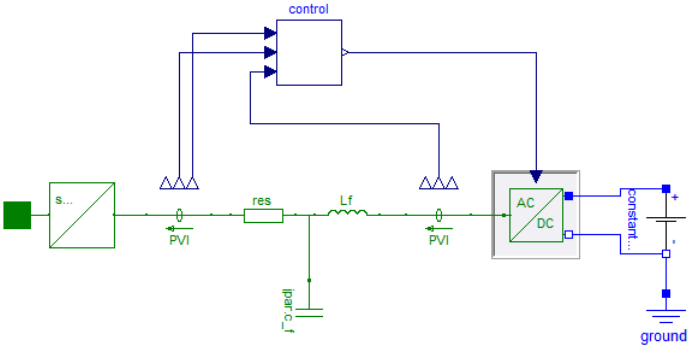

Figure 7: Main circuit of converter based sources.

2.3.3 DER Unit Representation

The benchmark system contains various types of DER as listed in Table 1.

In the project, the objective was not to develop new grid forming or grid following converter control system, but rather to study the impact of such. Therefore the converter control schemes have been adopted from scientific literature. However, a detailed review and comparison of various schemes from the scientific literature was carried out in a parallel Master's project [35] and supported through supervision enabled by the ACSICON project. All converter based generation is modelled using an average representation of the converter and with an LC output filter as shown in Figure 7. The photovoltaic units, residential fuel cells and CHP fuel cells are modelled as current controlled converter systems. These converters have a dq current reference that is initialized at the start of simulation and then tracked by PI controllers in d- and q- components, respectively. The control scheme is illustrated in Figure 8. These converters use a reduced version of the scheme in [5] where all loops except the current control loops have been removed. This control scheme is representative of control scheme used in typical PV and wind power converters today.

The battery and wind turbine are modelled using converter systems equipped with the full virtual synchronous machine control scheme described in [5]. Thus, they provide virtual inertia to contain frequency deviations and reactive power to support voltage control.

Initially all converters control system are tuned with the default parameter values given in [5] and the whole DER model is scaled based on the unit rating. These parameters have been well chosen to give good control performance for operation in a distribution system with typical grid strength, but without explicitly considering the potential of interaction with other DER controllers and the specific CIGRE benchmark case considered in this report.

The CHP diesel is modelled using a simplified third order synchronous machine model combined with standard excitation and governor control systems shown in Figure 10.

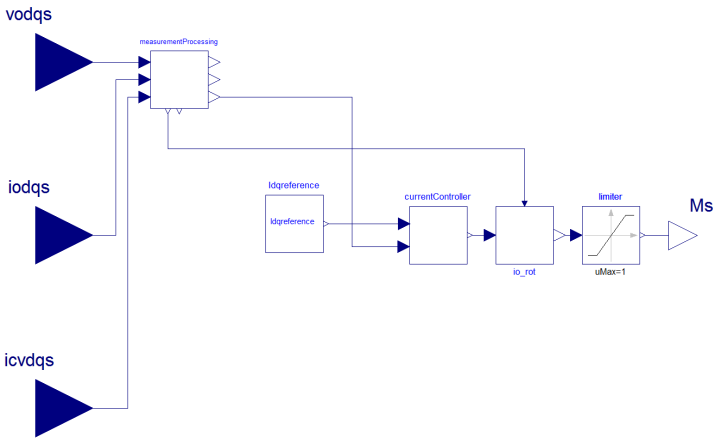

Figure 8: Grid following control system used by photovoltaic, residential fuel cell and CHP fuel cell DERs.

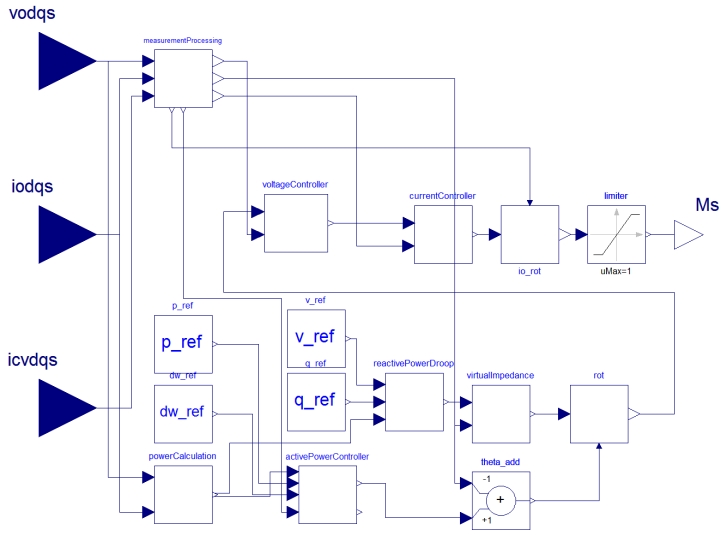

Figure 9: Grid forming control system used by battery and wind turbine DERs.

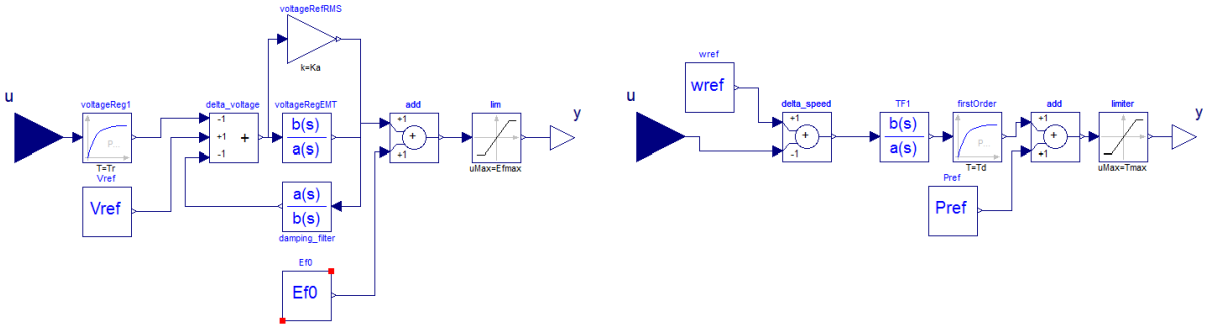

Figure 10: Excitation (left) and governor control systems used by diesel generator.

2.3.4 Validation of the Simulation engines

2.3.4.1 Overview

The two simulation engines used in the project are:

- The commercial simulation tool DYMOLA based on the modeling language Modelica and dedicated power system libraries (developed and used by Hitachi ABB Power Grids). Simulations can be performed in EMT or RMS mode, a graphical user interface is available.
- The in-house developed simulation tool FLEXDYN, using text-based symbolic power system models, translated to C++ code, and parameter files using the JSON-format. Simulations can be performed in RMS mode in a rotating dq-frame, allowing very efficient simulations of large power systems.

DYMOLA is used for the investigations in WP1 (modeling of distribution grids) and WP2 (linear distribution grid aggregation). FLEXDYN is used for the investigations in WP2 (nonlinear distribution grid aggregation) and WP3 (transmission grid investigations). Besides, an interface is established between the simulation tools, allowing to exchange symbolic models (in particular of the converter models), as well as aggregated power system models.

It is essential to ensure the consistency of the simulated results, allowing to exchange data and presenting the project findings irrespective of which of the two simulators has been used. To compare the converter simulation tools FLEXDYN (used at ETHZ-FEN) and DYMOLA (used at Hitachi ABB Power Grids), a simple reference network undergoing a large transient disturbances has been simulated and compared.

Both the HAPG and FEN models follow the implementation of [35]. Several differences of the HAPG and FEN converter model implementation have been identified, discussed and iteratively eliminated. A key difficulty involved the implementation of the PLL model. The internal converter angle and the dynamic model used for its tracking is essential for the performance of the Virtual-Synchronous-Machine(VSM)-functionality of the converter.

2.3.4.2 Validation test model

The test model used for validation of the ABB and the FEN simulator is depicted in Figure 11. During the validation, the grid undergoes an event sequence of voltage steps, load steps, islanding and re-synchronization to test the validity of the implemented converter model. The resulting trajectories of all dynamic variables are generated with both simulators and compared.

2.3.4.3 Disturbance scenario and converter models

The basis is the DYMOLA-case "ConverterSystems.Test.StrongGrid.Basecase". The converter simulation tools are tested with the following scenario:

- Linear network of 3 buses in a row
  - Bus 1 is connected to a Feeder
  - Bus 2 is connected to a Load (initial load $0.6 + 0.15iMVA$)
  - Bus 3 is connected to a VSM-converter (initial injection $0.2 + 0.1iMVA$)
- After initialization, a sequence of disturbances is applied:
  - 1 second: 5% Step of Reference Voltage
  - 4 second: Step of Converter Active Power (from $0.2MVA.$ to $0.3MVA$)
  - 5 second: Load step (new load $0.5 + 0.1iMVA$)

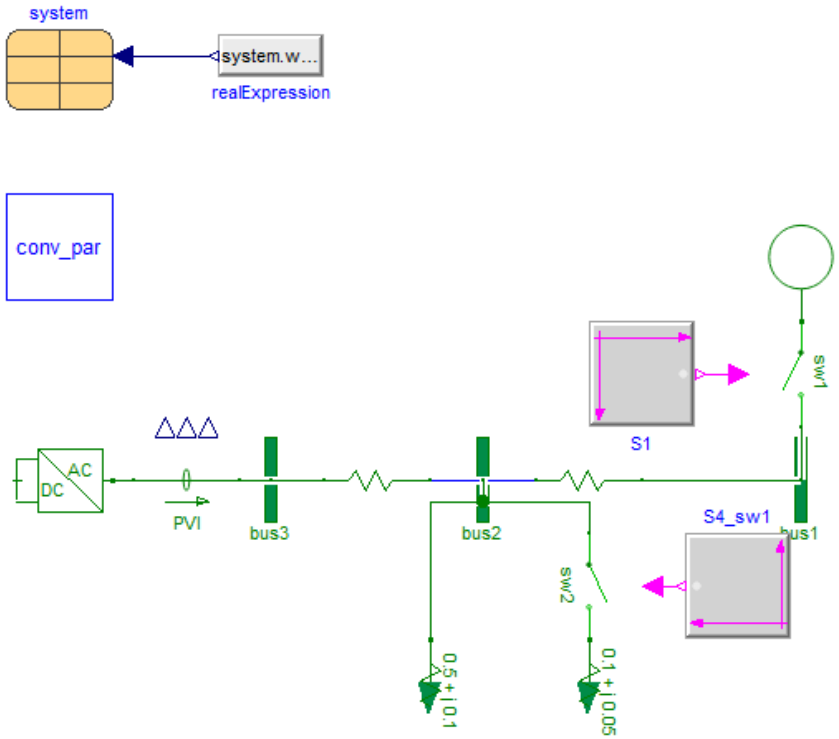

Figure 11: Reference grid model used for validation of the ABB and the FEN simulator. The grid undergoes an event sequence of voltage steps, load steps, islanding and re-synchronization to test the validity of the implemented converter model.

- 10 second: Disconnection of the Feeder (Islanding)
- 15 second: Reconnection of the Feeder

During the islanding, the converter has to supply the whole load demand and control the frequency of the islanded network.

The goal of the validation process is to implement the same control loop structures including a map of key parameters used in both simulation tools. Similar parameter settings should result in similar simulation results.

Three converter types are being implemented:

1. Converter with pure current control and no storage, representing a grid-following converter. The structure converter model is shown in Figure 12.
2. Converter with VSM functionality and storage. The structure converter model is shown in Figure 13.

The structure of the converter model implementation and the variable exchange between the modules is the same in both simulation frameworks. Small differences originate from the representation of the global grid frequency. The DYMOLA simulator also includes the option for EMT simulations and follows a more general modeling approach.

The storage can either be based on a storage with finite capacity (like a battery) or be modeled as an ideal stiff DC-voltage source (very large storage).

Note that the full disturbance sequence can only be applied for the VSM converter type, due to the islanding scenario.

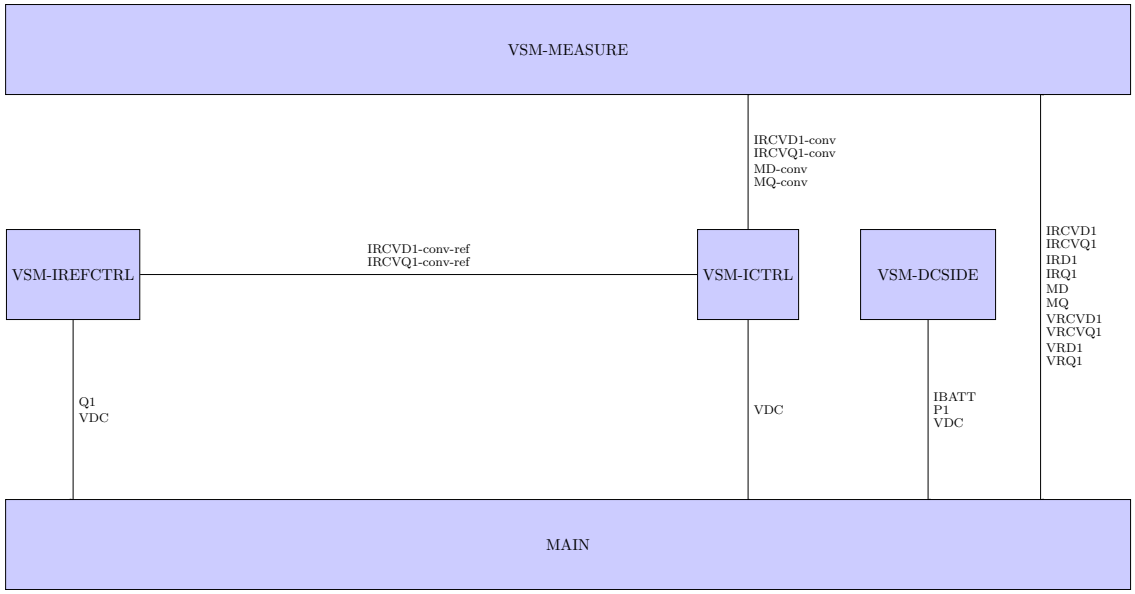

Figure 12: Structure of the current-controlled capacitor model. This represents classical PV-converters without connected battery storage.

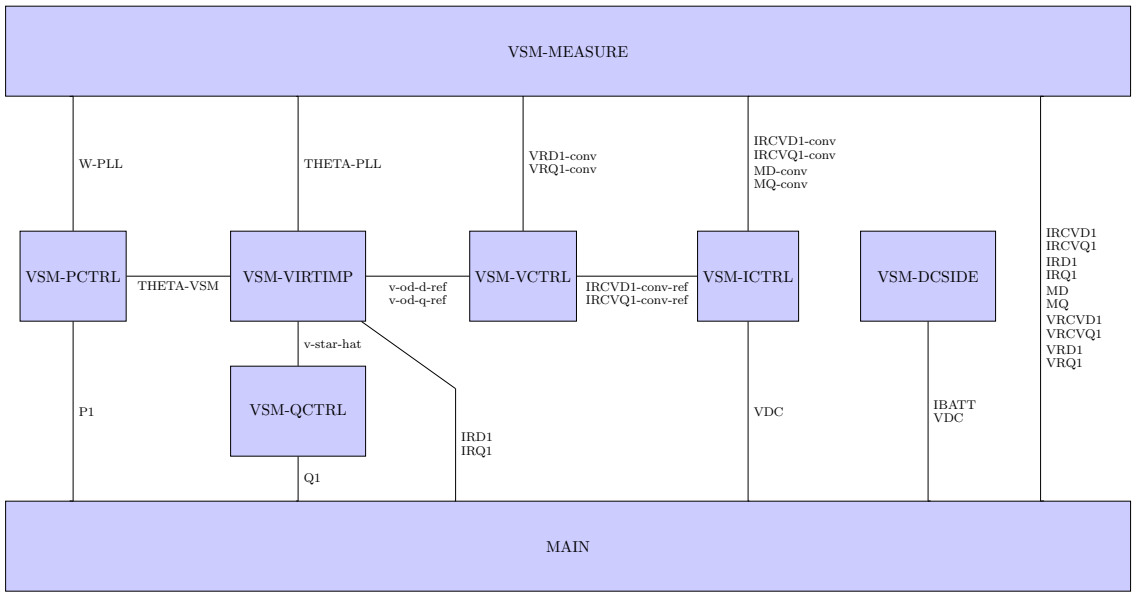

Figure 13: Structure of the VSM model. This represents an advanced converter control with connected battery storage, whose capacity is sufficient to support the grid during transients.

2.3.4.4 Resulting parameter map

Besides the topology, line parameters and nominal powers of loads, generators and voltages, the following map of converter parameters has been established as interface between FLEXDYN and DYMOLA. The purpose is to use this map for a fast exchange of adjusted converter tunings performed by the two project partners.

For the simulation results used for comparison, the DYMOLA parametervalues were used with both simulators.

2.3.4.5 Comparison Variables and Results

For validation of the 2 converter simulation tools, the following variables are plotted:

- Load Bus Voltage
- Load Bus Voltage Angle
- Converter Active Power
- Converter Reactive Power
- PLL frequency
- PLL angle
- Converter D-Current
- Converter Q-Current

The following plots show the comparison of the converter's terminal active power and internal PLL frequency in both simulation environments. The trajectories were exported with the two simulation tools and are jointly presented for a selection of relevant variables.

The full plot shows the complete disturbance scenario, with zooms after each of the 4 disturbances.

As can be seen, the final model implementation and parameter map result in a very similar qualitative and quantitative shape of the trajectories.

The plots for the other comparison variables show a similar match between both simulators. *FLEXDYN* refers to the FEN-Simulator while *DYMOLA* refers to the HAPG-Simulator.

DYMOLA			FLEXDYN		
Variable	Value	Description	Model	Variable	Original Value
conv.par.c_dc	1	DC capacitor (pu)	PSC_ABB_CONVERTER	Cdc	1
conv.par.c_f	0.074	Filter capacitance (pu)	PSC_ABB_CONVERTER	Cf	0.08
conv.par.l_f	0.08	Filter inductance (pu)	PSC_ABB_CONVERTER	Lf	0.074
conv.par.r_f	0.003	Filter resistance (pu)	PSC_ABB_CONVERTER	Rf	0.003
conv.par.w_b	314.1593	Rated angular frequency	PSC_ABB_CONVERTER	ws	314.159
conv.par.T_a	2	VSM Inertia constant (s)	PSC_ABB_VSM_PCTRL	Ta	2
conv.par.k_d	400	VSM Damping coefficient	PSC_ABB_VSM_PCTRL	kd	400
conv.par.k_w	20	Frequency droop gain (pu)	PSC_ABB_VSM_PCTRL	kw	20
conv.par.w_star	1	Frequency reference (pu)	PSC_ABB_VSM_PCTRL	ws	314.159
conv.par.k_q	0.01	Reactive power droop gain (pu)	PSC_ABB_VSM_QCTRL	kq	0.01
conv.par.l_f	0.08	Filter inductance (pu)	PSC_ABB_VSM_ICTRL	Lf	0.08
conv.par.k_ic	60	Current controller integral gain	PSC_ABB_VSM_ICTRL	k_ic	30
conv.par.k_pc	1	Current controller proportional gain	PSC_ABB_VSM_ICTRL	k_pc	0.3
conv.par.uv_max	1.1	Valve voltage limit (pu)	PSC_ABB_VSM_ICTRL	limit_uv_max	1.1
conv.par.w_b	314.1593	Rated angular frequency	PSC_ABB_MEASUREMENT	K	314.159
conv.par.k_i_PLL	15	PLL integral gain (pu)	PSC_ABB_MEASUREMENT	kipll	5
conv.par.k_p_PLL	0.6	PLL proportional gain (pu)	PSC_ABB_MEASUREMENT	kppll	0.4
conv.par.c_f	0.074	Filter capacitance (pu)	PSC_ABB_VSM_VCTRL	Cf	0.074
conv.par.k_iv	250	Voltage controller integral gain	PSC_ABB_VSM_VCTRL	k_iv	500
conv.par.k_pv	0.05	Voltage controller proportional gain	PSC_ABB_VSM_VCTRL	k_pv	0.11
conv.par.iv_max	1.05	Valve current limit (pu)	PSC_ABB_VSM_VCTRL	limit_iv_max	1.1
conv.par.l_v	0.2	Virtual Inductance (pu)	PSC_ABB_VIRTUAL_IMPEDANCE	l_v	0.2
conv.par.r_v	0.05	Virtual Resistance (pu)	PSC_ABB_VIRTUAL_IMPEDANCE	r_v	0.05
conv.par.uv_max	1.1	Valve voltage limit (pu)	PSC_ABB_VIRTUAL_IMPEDANCE	limit_uv_max	1.1
conv.par.u_dc_nom	1	Nominal dc voltage (pu)	PSC_ABB_VSM_DCSIDE_STIFF	VDCREF	1
conv.par.u_dc_nom	1	Nominal dc voltage (pu)	PSC_ABB_VSM_IREFCTRL_VDC	VDCREF	1
conv.par.T_i_dc	0.1	DC voltage controller integral gain	PSC_ABB_VSM_IREFCTRL_VDC	k_idc	0.01
conv.par.k_p_dc	30	DC voltage controller proportional gain	PSC_ABB_VSM_IREFCTRL_VDC	k_pdc	300
conv.par.c_dc	1	DC capacitor (pu)	PSC_ABB_VSM_DCSIDE_CAP	Cdc	1

Table 3: Parameter map between DYMOLA and FLEXDYN. The DYMOLA parametervalues were used in both simulators.

Comparison of Terminal Active Power

The following plots show a comparison of the Active Power at the converter terminal.

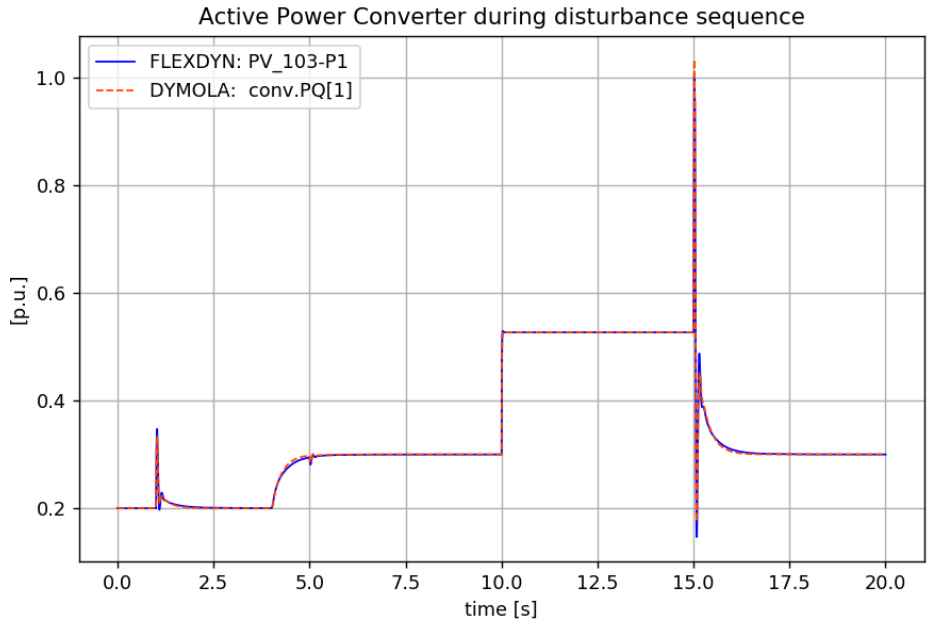

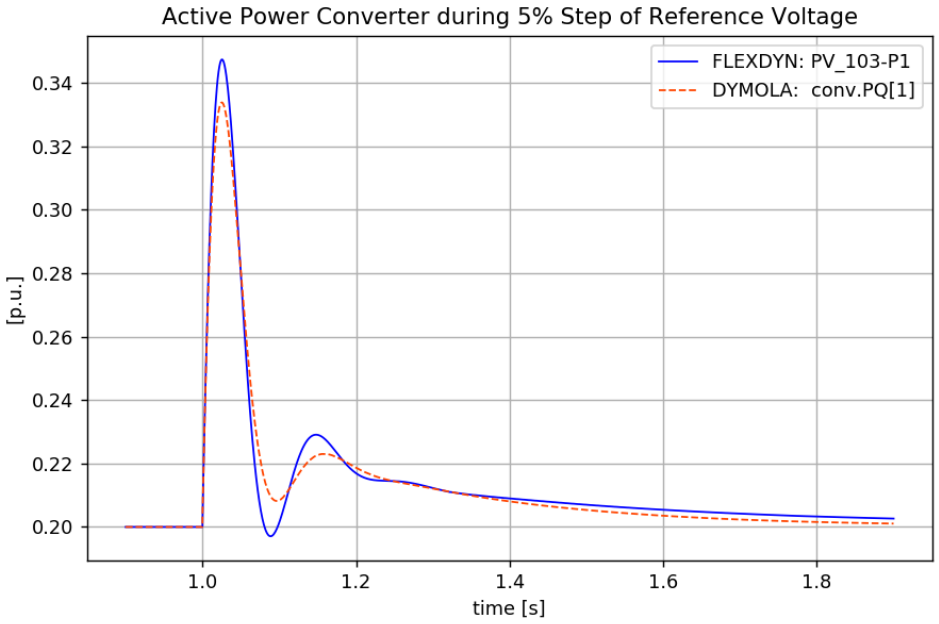

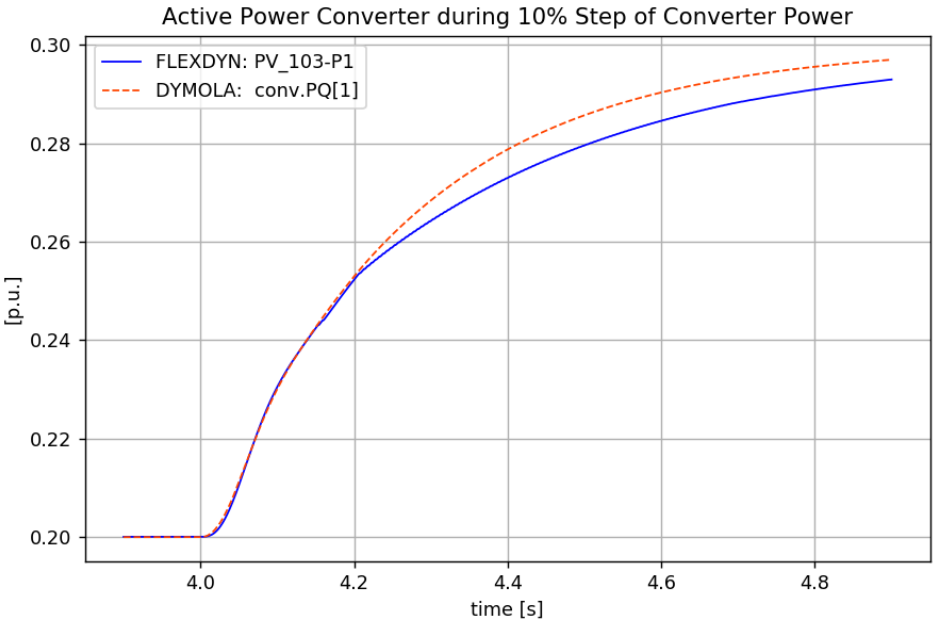
Active Power Converter during 10% Step of Converter Power
FLEXDYN: PV_103-P1
DYMOLA: conv.PQ[1]
0.30
0.28
0.26
0.24
0.22
0.20
[p.u.]
4.0
4.2
4.4
4.6
4.8
time [s]

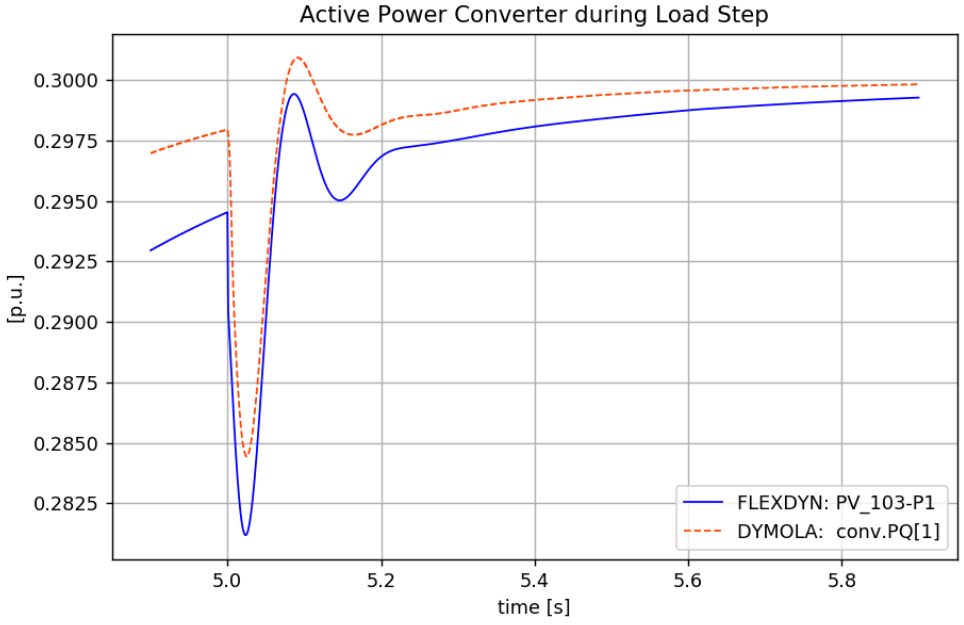
Active Power Converter during Load Step
0.3000
0.2975
0.2950
0.2925
0.2900
0.2875
0.2850
0.2825
[p.u.]
FLEXDYN: PV_103-P1
DYMOLA: conv.PQ[1]
5.0
5.2
5.4
5.6
5.8
time [s]

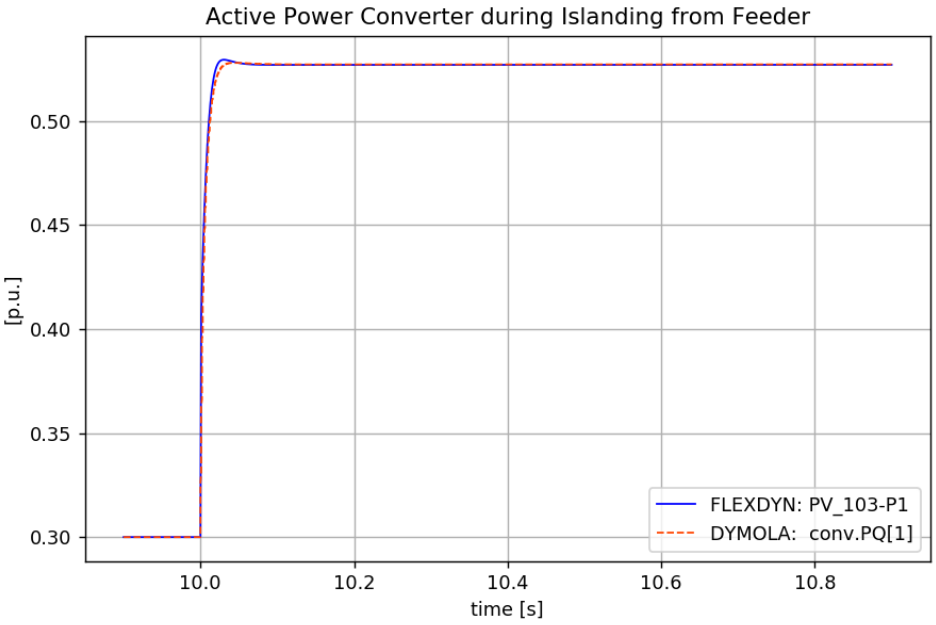
Active Power Converter during Islanding from Feeder
0.50
0.45
0.40
0.35
0.30
[p.u.]
10.0
10.2
10.4
10.6
10.8
time [s]
FLEXDYN: PV_103-P1
DYMOLA: conv.PQ[1]

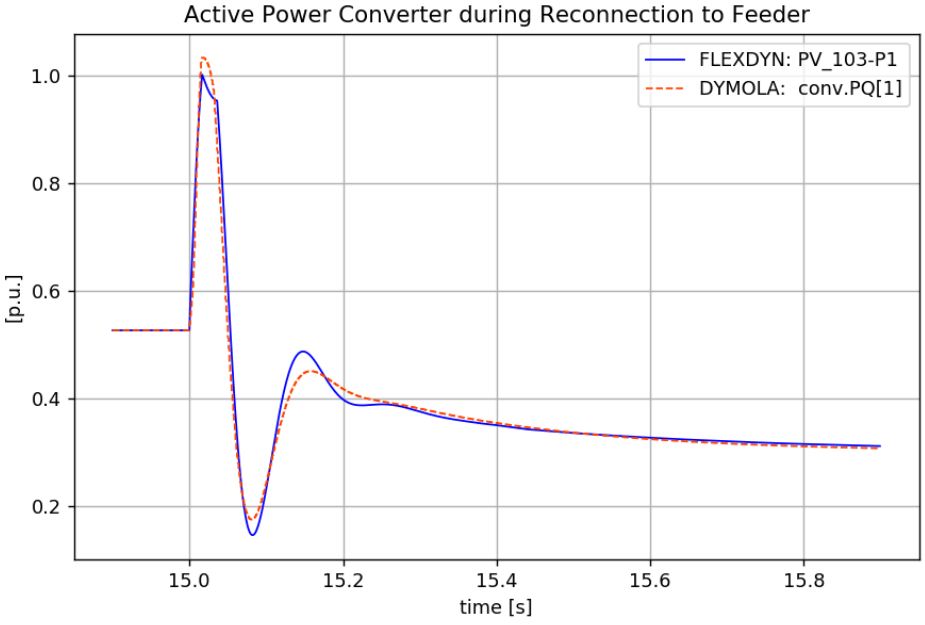
Active Power Converter during Reconnection to Feeder
1.0
0.8
0.6
0.4
0.2
[p.u.]
15.0
15.2
15.4
15.6
15.8
time [s]
FLEXDYN: PV_103-P1
DYMOLA: conv.PQ[1]

Comparison of PLL frequency
The following plots show a comparison of the PLL frequency estimated by the converters.

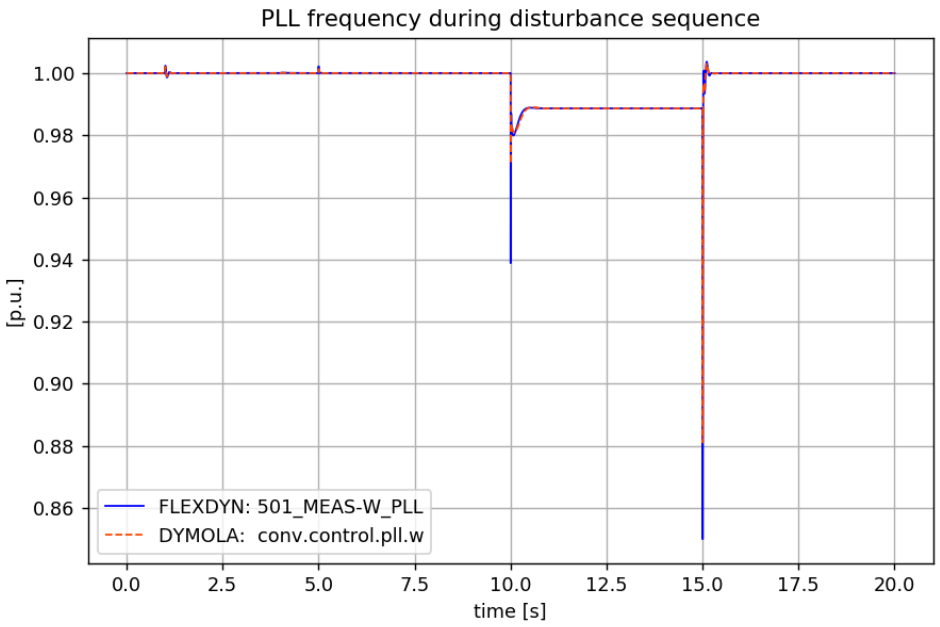

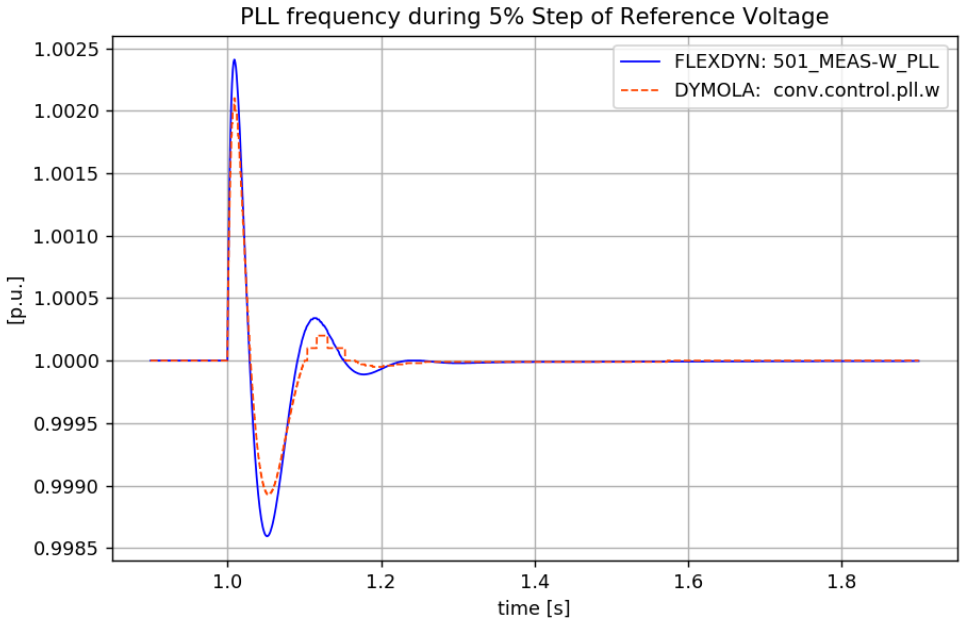

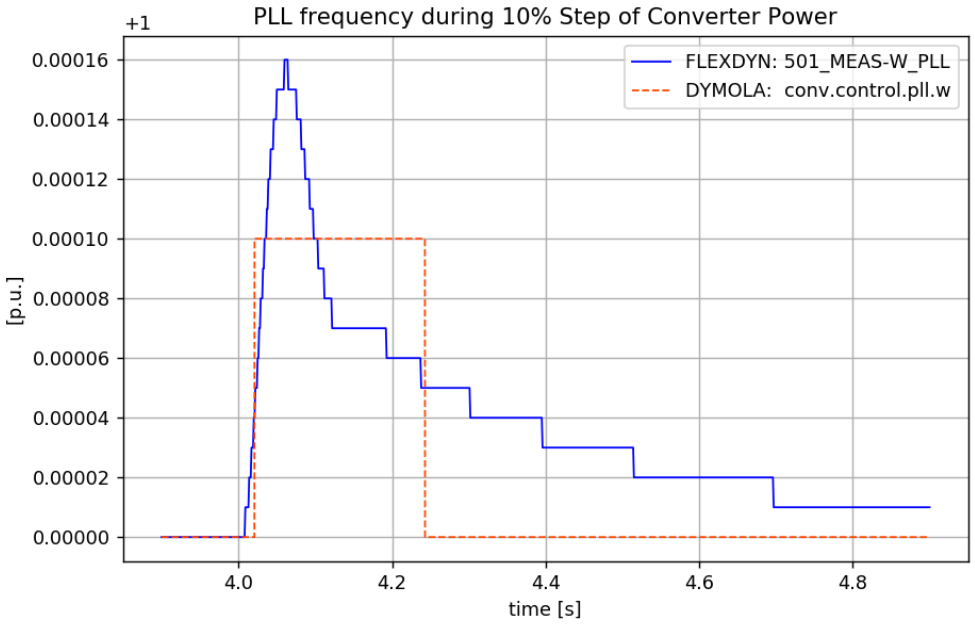
PLL frequency during 10% Step of Converter Power
+1
0.00016
0.00014
0.00012
0.00010
0.00008
0.00006
0.00004
0.00002
0.00000
[p.u.]
4.0
4.2
4.4
4.6
4.8
time [s]
FLEXDYN: 501_MEAS-W_PLL
DYMOLA: conv.control.pll.w

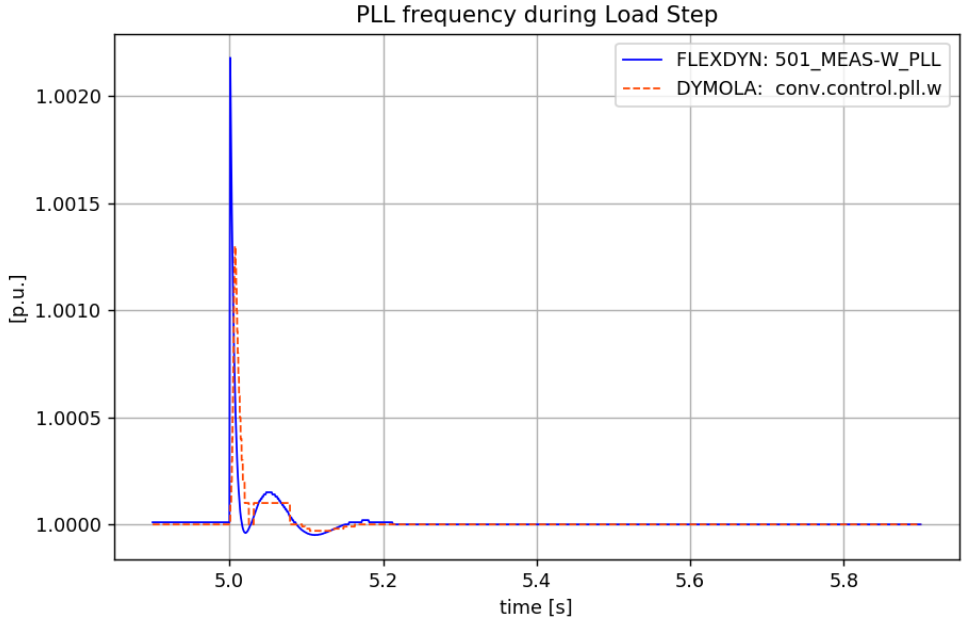
PLL frequency during Load Step
1.0020
1.0015
1.0010
1.0005
1.0000
[p.u.]
5.0
5.2
5.4
5.6
5.8
time [s]
FLEXDYN: 501_MEAS-W_PLL
DYMOLA: conv.control.pll.w

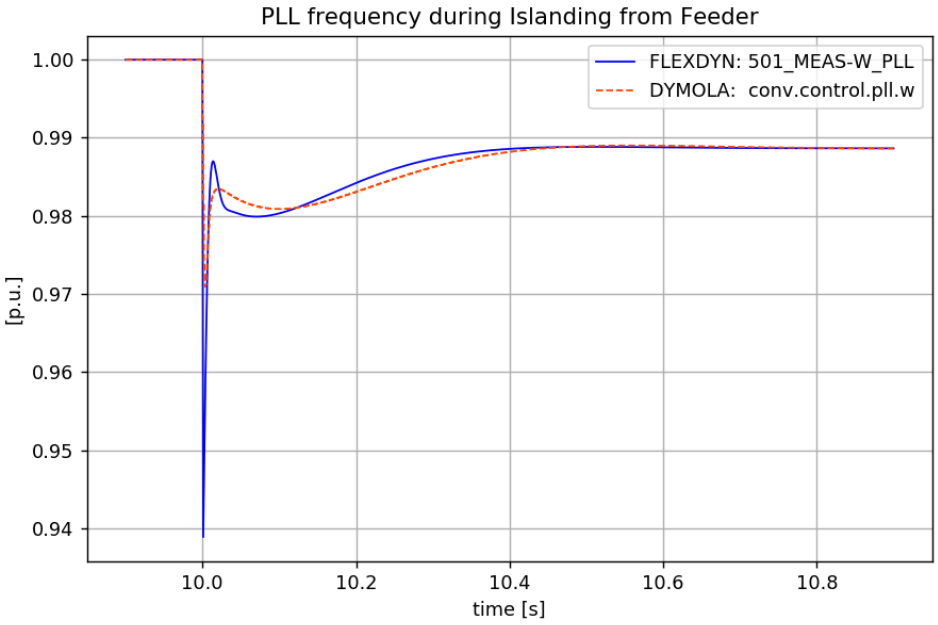
PLL frequency during Islanding from Feeder
FLEXDYN: 501_MEAS-W_PLL
DYMOLA: conv.control.pll.w
[p.u.]
time [s]
1.00
0.99
0.98
0.97
0.96
0.95
0.94
10.0
10.2
10.4
10.6
10.8

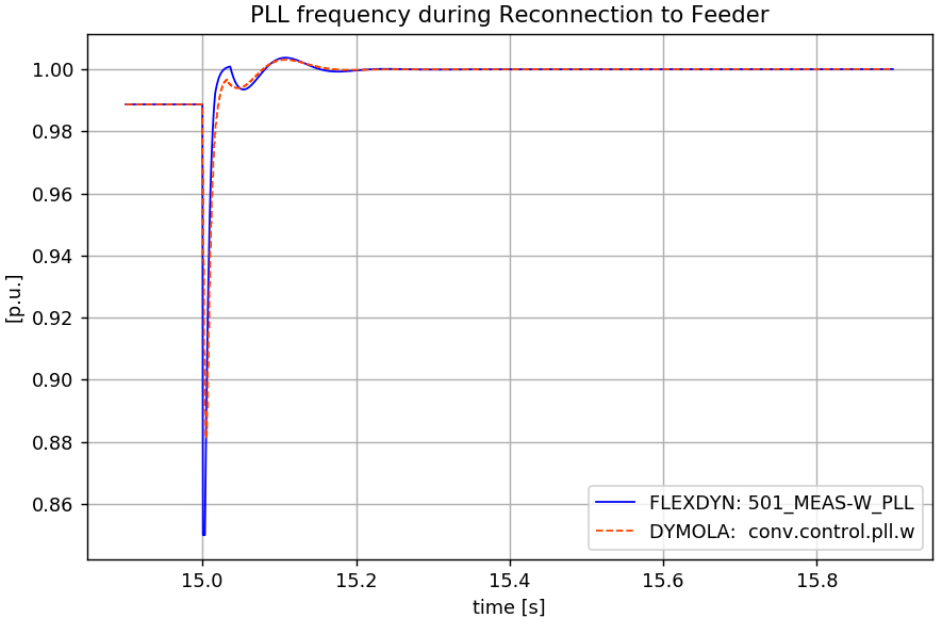
PLL frequency during Reconnection to Feeder
FLEXDYN: 501_MEAS-W_PLL
DYMOLA: conv.control.pll.w
[p.u.]
time [s]
1.00
0.98
0.96
0.94
0.92
0.90
0.88
0.86
15.0
15.2
15.4
15.6
15.8

2.3.5 Reference Test Scenario

To evaluate the performance of DERs in the CIGRE benchmark grid environment a case with islanding in the grid is chosen. This is a particularly challenging test case with respect to stability and simulation accuracy since it causes off nominal frequency operation during the islanding and contains two line switching events. Those switching events result in time based discrete events during simulation. As a consequence of those events, there are also signal based events due to saturation logic of the control schemes for some of the inverters and the diesel generator.

As shall be seen, the islanding poses a significant challenge for the DERs which in the initial phase are tuned for operation in grid connected mode and for a rather strong grid. The simulations are carried out using both EMT and a reduced RMS models to allow a larger time step in the RMS simulation, and align the fidelity to those used in the large-scale scenario studies in WP3.

The numerical simulation of differential equation arising in grid simulation models introduces an approximation error that is dependent on the the integration step size h. By example, for the Euler method this error is proportional to h^2, thus the error will rapidly decrease when the time step is made smaller. More importantly, the Euler iteration can experience instability if the time step is too large in relation to the fastest dynamics of the system. An approximate stability bound on h can be given by

$$|1 + h\lambda_{max}| \leq 1 \tag{1}$$

where λ_{max} is the largest eigenvalue of the Jacobian matrix A in (4) [32]. Thus, the maximum possible time step is heavily influenced by the dynamics of the system unde study. The largest eigenvalue can be interpreted as a measure of the speed of the fastest dynamics in the system. As discussed in [32], higher order methods requiring multiple derivative evaluations per time step can be used to allow substantially larger time steps while retaining a predictable update time, but the Euler assumption yields a conservative estimate.

Table 4 shows the largest eigenvalues along with the dominant states for the various EMT component models along with the resulting stability bound on h for the various grid and component models in the CIGRE benchmark system. As shown, the time step required for stability of the Euler method on the EMT components models is very small. For the grid, this is due to the short cable segments–the shortest being only 0.24 kms long. This results in very fast dynamics related to the electromagnetic phenomena of the grid component which the explicit Euler approximation is very poor in handling. For the EMT model, therefore an implicit method should be used.

To reduce the DER models for RMS simulation, modal analysis (see Section 2.4.2.1) of the EMT component models was made to detect the fastest dynamics. On the basis of that analysis, which is summarized in Table 4, the following changes was made to the EMT model resulting in the simplified model referred to as the RMS model:

- neglecting electromagnetic transients related to inductive and capacitive elements in the grid, load and converter filters,
- assuming and instantaneous response of the converter current controls,
- and assuming an instantaneous response of the diesel generator automatic voltage regulator (AVR).

This eliminates all fast states in the component models and results in the new time step bound shown in Table 2.3.5. The adapted model is accurate enough to study low-frequency behaviour up to around 5 Hz, and of the required accuracy for RMS based simulation tools.

Figures 14-15 show simulation results of the islanding case using default parameters of the various converter control systems. At time 1 s, a voltage step of 2 % is applied on the feeding grid and at time 5 s the switch S4 is opened. Since switches S1-S3 are normally open, this results in islanding of the section of the grid containing buses 7-11. The other buses remain connected to the main grid. The simulation results are discussed in the following sections.

Component	λ_{max} (s^{-1})	Dominant State	h_{max} (s)
Grid	-217.52+j405058.83	C6_7.RX.i[1]	4.8e-09
Photovoltaic	-1415119.99+j314.16	Cf.T.v[1]	1.4e-06
Fuel Cell	-1415119.99+j314.16	Cf.T.v[1]	1.4e-06
Battery	-1415045.06+j419.61	Cf.T.v[2]	1.4e-06
CHP Diesel	-12.16+j3.07	governor.damper.lowpass.x_scaled[1]	0.02
CHP Fuel Cell	-1415119.99+j314.16	Cf.T.v[1]	1.4e-06

Table 4: Maximum eigenvalues and resulting step size upper stability bound for the various EMT component models

Component	λ_{max} (s^{-1})	Dominant State	h_{max} (s)
Grid	NaN+j0.00	n/a	NaN
Photovoltaic	-13.19+j36.05	control.measurementProcessing.pll.pi.x	0.018
Fuel Cell	-13.19+j36.05	control.measurementProcessing.pll.pi.x	0.018
Battery	-31.82+j149.56	control.voltageController.PI[2].x	0.0027
CHP Diesel	-12.16+j3.07	governor.damper.lowpass.x_scaled[1]	0.02
CHP Fuel Cell	-13.19+j36.05	control.measurementProcessing.pll.pi.x	0.018

Table 5: Maximum eigenvalues and resulting step size upper stability bound for the various RMS component models

2.3.5.1 RMS Model

The voltage step at 1 s is handled without incident in the RMS simulation. There is a well damped oscillation in the voltage at Bus 7 which is also visible in the generated power by the wind turbine. There is also poorly damped but stable low frequency oscillation in the speed of the diesel generator. Thus, it appears that the control of the diesel generator which has been designed primarily with island operation in mind is not adequate for the grid connected mode.

When the network is islanded at 5 s the frequency of the islanded part of the grid rapidly decreases due to the power imbalance in the island. Furthermore, the voltage at bus 7 rapidly declines but is contained through the voltage support by the diesel generator, wind turbine and battery energy storage system. The voltage and frequency control of the DERs in the island stabilizes the frequency resulting in a frequency nadir of around 0.96 pu. However following the stabilization of the frequency, there is a negatively damped oscillation in the voltage and generated power by the wind turbine at approximately 24 Hz. Because of this instability the simulation prematurely terminates due to singularities in the model.

Thus, although the DERs operate stably in the grid connected mode, there is an instability in islanded mode.

2.3.5.2 EMT Model

Initially the response is similar to the response of the RMS simulation. The same oscillation directly following the voltage step as in the RMS simulation is visible and shows a slight negative damping. This qualitative difference from the RMS simulation can be attributed to the dynamics of the converter current control loops and the electromagnetic transients related to inductive and capacitive elements that are neglected in the RMS model (see Figure 21). The negatively damped mode results in a slowly growing oscillation also in grid connected mode that starts to become visible particularly in the Bus 7 voltage and the power injection from WT7. The poorly damped frequency control mode of the diesel generator shows similar low damping as in the RMS simulation.

Thus, it is clear that the default parameter settings of the DERs are not adequate for the considered benchmark grid. The analysis in Section 2.4.3.2 will describe ways of improving stability and derive tuning for the DERs that is adequate in the CIGRE benchmark system.

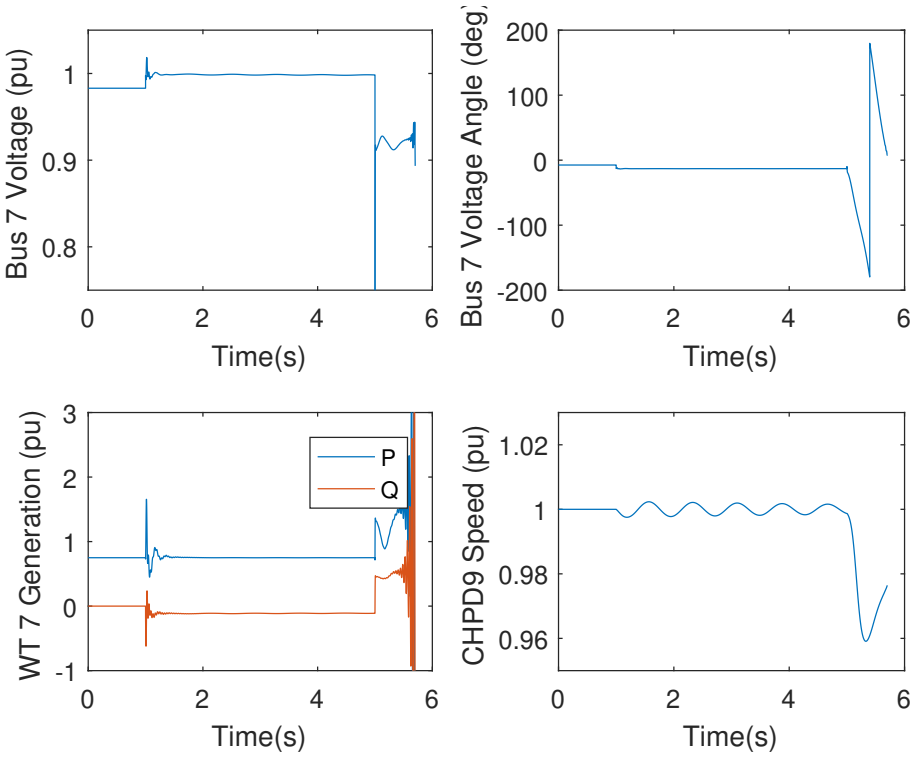

Figure 14: Islanding scenario with RMS simulation.

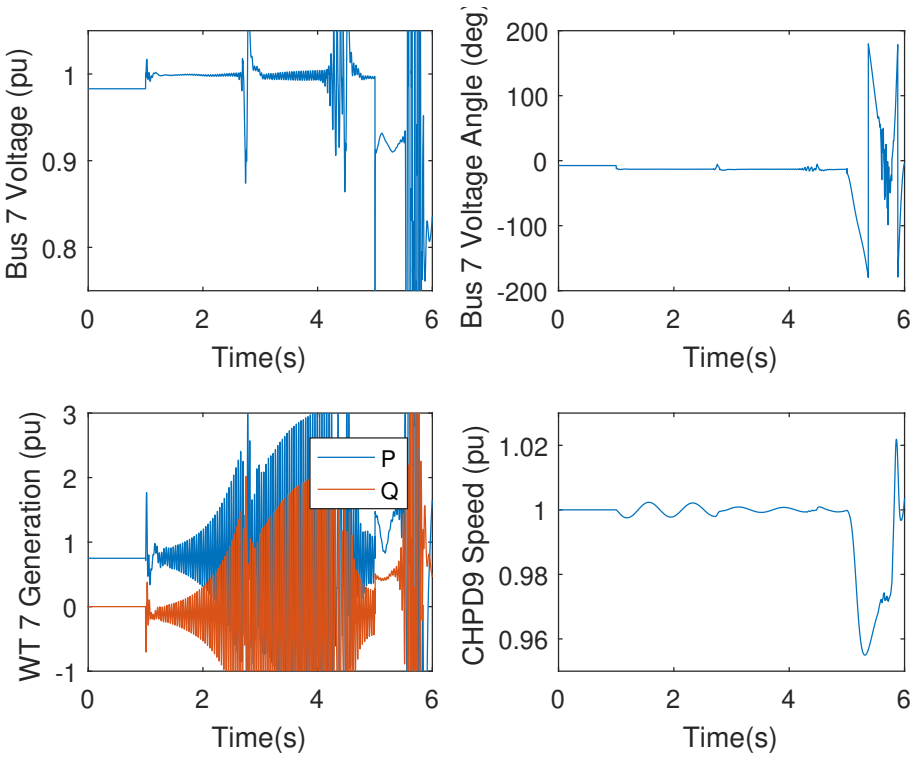

Figure 15: Islanding scenario with EMT simulation.

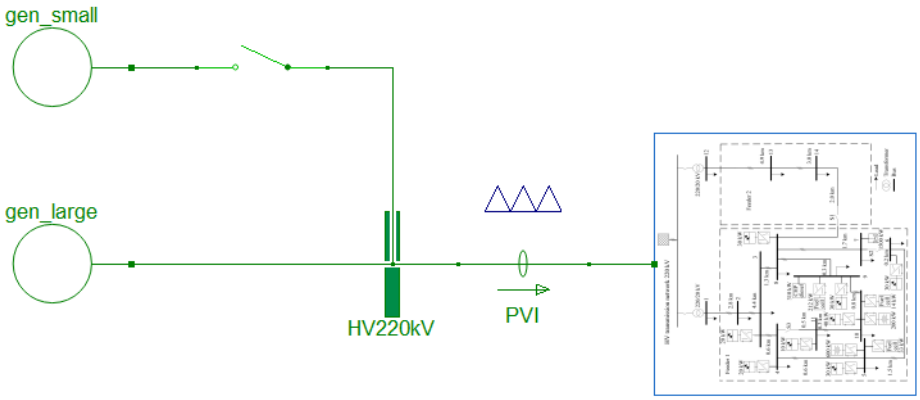

Figure 16: Single line diagram of the generator to grid test case.

2.3.6 Scenario Definition for Varying DER Penetration Level

To allow study of the benchmark system under varying penetration of grid supporting converters, the following scalings have been applied to the original ratings shown in Table 1. Scenarios with different penetration levels are generated by linear scaling of the rating of the grid supporting DERs in the CIGRE benchmark system shown in Figure 5. The penetration level is then defined as

$$p = \frac{\sum S_{gsconverter}}{\sum P_{load}} \tag{2}$$

That is, the penetration level is a relative measure of to what degree the distribution grid load can be supplied locally. Thus, grid with a penetration level higher than one would be capable of islanded microgrid operation.

To study the impact of the active DERs, the CIGRE benchmark grid was connected to simple grid equivalent used to simulate frequency and voltage disturbances from the transmission side. The grid is modelled as a single generation unit with a rating of 100 MVA, corresponding to approximately twice the load in the supplied grid. In the base case 3 MW of load is supplied by a smaller machine which is disconnected at simulation time 10 s. This creates a power imbalance in the system that needs to be compensated by the remaining synchronous machine through rotational energy stored in its rotor and subsequent production ramp up by its governor control system. Additionally the grid supporting converters in the distribution grid will respond with both inertial response and frequency response that can also be faster than that of the synchronous machine.

The resulting response of the system frequency under varying level of penetration of grid supporting converters is illustrated in Figure 18. The initial rate of change of frequency (ROCOF) following the generator trip at 10 s is almost identical in the cases with and without DERs indicating that the virtual inertia supplied by the VSMs embedded in the DERs has a very small effect on the ROCOF even under high penetration. Since the load is to a larger extends supplied by the DER in the high penetration cases, those cases also have a significantly lower demand on the transmission grid.

Figure 17 shows the active and reactive power load in the interconnection point between transmission and distribution during the generator trip scenario described above. Cases with high penetration level has substantially lower load at the initial time, and it can be seen that the load decrease thanks to the frequency support of the DERs is more prominent.

The frequency nadir is significantly lower in cases with low penetration of DER, indicating that the fast regulation capability of the VSM very effectively supports the grid frequency even when the DER penetration level is only around 10 %. It should be noted that the inertia emulation and frequency controllers in the grid forming DERs are using the parameter settings proposed in the original reference [5] and that the virtual inertia support could be improved by changes in the tuning.

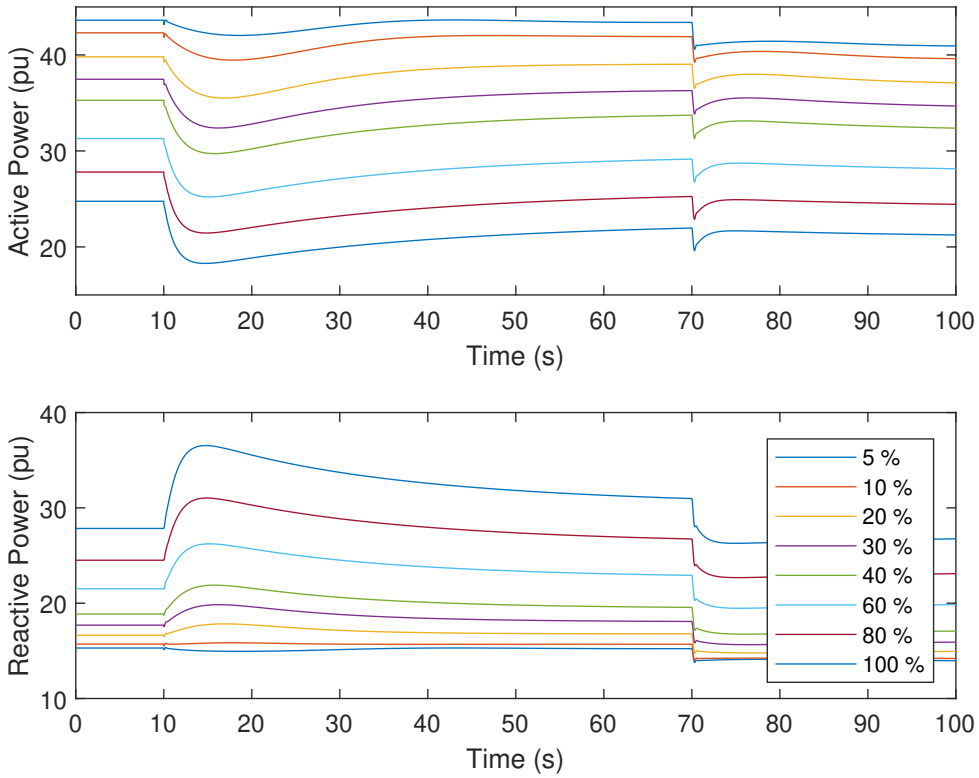

Figure 17: Response of active and reactive power consumption of the distribution grid during generator trip scenario.

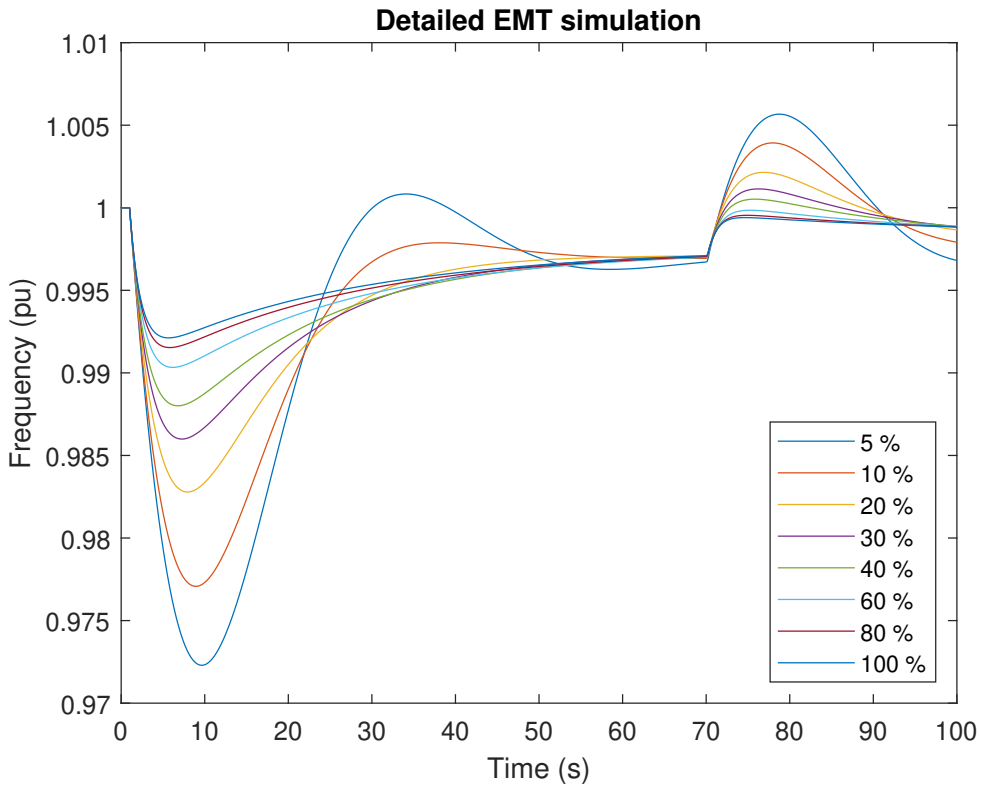

Figure 18: Response of system frequency during generator trip scenario.

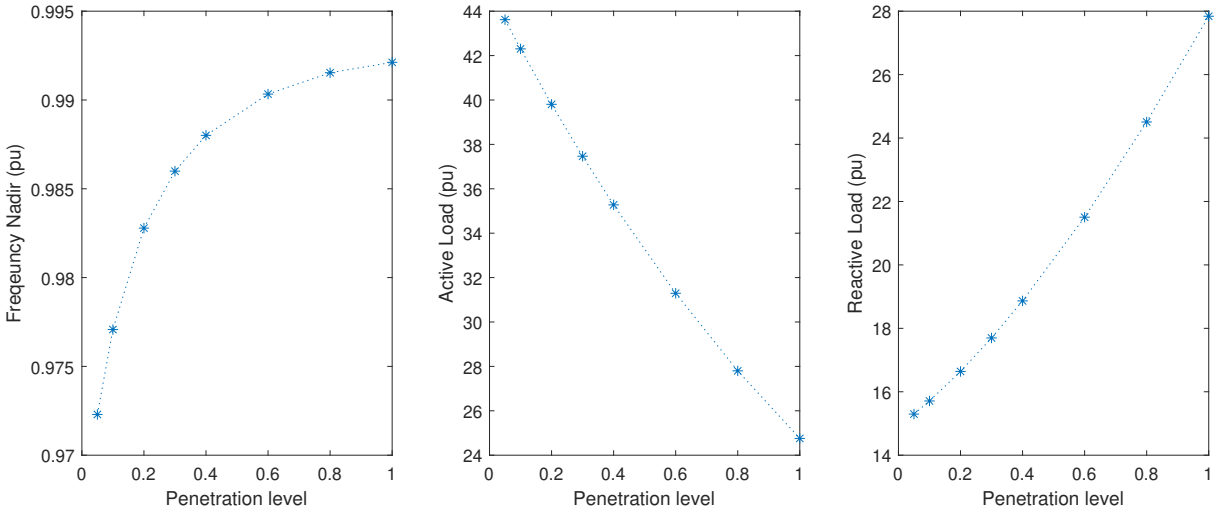

Figure 19: Dependency of Nadir frequency and active/reactive power load on penetration level.

Figure 19 (left) illustrates the effect of DER penetration on the frequency nadir following the applied disturbance and the pre-disturbance active and reactive load as seen from the interconnection point between transmission and distribution. The decrease in load is almost linear with the penetration level however the effectiveness of frequency support in terms of the nadir frequency exhibits a diminishing return as the penetration level increases. For example, at the penetration level of 5 %, the frequency nadir occurs at around 0.972 pu whereas at 10 % it occurs at around 0.977 pu, which is an an improvement of about 0.1 pu frequency per per penetration level. On the other hand, comparing the improvement between 80 % and 100 % penetration shows only a marginal improvement. Thus, it is clear that there is an effect of diminishing return as the penetration level increases.

2.3.7 Key results and connection to other tasks

This section has presented the CIGRE benchmark distribution grid that is used as a representative test case. This grid has been equipped with grid following and grid forming DERs employing the control strategies described in Section 2.3.2. It was demonstrated that typical controller parameters of grid forming and grid following converters are not necessarily adequate for a particular distribution network usually need adaptation for the grid environment considered. Tools and techniques to do that will be discussed in Section 2.4.3.2.

Furthermore, a procedure for scenario creation through scaling of the DERs has been presented and applied to the benchmark grid. Simulation experiments on the detailed model of the CIGRE benchmark system under varying levels of DER penetration has demonstrated the effectiveness of the distributed freqeuncy support.

This detailed model with parameterization of DER penetration level and representative control schemes will be used in WP2 as basis for the derivation of simplified aggregated models of the distribution grid.

2.4 Local distribution grid interactions

2.4.1 Problem description

This work package focussed on the determination of appropriate tuning for the selected control schemes for use in the benchmark system to allow demonstration of the aggregation methods. This section outlines the fundamentals of and illustrates harmonic stability by simple examples in a tutorial that has previously appeared in shortened form in [23] and applies the proposed methodology to a case study on the CIGRE benchmark system.

2.4.2 Harmonic Stability

Harmonic stability is an emerging form of power system stability that can be seen as an extension of the classical small-signal stability as defined for example by [20]. Classical small-signal stability typically relates to electro-mechanical dynamics of synchronous machines and their control system and interaction through the grid and considers a frequency range up to a few Hz. On the other hand, harmonic stability relates to electromagnetic dynamics of the grid and their interaction with power electronic converter systems (PECs) and their associated control systems. Since PECs are typically driven by open-loop power electronic switching in a frequency range of several kHz, high-bandwidth control can be associated with their grid side converters, and harmonic stability analysis therefore requires extension of the small-disturbance stability concept to a much wider frequency range.

In short, harmonic instability relates to the destabilization of grid resonances through their interaction with converter control or a harmful interaction between different converter systems through their grid connection. In both cases, harmonic instability leads to extreme inter-harmonic distortions that can usually not be predicted by classical harmonic power flow studies. Such instabilities can cause failure of cables and filter capacitors if allowed to persist, as the resulting harmonic distortions often are far beyond the design requirements for the filter components.

The observation of unstable interactions between converter and grid systems is not new. Early observations and some early analysis results were presented in [1], however the topic has recently gained significantly in importance due to the proliferation of power electronics in the grids. Some examples where issues have been reported are railway power systems following the introduction of variable speed drives in trains [27] as well as offshore wind farms and large solar PV installations [25]. Rigorous analytical studies are available for other applications such as aircraft [26], marine power systems [28] and microgrids [8].

2.4.2.1 Modal Analysis

Modal analysis is a convenient tool to assess harmonic stability in converter based power systems. It is based on the observation that the behaviour of any linear system can be decomposed into a number of independent oscillatory and non-oscillatory modes. For harmonic stability analysis the oscillatory modes are of primary interest. Modal analysis has been used extensively for power system stability studies involving low-frequency oscillations and sub-synchronous torsional interactions. The mathematical framework used there is also applicable in the study of harmonic stability. For power systems of nontrivial size, modal analysis is most conveniently carried out using a state-space representation of the system dynamics as described for example by [20, 15], which also give a detailed description of the required mathematical framework that is only briefly reviewed here. The behaviour of a dynamic system, for example a power system, can be described in the ordinary differential equation form:

$$\dot{x} = f(x) \tag{3}$$

The vector x is referred to as the state vector that contains all information necessary to predict the future evolution of the system behaviour together with the function $f(x)$ given an initial state. This vector typically includes currents of inductive elements and voltages of capacitive elements, but also internal states associated with integrators in converter control systems and delay approximations.

Any point x^* where $f(x^*) = 0$ is referred to as an equilibrium point or rest state, where the system will remain unless it is perturbed. Small-signal stability analysis is used to predict whether a system will return to the same rest state given a small perturbation. Modal analysis is carried out around an equilibrium point yielding,

$$\frac{d\Delta x}{dt} = \frac{\partial f}{\partial x}(x^*)\Delta x = A\Delta x \tag{4}$$

Here, A is referred to as the Jacobian matrix, whose eigenvalues can be used to assess stability [19] as follows:

- The equilibrium point x^* is asymptotically stable if all eigenvalues of A have negative real part.
- The equilibrium point x^* is marginally stable if at least one eigenvalue has a zero real part and all other eigenvalues have negative real part.
- The equilibrium point x^* is unstable if one or more of the eigenvalues of A have a positive real part.

There are some important restrictions to these results however. Firstly, and similarly to the impedance based and passivity approaches, the conclusion regarding stability is only valid in a neighbourhood of the studied equilibrium point. For the study of harmonic stability in converter based power systems, the equilibrium point is determined by e.g. the loading level of the converters and repeated analysis for varying operating points is necessary. Secondly, it is assumed that the function $f(x)$ is differentiable, which requires averaging of the converter switching behaviour and sampling behaviour of the control system. Tools and techniques for averaging the converter and control system behaviour and calculating the Jacobian matrix in (4) are reviewed in [22].

Given any initial state $x(0)$, the free response of the system can be written as

$$x(t) = e^{At}x(0). \tag{5}$$

If A has distinct eigenvalues, the matrix exponential can be computed by via spectral decomposition as a series of independent terms, where each term is referred to as an (eigen-)mode of the system [29]:

$$e^{At} = \sum_{i=1}^{n} e^{\lambda_i t} r_i l_i, \tag{6}$$

where λ_i are the eigenvalues of A, and $R = [r_1, \ldots, r_n]$ and $L = [l_1, \ldots, l_n]^T$ are matrices composed of corresponding right and left eigenvectors. Furthermore, (6) can be expanded into the respective exponential part that models the attenuation or amplification of the mode, the oscillatory part that represents the resonance frequencies of the system and the participation part that can be used to identify what physical components in a system are contributing to a mode:

$$x(t) = \sum_{i=1}^{n} \underbrace{e^{\alpha_i t}}_{\text{exponential}} \underbrace{(\cos\omega_i t + j\sin\omega_i t)}_{\text{oscillatory}} \underbrace{r_i l_i^T}_{\text{participation}} x(0). \tag{7}$$

Based on inspection of (7) and the observation that each term i in the sum corresponds to an eigenmode of the system, it can be seen that:

- right half plane eigenvalues (α_i positive) correspond to unstable, exponentially growing modes,
- left half plane eigenvalues (α_i positive) correspond to stable, exponentially decaying modes,
- complex eigenvalue pairs (ω_i nonzero) correspond to oscillatory modes, and
- real eigenvalues (ω_i=0) correspond to non-oscillatory modes.

Based on the eigenvalues one can also define the modal characteristics: *attenuation* $-\alpha_i$ which is a measure of the speed of decay or growth of a mode, *frequency* ω_i which is the resonance frequency related to a mode. The *relative damping* is defined as

$$\zeta_i = \frac{-\alpha_i}{\sqrt{\alpha_i^2 + \omega_i^2}}. \tag{8}$$

In addition to these characteristics which classify the nature of the behaviour of the mode, one can also calculate *participation factors* as described in the original reference [34] as

$$R \odot L = [r_1 \dots r_n] \odot [l_1 \dots l_n] = \begin{bmatrix} r_{11}l_{11} & \cdots & r_{1n}l_{1n} \\ \vdots & \ddots & \vdots \\ r_{n1}l_{n1} & \cdots & r_{nn}l_{nn} \end{bmatrix} = \begin{bmatrix} p_{11} & \cdots & p_{1n} \\ \vdots & \ddots & \vdots \\ p_{n1} & \cdots & p_{nn} \end{bmatrix}.$$

Here, the elements r_{ij} shall be interpreted as the i-th element of the j-th right eigenvector. For the left eigenvector the opposite convention is used such that l_{ij} refers to the j-th element of the i-th left eigenvector. The resulting participation factor p_{ij} then corresponds to the relative participation of the i-th state in the j-th mode and can be used to trace which states in the model contribute to a certain mode.

2.4.2.2 Harmonic Stability Improvement

There are two different sources of the non-passive behaviour of converters and both play an important role in harmonic instabilities. In general, both types result in extreme harmonic distortion at interharmonic frequencies. Firstly, there is one related to the time delay in the converters which may cause high-frequency harmonic instabilities in a frequency range of the same order of magnitude as the converter switching frequency. The risk of this type of problems is larger in high voltage networks with a large share of overhead lines whose inductance in combination with their own capacitance or shunt capacitors can create poorly damped resonances in the kHz range. These resonances are typically beyond the bandwidth of the converter control loops meaning that it is very hard to solve such problems by extending or adapting the tuning of the converter control system. For this type of problems, a solution may be to avoid certain switching configurations where resonances in known converter active regions can be foreseen. One may also consider additional damping resistors in the converter filters or control hardware upgrades that increases the sampling frequency to ensure converter system passivity or push the non-passive region to a higher frequency band. Simply shifting the non-passive region to a higher frequency band can be an effective solution since transformers and overhead lines can be expected to provide larger resistive losses at high frequencies, meaning that a stronger non-passive behaviour of converter systems can be tolerated at higher frequencies. Another solution that may be considered is grid side passive filters. However, the design of these should be coordinated with converter control design to ensure that they do not introduce new resonances coinciding with active regions of converters. Also, passive filters may also add significant capacitance to the grid impedance, which in itself poses a stability challenge for current controlled converter systems. In other types of networks, such as microgrids, offshore wind or solar farms with long cable connections, grid resonances tend to appear in a much lower frequency range, in the order of a hundred or a few hundred Hz. In these grids, problems are more often related to the converter outer converter control loops, and are referred to as low-frequency harmonic instabilities. These resonances are typically well within the bandwidth of the converter control system and active damping strategies can be effectively used. This involves designing special control extensions to perform targeted or broad spectrum damping of resonances. Such methods are usually economically preferrable since they do not require any new physical hardware and are also very effective in suppressing harmonic amplification of steady-state harmonics, even when no stability problem is present.

2.4.2.3 Challenges for the Future

Harmonic stability is most likely to be an issue in systems where the rating of converter connected load and generation is large compared to the amount of directly connected resistive loads. This is already the case today for certain types of specialized grids. Several practical cases have been experienced, and

active research is being performed for other types of specialized grids. Perhaps the next challenges will arise from the proliferation of electric vehicles that will lead to massive deployment of charging infrastructure in the low and medium voltage grids. Such charging infrastructure will add significant amounts of converters from different vendors and will highlight grid integration and inter-operability requirements for stable operation. This may force grid operators to do more detailed harmonics and power quality studies. Converter system manufacturers may need to take further steps improve and tailor their control design for specific grid environments, and more seriously consider the inter-operability of their converters with other manufacturers' which will often be connected in parallel. Currently, grid codes do not consider explicitly harmonic stability although some proposals are under development for HVDC systems and offshore wind [33] and for rail power systems [2]. It is foreseen that future grid codes and study recommendations also for traditional distribution grids will need extension to incorporate harmonic stability and converter inter-operability as the degree of converter penetration increases both on the load and generation side.

Providing models that are good enough for harmonic stability studies while preserving the protection of intellectual property for converter manufacturers will be a major challenge. A promising approach is that manufacturers exchange impedance profiles as foreseen by [33, 2], but standardization of measurement and computation techniques for such impedance profiles are still open topics. In the long run, standardization of modulation techniques and control structures may be a solution.

Currently analysis techniques for harmonic stability is maturing field. So far most results has been based on impedance matching techniques, which however are difficult to apply in practical cases where topologies become complex. The adoption of the modal analysis approach is more recent but shows some advantages, particularly related to its ability to pinpoint root-causes of stability problem, universal applicability and scalability to grids with complex topologies and large number of converters.

Mode	Frequency (Hz)	Damping (%)	Dominant State:
1	1.33	1.4	CHPD9.gen.w
2	24.60	1.9	Bat10.control.voltageController.PI[1].x
3	24.74	3.2	Bat5.control.voltageController.PI[1].x
4	27.77	18.5	WT7.control.voltageController.PI[1].x

Table 6: Oscillatory modes with damping less than 25 % in the RMS model.

Mode	Frequency (Hz)	Damping (%)	Dominant State:
1	24.67	-2.5	Bat10.control.voltageController.PI[1].x
2	24.69	-1.3	Bat5.control.voltageController.PI[1].x
3	1.33	1.3	CHPD9.gen.w
4	25.72	12.2	WT7.control.voltageController.PI[1].x

Table 7: Oscillatory modes with damping less than 25 % in the EMT model.

2.4.3 CIGRE MV Benchmark System Case Study

As shown in Section 2.3.5 default tuning parameters taken form the original reference [5] for the DERs are not appropriate for stable operation in the CIGRE benchmark system. In this section the stability analysis techniques discussed in the previous sections are used to define a set of adequate tuning parameter to allow scenario derivation.

2.4.3.1 Modal analysis

Since the simulation model has been formulated in the dq-frame, modal analysis can be used to investigate the source of the poor performance of the diesel generator control and the control instability of the DERs. In this report, the toolbox ConverterStab [22] is used for this purpose.

RMS Model Modal analysis of the RMS model at time 0 s reveals 4 oscillatory modes with damping less than 25 % that are listed in Table 6. The modal analysis can explain and confirm the results of the time domain simulation as explained in the following paragraphs.

The poorly damped mode at 1.34 Hz which is dominated by the speed state of CHP9 is responsible for the nearly undamped speed variation in the rotor speed of CHD9. This is confirmed by the participation factors shown in Figure 20 which also indicate a weak participation of the governor control system of CHPD9. There is no significant participation of the various converter control systems. Thus, it can be concluded that this mode is not a result of interaction between the diesel generator and the converter based DER control systems.

The poorly damped oscillation at 24 Hz that is visible predominantly in the generated active and reactive power of WT7 is linked to the voltage control loop of Bat10. Figure 20 clearly shows that this mode is linked predominantly to the voltage control loop of Bat 10, which also interacts with the voltage control loops of Bat5 and WT7 which have significantly lower participation. The voltage control mode of Bat5 is likewise poorly damped at 3.2 % and interacts with primarily WT7 in the same fashion. Also the WT7 dominates one of the voltage control models at a slightly higher frequency of 27.77 Hz and good damping of 18 %.

EMT Model Table 7 lists the modes with damping less than 25% in the EMT model. The modes appear with the same dominant states as for the RMS model, however the three modes related to the voltage control of the VSMs have significantly worse damping with two of the modes being unstable. This instability is clearly visible in the time domain results. Also the voltage control mode of WT7 appears with lower damping than in the RMS model, but is still moderately well damped at 12 %.

A notable qualitative difference between the modal analysis results with the EMT model compared to

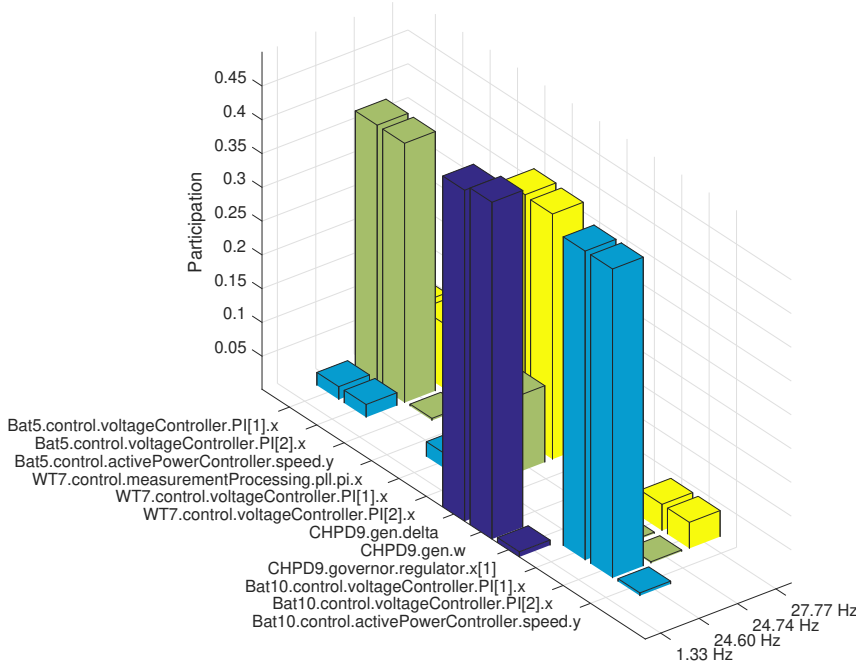

Figure 20: Modal participation in the RMS model.

to the RMS model is that the DER controls exhibit also an interaction with the inductive and capacitive elements of the grid. This in particularly true for the 25.72 Hz mode related to the voltage control of Bat10. This can also explain why the damping is lower in the EMT model.

2.4.3.2 Dynamic Performance Improvement

As discussed in he previous sections, the default parameter settings of the diesel generator are not appropriate for grid connected operation and the converter controls. Furthermore, particularly the VSM controls are not appropriate for the operation in islanded mode. Therefore improvements are necessary before the model can be used for validation of the decomposition approach for simulation.

Modal analysis offers a systematic way of improving tuning to achive stability and adequate damping also for islanding case. Since the RMS model fails to accurately represent the stability properties of the converter controls, the tuning improvement is based on the EMT model.

Subsynchronous Modes Firstly, stabilization of the voltage control modes around 25 Hz will be considered. To find out what parameters to modify, modal sensitivity analysis with respect to the VSM controller parameters is carried out. Normally, customized tuning could be applied to individual units, however for simplicity we here consider changes global such that they apply to all units. The VSM controllers each have 13 parameters that can be considered as tuning parameters.

Consider an in relative terms small change of a parameter j, $\Delta p_j = p_j^{new} - p^{nom}$, compared to its nominal value which results in a change of the modal damping $\Delta\zeta = \zeta_i^{new} - \zeta_i^{nom}$ and frequency and $\Delta f_i = f_i^{new} - f_i^{nom}$. The modal sensitivities are then defined as

$$\frac{\partial \zeta_i}{\partial p_j} \approx \frac{\Delta \zeta}{\Delta p_j} \tag{9}$$

and

$$\frac{\partial f_i}{\partial p_j} \approx \frac{\Delta f}{\Delta p_j} \tag{10}$$

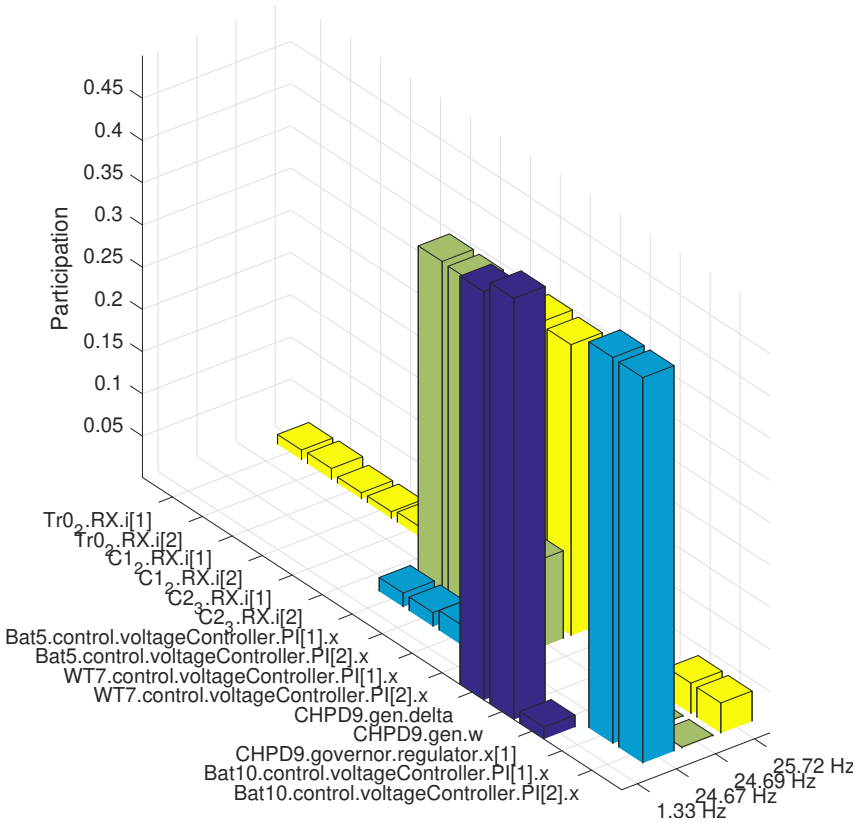

Figure 21: Modal participation in the EMT model.

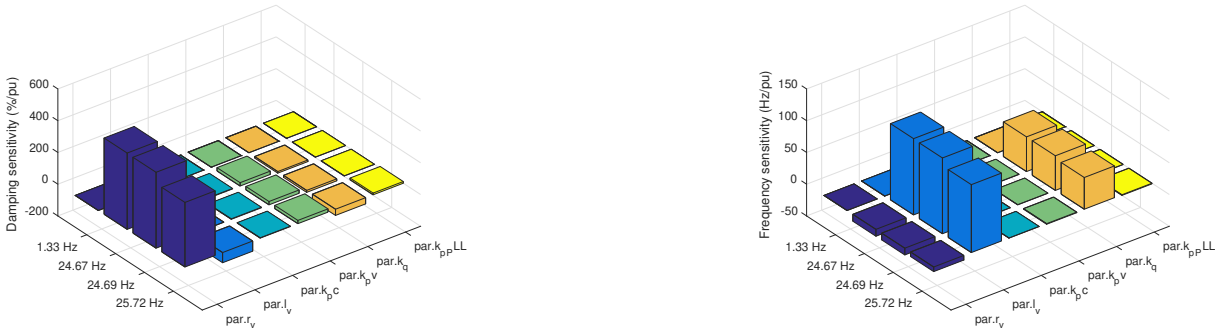

Figure 22: Modal sensitivity with respect to VSM control parameters of Bat10.

Mode	Frequency (Hz)	Damping (%)	Dominant State:
1	1.33	1.3	CHPD9.gen.w
2	24.23	16.6	Bat10.control.voltageController.PI[1].x
3	24.27	17.6	Bat5.control.voltageController.PI[1].x

Table 8: Oscillatory modes with damping less than 25 % in the EMT model the virtual resistance parameter of all VSM controlled DERs increased to 0.04 pu.

Modal sensitivites can be used to investigate how strongly a change of a parameter change influences the modal damping. Note however that the absolute value of the sensitivities are not straightforward to compare since different parameter may have completely different allowable ranges. However, the sensitivities still can be used to identify which parameters are connected to the damping of different modes.

As shown in Figure 22, the damping sensitivity of all three modes around 25 Hz are the the strongest in the parameter r_v which is the virtual resistance emulated by the VSM controller. Also this parameter has a relatively weak influence on the frequency. Other parameters that can influence the model are the voltage controller gain k_{pv} and the reactive power controller gain k_q. All these parameters could be considered to improve the damping of the unstable modes. A rule of thumb is to consider the parameters that do not strongly influence the frequency of the modes. The rationale behind this is that control energy should be spent on providing damping, not to force a change in the natural resonance frequencies in the system.

Therefore we choose the parameter k_{pv} as a first candidate for damping improvement. The sensitivity coefficient of the critical 24.67 Hz Mode evaluates to around 450 % per per unit. With a target damping of 15 % and the current damping of -2.5%, the required increment in the parameter r_v can be estimated to around

$$\frac{15\% - (-2.5\%)}{450\%} \approx 0.04 \text{ pu} \tag{11}$$

The resulting modal analysis results are shown in Table 8. The damping of the critical model has increased to about 16 %, close to the value predicted by the modal sensitivity analysis. The damping of the poorly damped mechanical mode remains low at 1.3% as expected.

Low frequency oscillation Once the subsynchronous control modes have been stabilized an improvement to the diesel generator CHPD9 control will be considered. As discussed, this mode is dominated by the CHPD9 itself with little to no interaction with other DERs. Therefore the best approach is to consider modifying its own controls rather than implementing a damper using the other DER controls. Low damping of low frequency mechanical modes of small generators remotely connected to stiff system over weak links is a well known problem in power systems. The classical approach to this problem is to implement additional damping via power system stabilizers acting on the excitation voltage which the output of the excitation system [15]. This was attempted as a first resort, but very little damping

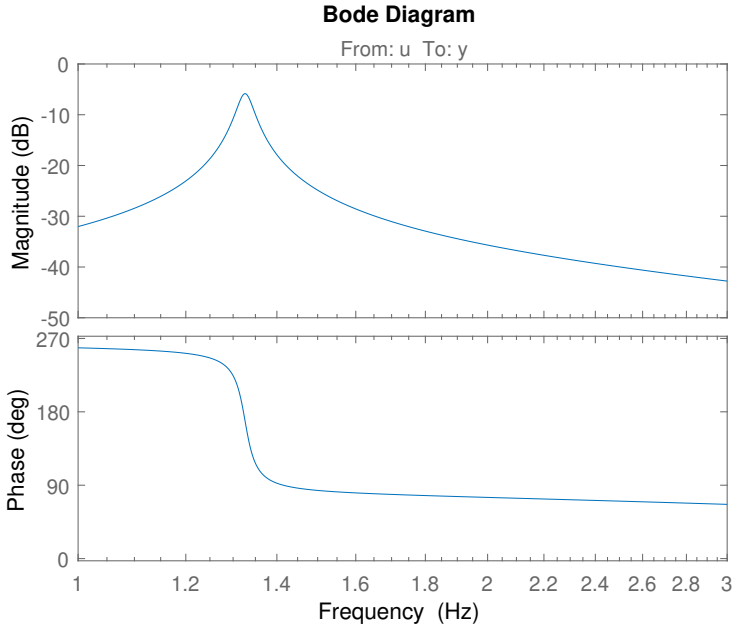

Figure 23: Bode plot for transfer between engine input and resulting generator speed for CHPD9.

Mode	Frequency (Hz)	Damping (%)	Dominant State:
1	1.32	15.3	CHPD9.gen.w
2	24.23	16.6	Bat10.control.voltageController.PI[1].x
3	24.27	17.6	Bat5.control.voltageController.PI[1].x

Table 9: Oscillatory modes with damping less than 25 % in the EMT model with the damping compensator in CHPD9 enabled.

improvement could be achieved with this method and therefore that solution was abandoned.

Since the mode is clearly visible in the governor control system, another possibility would be to retune the governor control system. This has three parameters: regulator time constant (T) regulator gain (K) and engine delay (T_d). However modal sensitivity analysis reveals a very low sensitivity to all three parameter such that a tenfold decrease of the regulator gain would be necessary to achieve an additional damping of one percent. Therefore also this candidate solution was abandoned.

The best solution appears to be adding an additional damper in parallel to the regulator block in Figure 10. Figure 23 shows the transfer function between an incremental perturbation on the input to the engine delay block and the generator speed. A clear resonance peak can be seen around the modal frequency of 1.3 Hz. Based on the linearized model, a modal residue $r = -0.1052 + 0.0202i$ and modal eigenvalue $\lambda = -0.1110 + 8.3840i$ can be determined. Application of the modal residue based damper design method described in [22] yields the compensator

$$G_{damper}(s) = 9.7121 \frac{0.23855s}{0.23855s + 1} \left(\frac{0.14208s + 1}{0.097481s + 1} \right) \frac{1}{0.059638s + 1} \tag{12}$$

Table 9 shows revised modal analysis results for the retuned EMT model with the damping compensator enabled. As shown, the low frequency mode is well damped at its target value of 15 %. The dampings of the other modes remain more or less unchanged, thus the compensator can effectively damp the desired mode without any detrimental effects on the other modes.

2.4.3.3 Reference Scenario with retuned model

Following the optimization of the control parameters and addition of the damping loop in the CHP9

diesel generator, the islanding scenario was simulated again, resulting in the reference benchmark results shown in Figure 24 for the RMS model and Figure 25 for the EMT model. The results are now qualitatively the same with the only difference being a slighly better damping in the RMS model. The DER controllers perform well and the low-frequency mode related to the diesel generator is adequately damped both in islanded and grid connected mode.

Although the RMS model was not adequate to properly tune the converter control system, with well-tuned primary control systems the responses with the RMS and EMT models are near identical. Therefore the RMS model can be considered adequate for validation of supervisory microgrid control schemes.

2.4.4 Key results and connection to other tasks

This section has presented a tutorial on harmonic stability and converter control system tuning based on modal analysis. Modal analysis was then applied to adapt the tuning of the DERs to the CIGRE grid yielding a robust set of parameters with which the DERs can operate reliably, both in grid connected and islanded mode. This parameter set has been used in the simulation in Section 2.3.6 as well as the linear aggregation studies documented in [14].

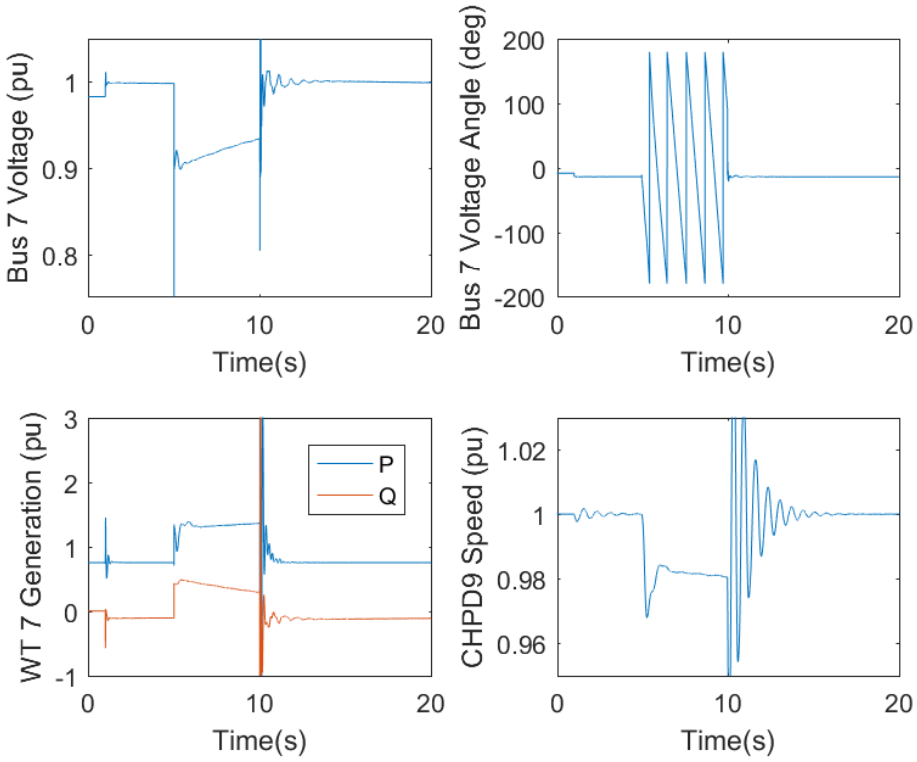

Figure 24: Islanding scenario with RMS simulation.

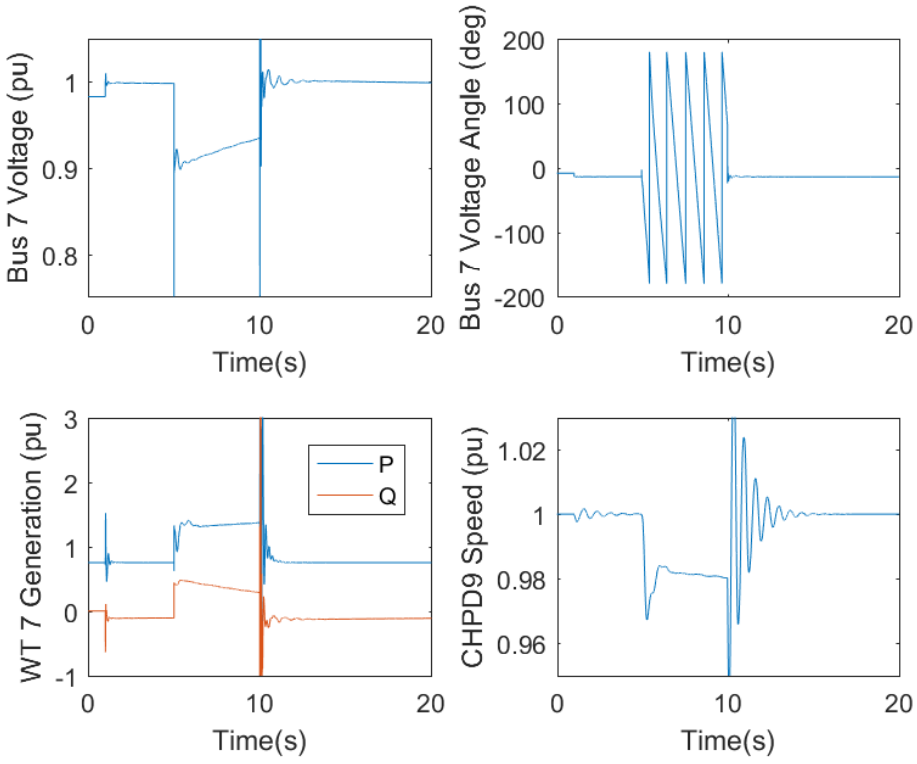

Figure 25: Islanding scenario with EMT simulation.

3 Dynamic distribution grid aggregation (WP2)

3.1 Introduction

3.1.1 Objective

Based on the converter system and CIGRE benchmark modelling developed in workpackage 1, an aggregation procedure that yields low order equivalent models has been developed. This required the development of a software framework to generate high-order linearized models of the distribution grid and a model reduction technique used to subsequently reduce the equivalent to a low order. The response of the original detailed EMT model is compared to that of the low order linearized equivalents to be used for the large-scale scenario study in workpackage 3.

3.1.2 Approach

For a specific penetration level p as defined in Section 2.3, a power network such as the distribution grid model in Figure 5 can be represented on the non-linear state space form according to

$$\dot{x} = f(x, u, p) \quad (13)$$

$$y = g(x, u, p) \quad (14)$$

Here, x is the state vector composed of the state variables x_i . Similarly, u is the input vector and y a vector of output or measurement signals to be monitored.

The formulation results in a high order model far too complex for implementation in large scale studies. This model captures the dynamics of each individual component in the grid, including each internal control loop of the DERs. However, from the point of view of the transmission system operator only the active and reactive power flows at the point of common coupling between transmission grid, and their response to disturbances in the transmission grid is of interest. This introduces the opportunity of model aggregation, that is, to represent the complex structure below the PCC between transmission and distribution with simplified and more computationally efficient representations.

The workpackage investigates how the dynamic behavior of distribution grids with many converter-based power sources is seen from the side of the transmission grid. These impacts on the global network can not be modeled by a simple collection of all individual converter models - both for reasons of computational complexity and analytical insight of the key dynamic interactions. The tasks review both linear and nonlinear aggregation procedures and conclude with a software implementation for the creation of aggregated distribution grid models:

1. **Linear model aggregation**:
   A linearization of the distribution grid model is performed, followed by a model reduction of the linear system. This approach makes use of standardized elaborate model reduction tools (e.g. balanced truncation). The individual linear states don't have a direct physical interpretation any more. For the implementation, the reduced model requires an estimate of the local transmission grid variables.
2. **Nonlinear model aggregation**:
   A simulation of the nonlinear distribution grid model is performed, followed by a comparison to a simplified model with reduction number of components. This approach maintains the nonlinear characteristics of the components and the physical interpretation of the dynamic states, but requires manual decisions to select the number of components in the reduced model. For the implementation, the reduced model can be directly interfaced with the transmission grid model.

The main outcome are two reduction approaches, that can be interfaced with a detailed transmission grid simulation.

3.2 Linear model aggregation

This section describes linear approaches to the aggregation of distribution grid with embedded DER.

3.2.1 Active/Reactive Power Based Model Aggregation

As frequency and voltage in power systems during normal operation typically exhibits small variations, linearized representations of the full nonlinear grid model can be expected to give results of sufficient accuracy. To study long-term evolution of transmission system grid frequency and voltage, frequency variations of say up to +/- 5 Hz and voltage variation of up to +/-10% are sufficient. Therefore the approach was chosen where the non-linear state space form (13)–(14) is linearized around an operating point (x^*, u^*, y^*) and formulated using perturbation variables as

$$\Delta\dot{x} = A(p)\Delta x + B(p)\Delta u \quad (15)$$

$$\Delta y = C(p)\Delta x + D(p)\Delta u \quad (16)$$

Here, $x = x^* + \Delta x$, $y = y^* + \Delta y$ and $u = u^* + \Delta u$.

The inputs and outputs of the models can be chosen freely, however for later compatibility and integration with RMS simulations, the quantities of primary interest is the active and reactive power demand of the entire grid as seen from the interconnection point with the transmission grid, and how this depends on changes in the grid frequency and voltage at the connection point. Therefore, the model takes perturbation variables in terms of the voltage magnitude at the connection point of the distribution grid to the transmission grid ΔV and the system average frequency $\Delta\omega$ as inputs and provides resulting perturbations of active ΔP and reactive power ΔQ as output. Here, the linearized models are linearized at nominal voltage and frequency, however a more accurate representation could be obtained if the model is linearized at the operating point where it actually is going to be used.

Based on the detailed EMT model developed in WP1, a wrapper model shown in Figure 26 was developed that encapsulates the full ADN with varying penetration level. This model can be used to generate linear models on the form (15)-(16) for selected inputs and outputs. This model reproduces the response of the ADN to disturbances introduced in the form of voltage or frequency variations on the transmission grid in detail, and could in principle be plugged directly into system simulations. However, the model is of high order and still too complex to be used in large-scale transmission grid simulations. This highlights the need for model reduction.

3.2.2 Linear Model Reduction

As discussed in the previous section, the models given by (15)–(16) and are high order models retaining the accuracy over a large frequency range due the EMT modelling as well as the internal dynamics of each converter control system. There are three main factors that allow significant reduction of the dimensionality of the models:

- For RMS simulation, only a frequency range of say up to 10 Hz is of interest since other components such as transmission lines and generators are modelled using a simplified representation.
- As long as the converter control are well tuned and remain stable, they tend to respond in a coherent manner to changes of voltage and frequency at the point of common coupling to the transmission grid.
- During operation, frequency and voltage is kept under quite tight control with frequency variations of maximum a few Hz and voltage around $\pm 10\%$.

Under such conditions also a linearized representation on the form (15)–(16) can be expected to provide adequate accuracy. Note however, that the linear model neglect saturation limits in the control, and thus

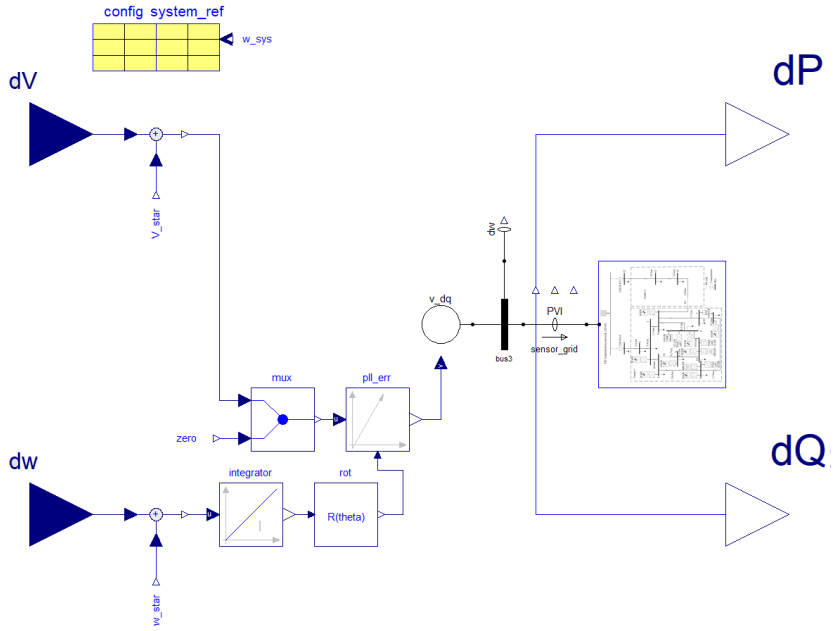

Figure 26: Wrapper model used for generation of aggregate distribution grid models.

for this application assumes that sufficient headroom in terms of active and reactive power is present in the DERs to provide voltage and frequency support.

To reduce the model order, balanced truncation [18] is applied to the full order linearized order using the following parameters

- Target frequency range: 0-20 Hz
- Model order: 4

This reduces the detailed linear model from an original order of 638 to an adequately low order of 4 for deployment in large-scale system studies.

Figure 27 shows a comparison of nonlinear, linearized and reduced linearized model responses for a penetration level of 5 % to simulated grid disturbances in the form of a 2% voltage decrease at time 1 s and a 1 % frequency decrease at 2 s. Following the voltage decrease, both the reactive and active consumption in the ADN reduces primarily due to the impedance characteristic of the load in the nonlinear model. For a small disturbance, this is reproduced near perfectly with also the full order and reduced order linear models. Following the frequency decrease, the characteristic second order response due to the inertia emulation of the grid forming converter can be seen in the active load demand. The reproduction of the behaviour is excellent with both the full order and reduced linear models.

Figure 28 shows the response to the same disturbances with a penetration level of 40 %. Reproduction of the active and reactive load is excellent with both the reduced and full order models. Following the frequency reduction, a more damped second order response can be observed however a slight offset in the frequency response can be seen in particularly the reactive power response. However, the accuracy is still adequate. The model reduction does not introduce additional error.

Figure 29 shows the response to the same disturbances with a penetration level of 100%. Reproduction of the active and reactive load is excellent with both the reduced and full order models. Here we can see that we are reaching the borderline of the validity of the linear model, as there is a noticable difference between the nonlinear and linear models. In steady state, the error is about 15 %. Also with penetration level model reduction does not introduce additional noticable error. The effect of this inaccuracy of the linear models will be studied in a more realistic grid environment in Section 3.4.4.

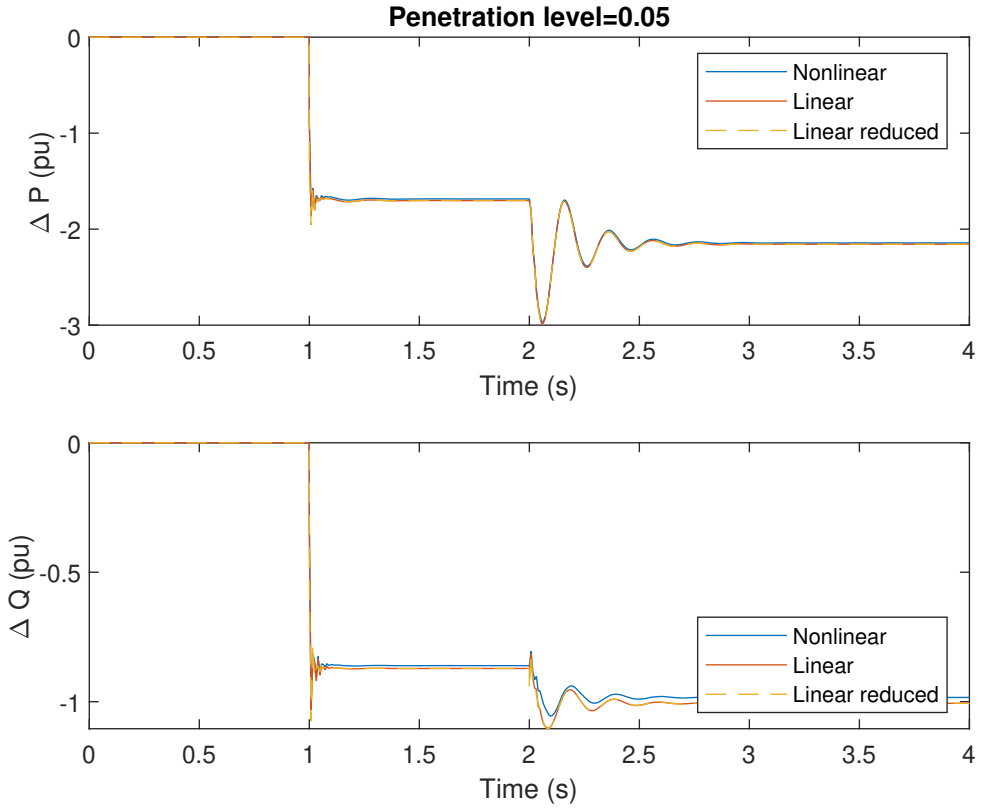

Figure 27: Model response to a 1% voltage decrease at time 1 s and a 1 % frequency decrease at 2 s. Comparison of nonlinear, linearized and reduced linearized model responses for a penetration level of 5 %.

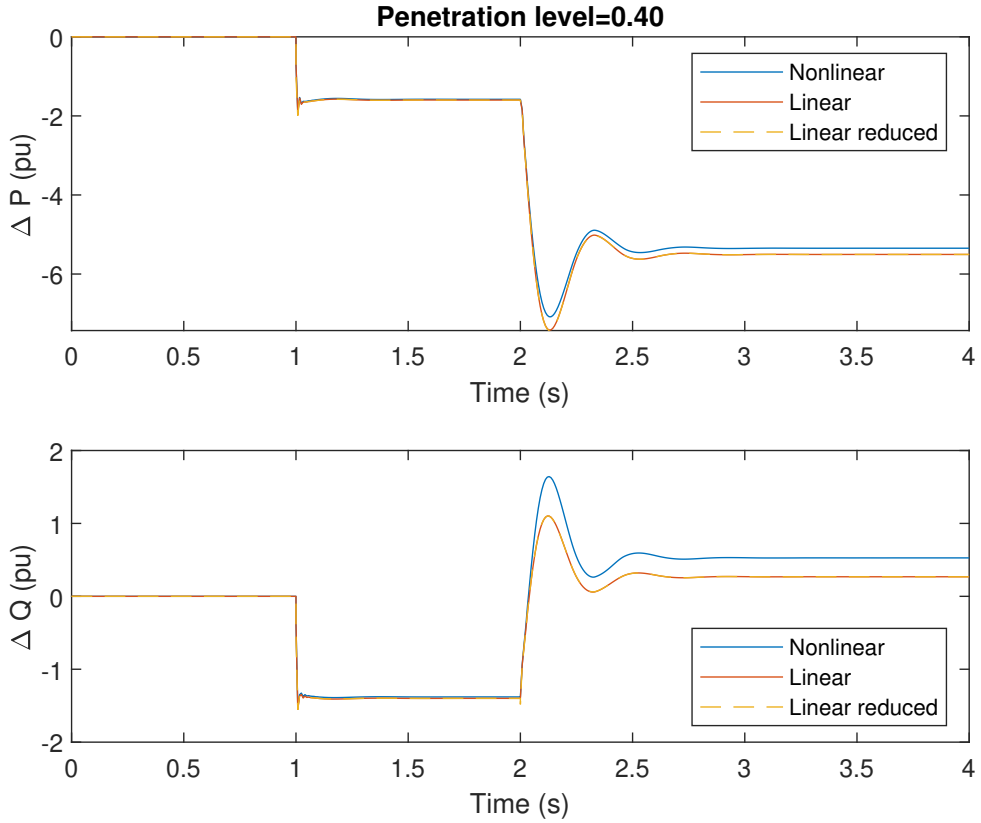

Figure 28: Model response to a 1% voltage decrease at time 1 s and a 1 % frequency decrease at 2 s. Comparison of nonlinear, linearized and reduced linearized model responses for a penetration level of 40 %.

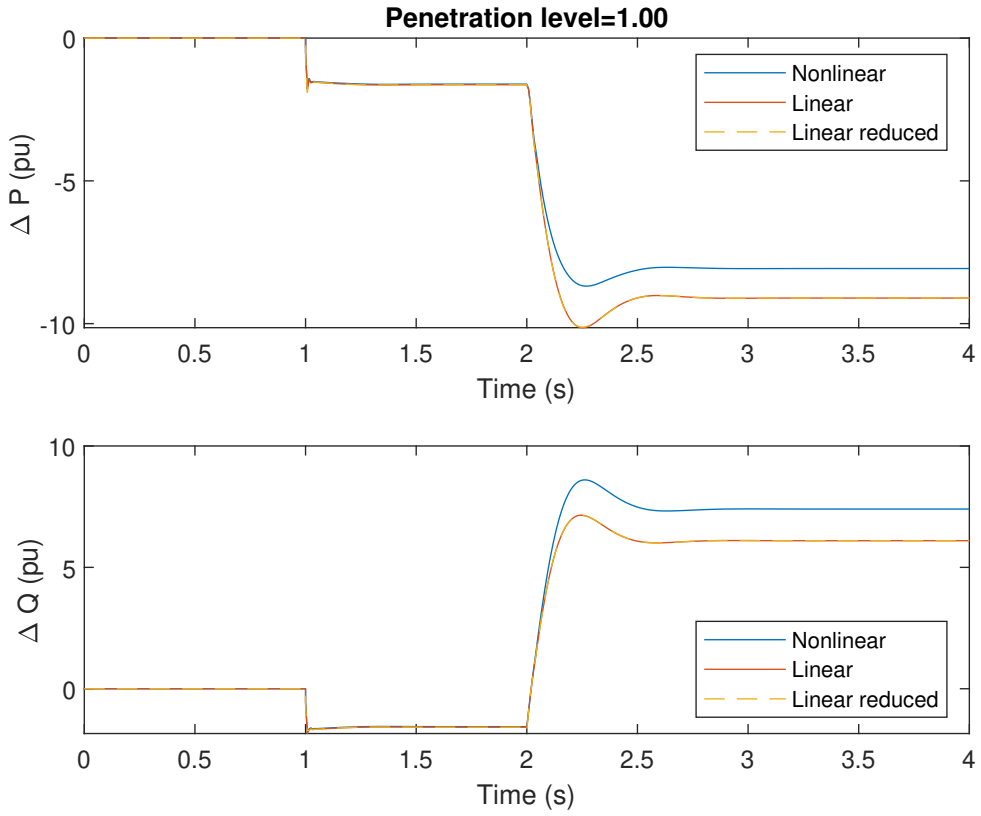

Figure 29: Model response to a 2% voltage decrease at time 1 s and a 1 % frequency decrease at 1 s. Comparison of nonlinear, linearized and reduced linearized model responses for a penetration level of 100 %.

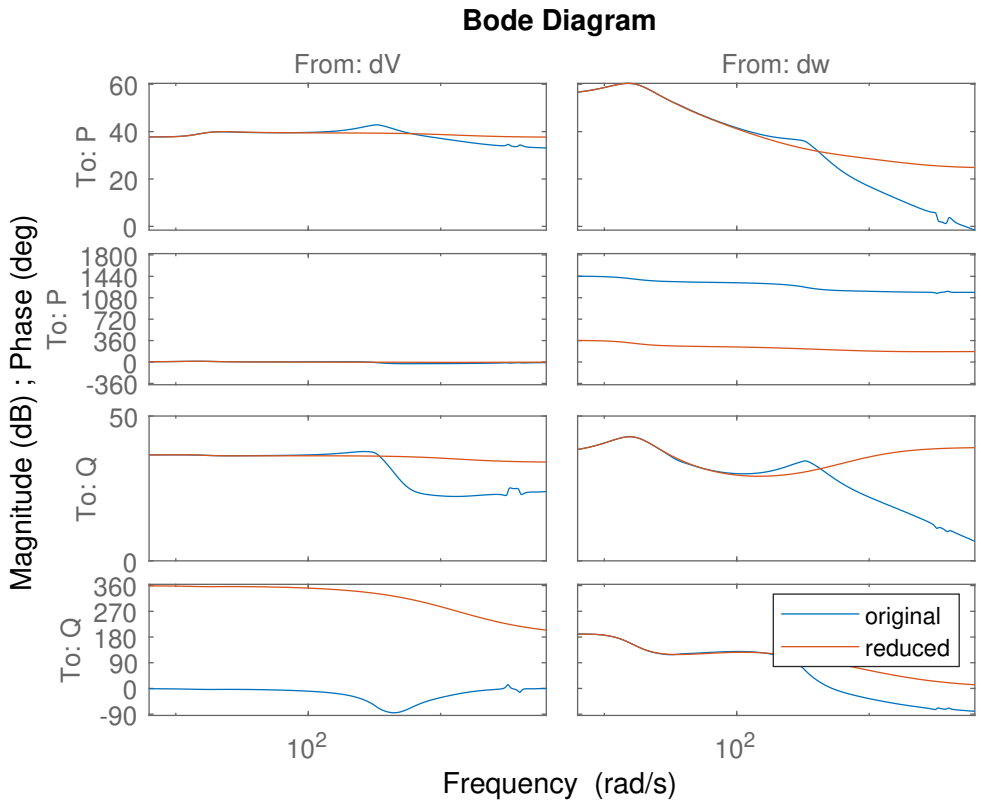

Figure 30: Bode plots of original and reduced models for a scenario with penetration level 40%.

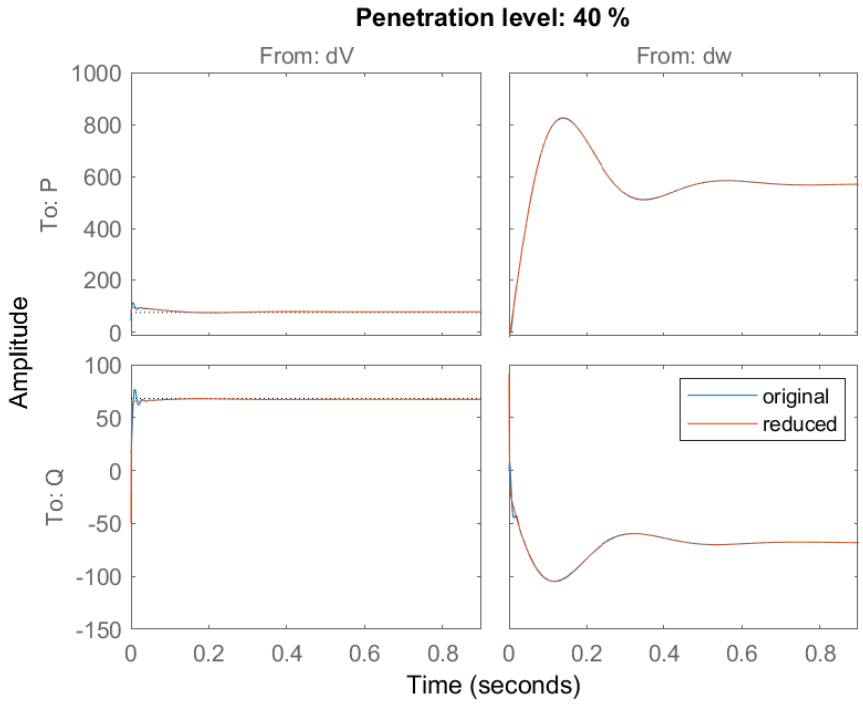

Figure 31: Step responses of original and reduced models for a scenario with penetration level 40%.

3.2.3 Key results and connection to other tasks

This section has described a developed linear aggregation procedure that can be used to generate low order equivalents of ADNs to be used as load models in large-scale RMS simulations. The models are of low order, typically 4, and can accurately reproduce the small-signal behaviour of the ADN in terms of its active and reactive power response to voltage and frequency disturbances in the transmission grid. The procedure has been tested on the CIGRE benchmark ADN under penetration levels ranging from 5-100 %. The main limitation of the model, is that it is linearized and thus ignores capacity constraints of DERs unless they were already activated at the operating point of linearization. Thus, the model makes the implicit assumption that sufficient headroom is available in each DER.

3.3 Nonlinear model aggregation

3.3.1 Problem description

While WP1 introduced the main power sytem components and the Cigre benchmark mark grid, WP2 has on the goal, to obtain a model that can be scaled up and down to represent typical distribution grids in a dynamic transmission grid simulation. To this end, the work of ETHZ-FEN in WP2 focuses on a nonlinear model with the same input-output relations as the linear model developed by HAPG.

The model provides the active and reactive power demand of the the distribution grid given a change of the d- and q-voltage components. To align the presentation with the linear model, the inputs triggering a transient are the voltage magnitude and the local grid frequency, also corresponding to the typical dynamic challenges in the transmission grid. We first show the scenario used to develop the distribution grid model characteristics, followed by the simulation results and a discussion of the aggregation.

3.3.2 Scenario for CIGRE grid simulation

Figure 32 and Figure 33 show the simple transmission grid model to identify the distribution grid characteristics and compare different aggregated models. The voltage disturbance is triggered by an infinite bus, imposing the voltage level near the distribution grid. The frequency disturbance is triggered by a load step next to a generator, both of which are much larger than the nearby distribution grid. The goal is not to identify the stability limit of the transmission grid (and the potential for support by the distribution grid), but to investigate the dynamic distribution grid characteristics when a transient is imposed from the transmission grid side.

All converters in the distribution grid inject only active power at 50% of the rated converter power. For the simulations, the rated power of grid supporting converters (the VSM control scheme developed and validated in 2019) is scaled relative to the active power loads in the distribution grid. This ratio corresponds to the penetration level of grid supporting converter, also used for the linear modeling. It ranges from 8.8% (the base case of the CIGRE MV grid) to 272.3%, the latter value corresponding to a 10MW net export from the distribution grid. The share of grid following converters is small and remains unchanged.

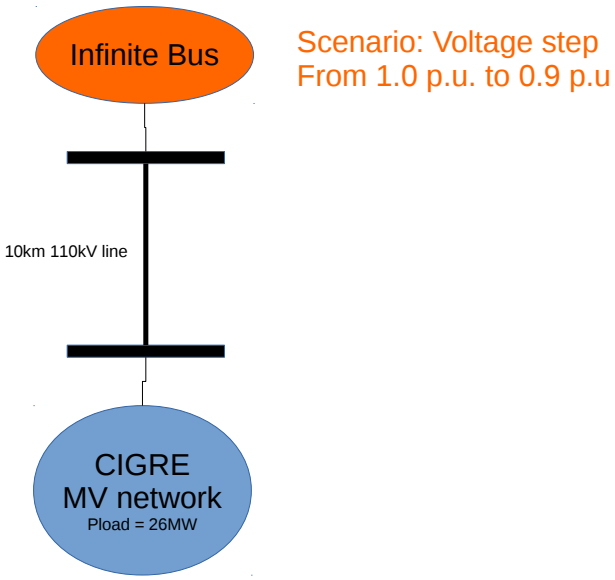

Figure 32: Simple transmission grid model to identify the distribution grid characteristics and compare different aggregated models (voltage disturbance).

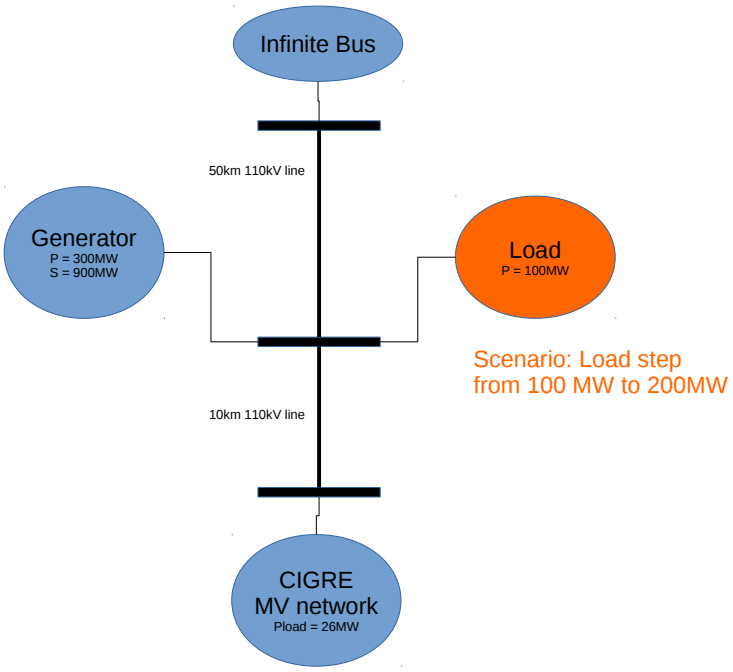

Figure 33: Simple transmission grid model to identify the distribution grid characteristics and compare different aggregated models (frequency disturbance).

3.3.3 Nonlinear simulation results and discussion

This section discusses the results of the dynamic simulation of the CIGRE MV grid in the reference disturbance scenarios. Figure 34 shows the response of the power demand of the active distribution grid after a negative voltage step near the distribution grid. Note that the figures do not show the absolute powers, but the change in power after the disturbance. As expected, it can be seen that both active and reactive power drop after the voltage drop. However, the change for different shares of grid supporting converters is opposite: The reactive power drop is larger for the higher shares of grid support to support the local grid voltage level, also shown in the top plot of Figure 35. As a result, the active power drop becomes smaller for higher shares of grid support. The lower plot of Figure 35 shows the PLL-frequency of a grid supporting converter in the distribution grid (used for damping control). It can be seen that with higher shares of grid support, smaller deviations of the PLL angle are required.

Similar results are obtained for the frequency transients. As shown in Figure 36, both active and reactive power demand of the distribution grid undergo a transient before settling at a reduced value. Again, the drop of reactive power is smaller for higher shares of grid support to support the voltage level, as shown in the top plot of Figure 37. The lower plot of Figure 37 shows the PLL-frequency of a grid supporting converter in the distribution grid. Again, it can be seen that with higher shares of grid support, smaller deviations of the PLL angle are required. Finally, Figure 38 shows the frequency transient of the generator. After a drop of about 80mHz, it reverts back to the nominal frequency due to the infinite bus in the system. The zoom in the bottom plot of Figure 38 shows that with more grid support, the frequency drop becomes smaller. The difference is small due to the relative size of the distribution grid, but noticeable.

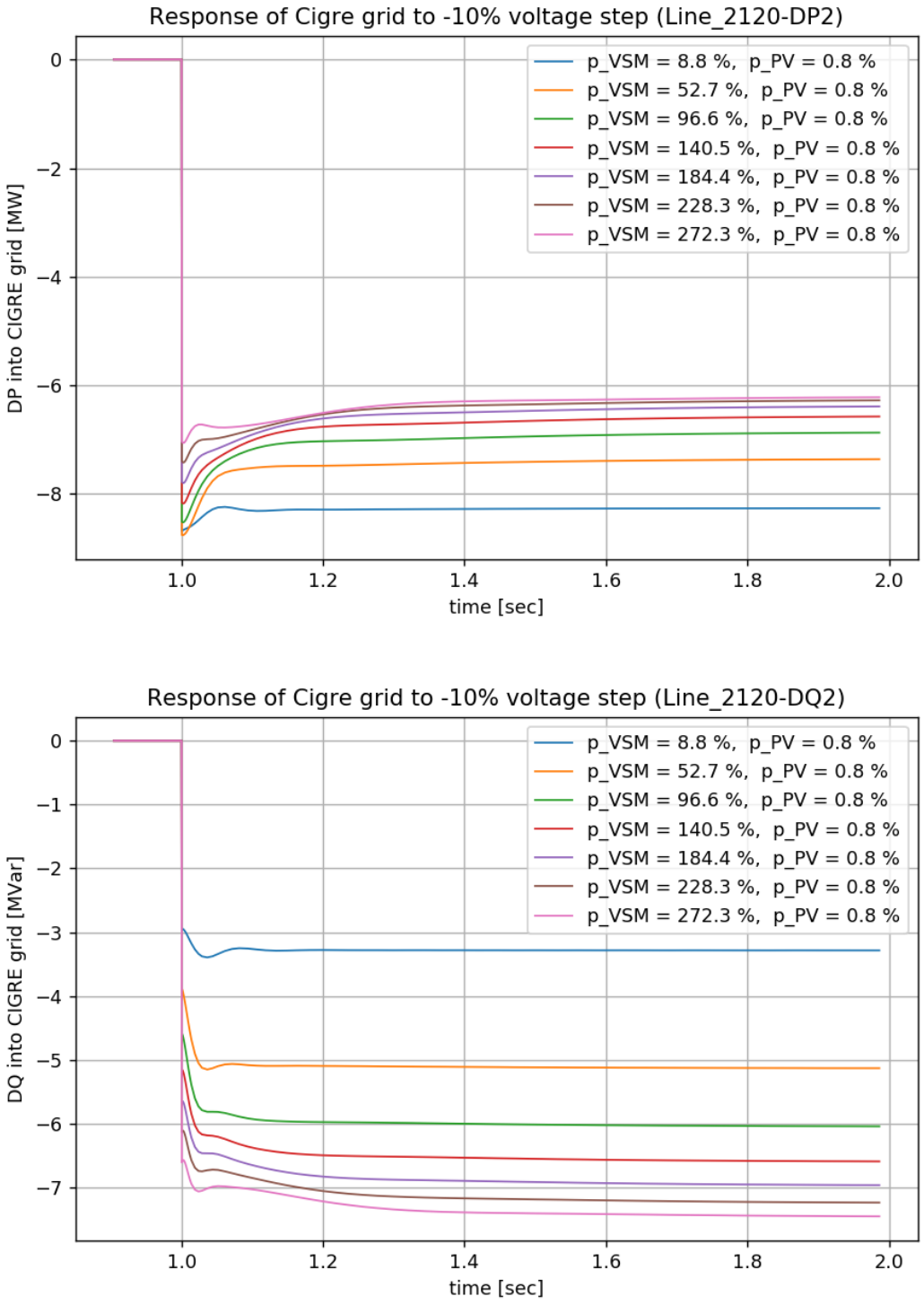

Figure 34: Cigre MW grid, response to a voltage step: change in active power (top) and reactive power(bottom) injected into the distribution grid.

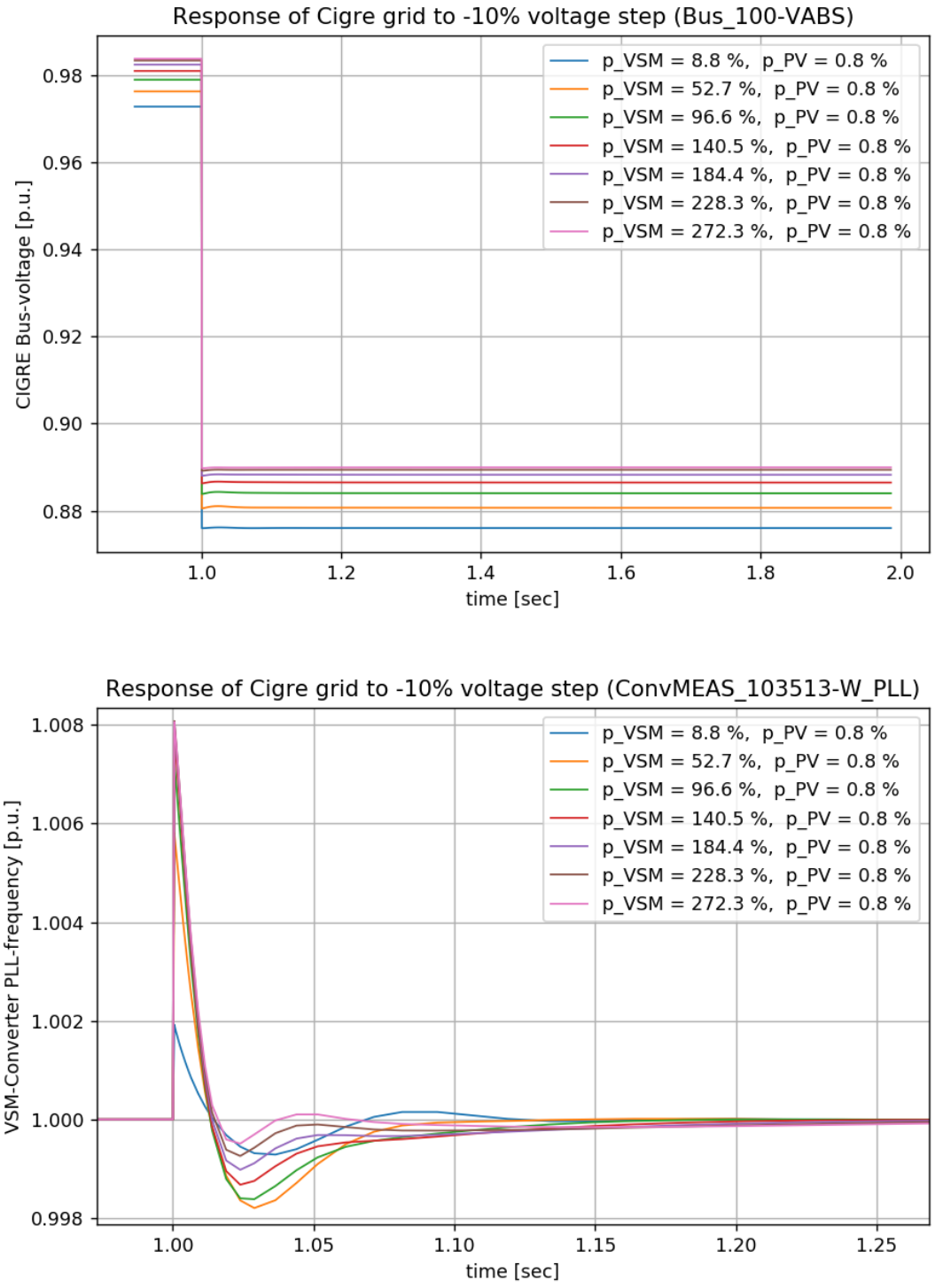

Figure 35: Cigre MW grid, response to a voltage step: change of local bus voltage level (top) and the PLL frequency of selected VSM converter in the distribution grid (bottom).

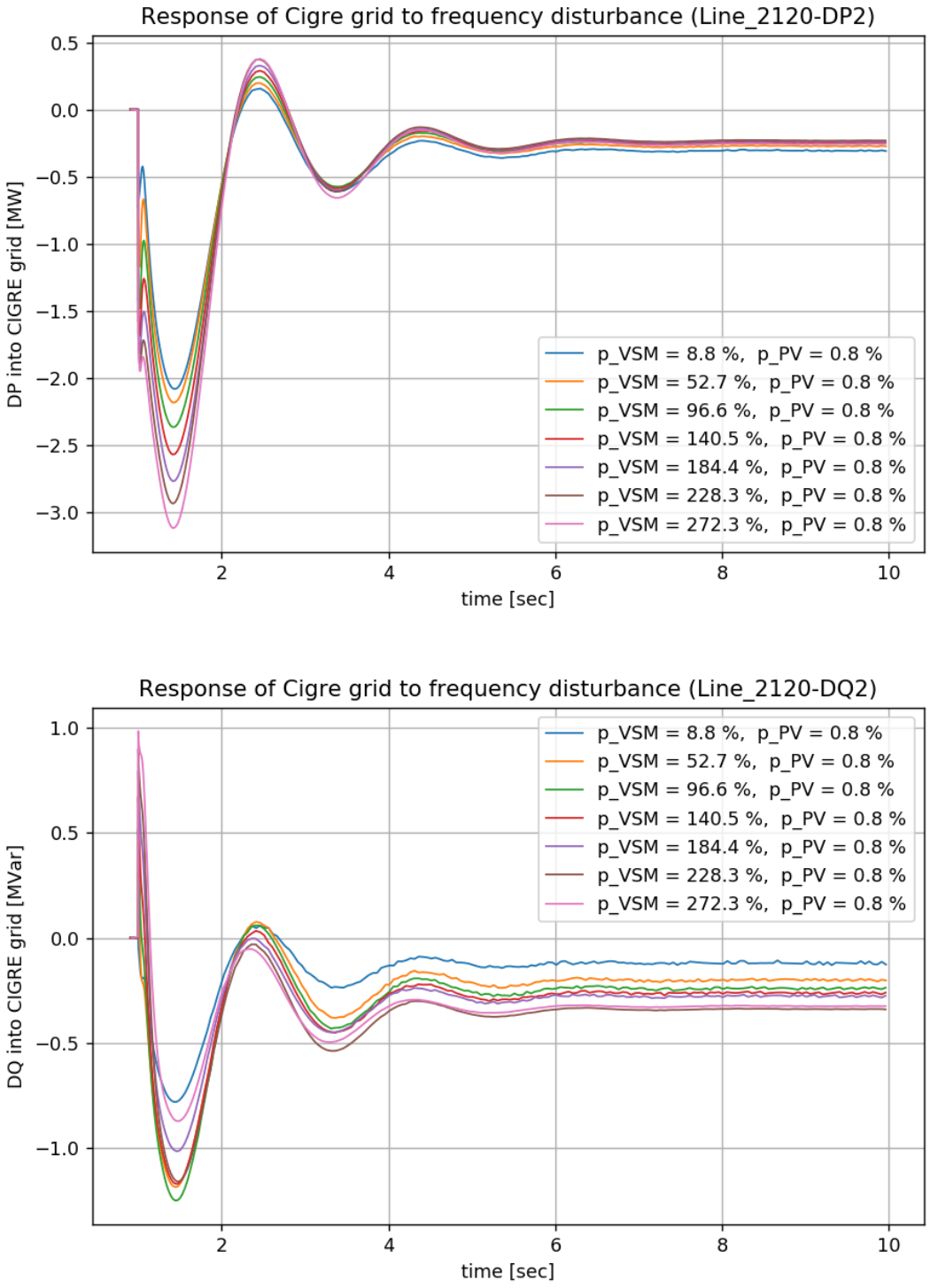

Figure 36: Cigre MW grid, response to a frequency transient of nearby generator: change in active power (top) and reactive power (bottom) injected into the distribution grid

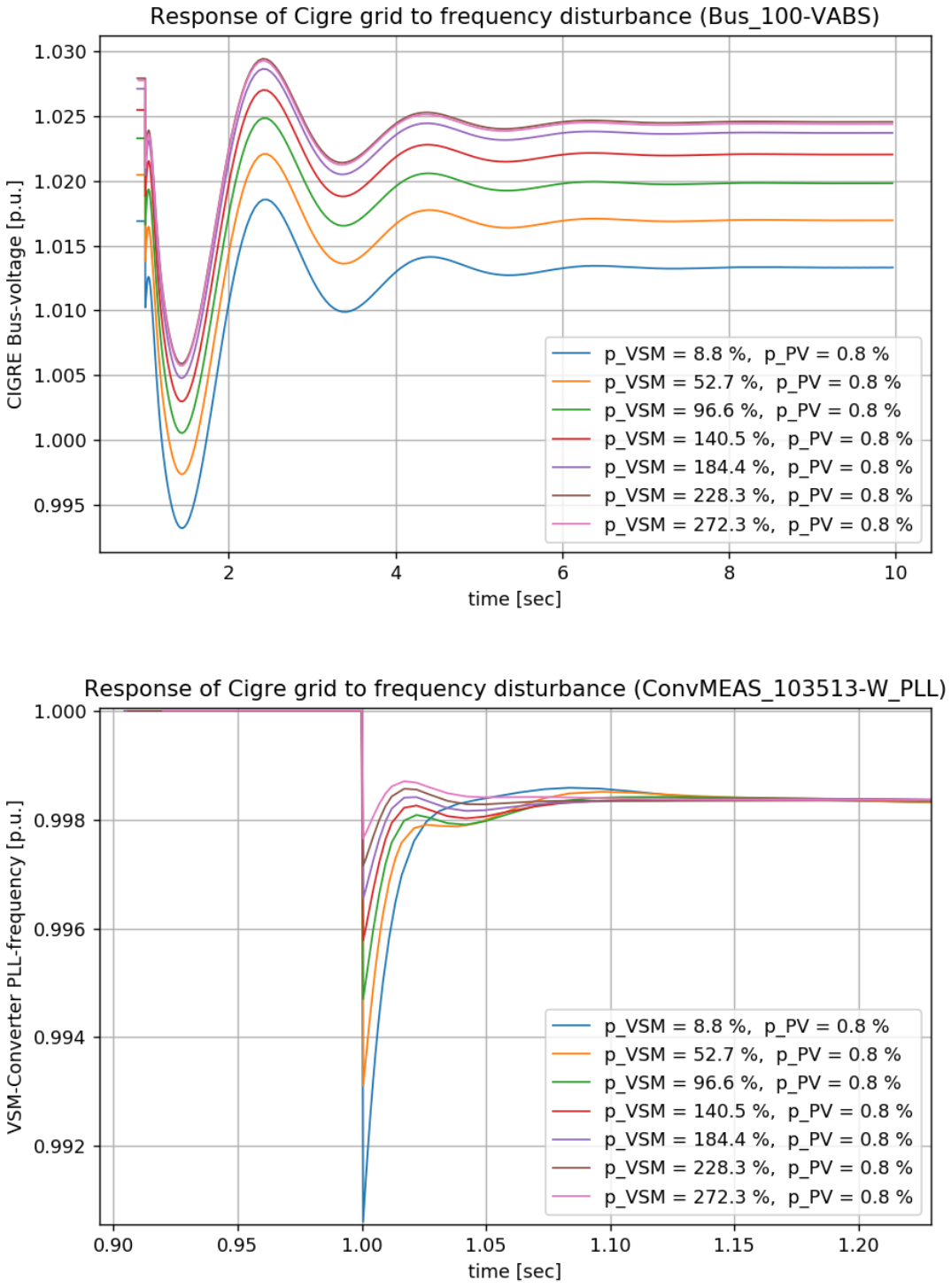

Figure 37: Cigre MW grid, response to a frequency transient of nearby generator: change of local bus voltage level (top) and PLL frequency of selected VSM converter in the distribution grid (bottom).

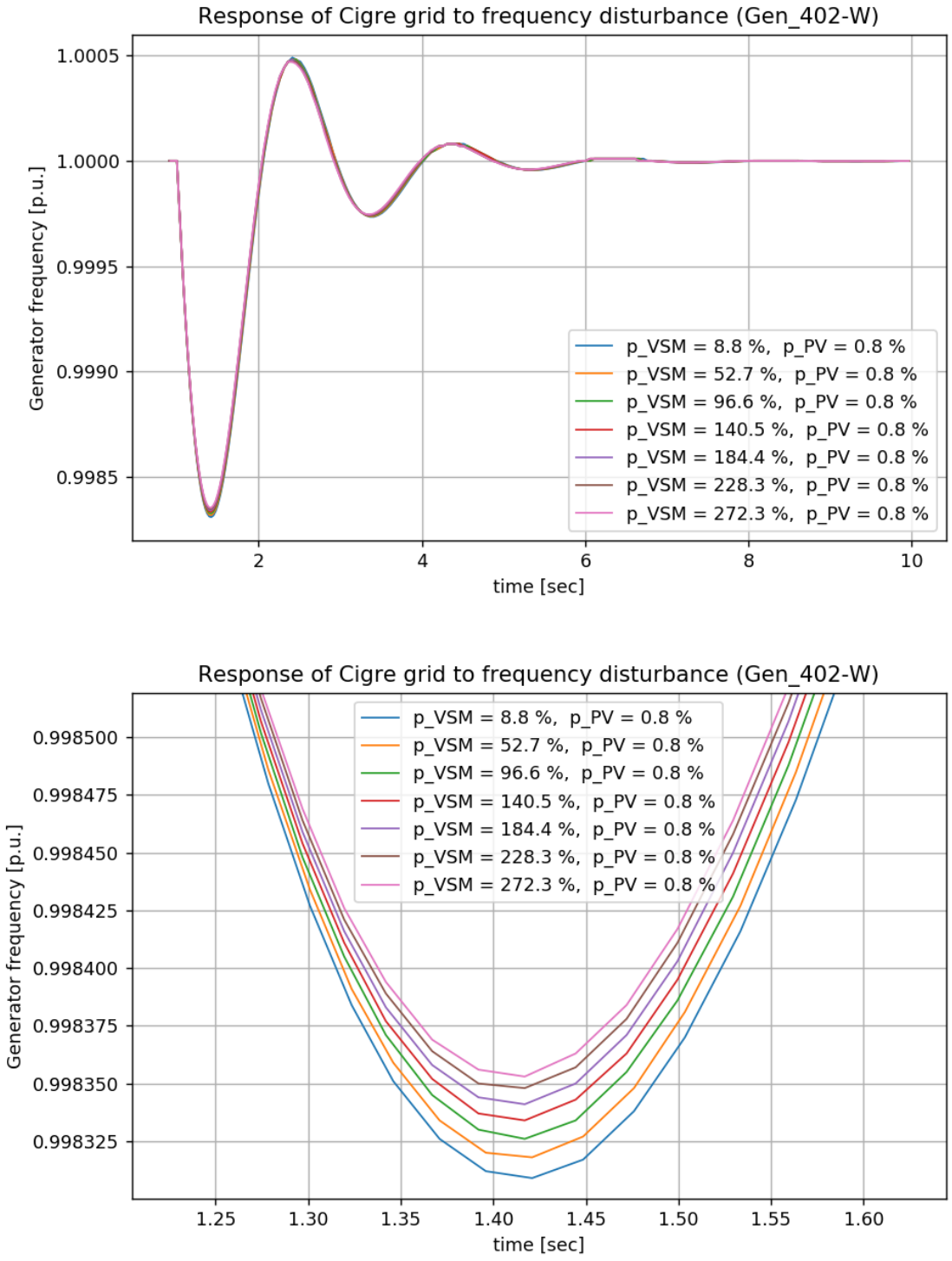

Figure 38: Cigre MW grid, response to a frequency transient of nearby generator: frequency of nearby generator (top) and zoom (bottom).

3.3.4 Nonlinear Aggregation

The nonlinear aggregation is obtained by simulating only 3 units instead of a full distribution grid,

- an aggregated load,
- an aggregated converter with grid support and
- an aggregated converter without grid support.

The parameter settings are topic of ongoing investigation and will be compared with the previous reference simulations.

The resulting nonlinear aggregated model is used in small scale transmission grid simulations as depicted in Figure 32 and Figure 33 and the Kundur system. The main observations are as follows:

- The aggregated nonlinear model with three components is sufficiently accurate to represent the detailed Cigre grid model with different shares of converter-based generation.
- The linear aggregation model performance is very similar to the nonlinear aggregation even for high loadings of the converter system. Only when less than 10% headroom is available, the internal converter constraints become critical.
- Since the nonlinear aggregation ignores the distribution grid interactions, it can in principle also go to higher shares of renewable production than the linear aggregation approach. However, this ignores local stability issues accounted for by the linear aggregation method.
- The transmission grid investigations in WP3 will use the linear aggregation models of the distribution grid. As an LTI system with only 4 states they are numerically more stable while delivering a high accuracy representing the distribution grid performance when sufficient headroom is available.
- Headroom of converter systems may be expensive, for instance requiring the curtailment of PV sources. A more detailed headroom analysis is currently performed to identify the minimum headroom required for the grid-forming DER's flexibility to be useful for grid support.

3.3.5 Key results and connection to other tasks

The key outcome of this task is the nonlinear simulation of the Cigre benchmark grid in the FLEXDYN simulator. A nonlinear aggregation with 3 components reduces the model complexity while maintaining the key constraint, the headroom of the DERs. It also allows a validation of the linear aggregation results performed by HAPG.

3.4 Software implementation

3.4.1 Problem description

The linear and nonlinear aggregated distribution grid models need to be interfaced with the transmission grid simulation in WP3.

Both aggregation procedures yield models that are scaled to match individual loads in the transmission grid simulation. While the nonlinear aggregated models can be directly interfaced with the transmission grid simulation, the linear aggregated models need some minor modifications in the form of estimated transmission grid variables as inputs.

The scaling of the loads is outlined in the following section. The interface on the transmission grid side is outlined in sections Section 4.2 (for the data import) and Section 4.4 (for the load representation in the FLEXDYN simulator).

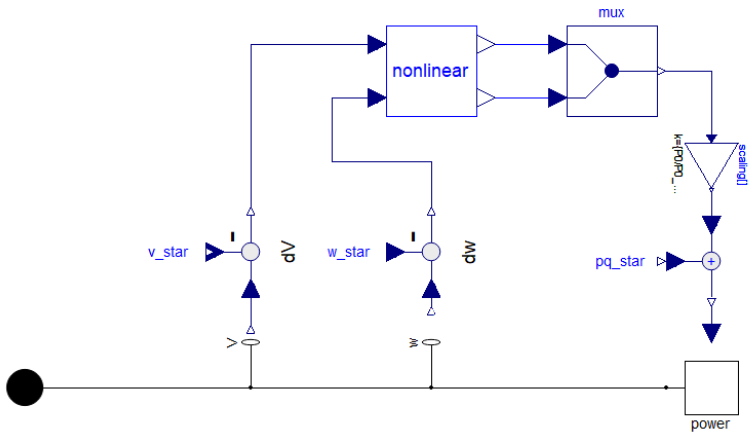

Figure 39: Wrapper model used for embedding aggregate distribution grid models in large-scale RMS simulation.

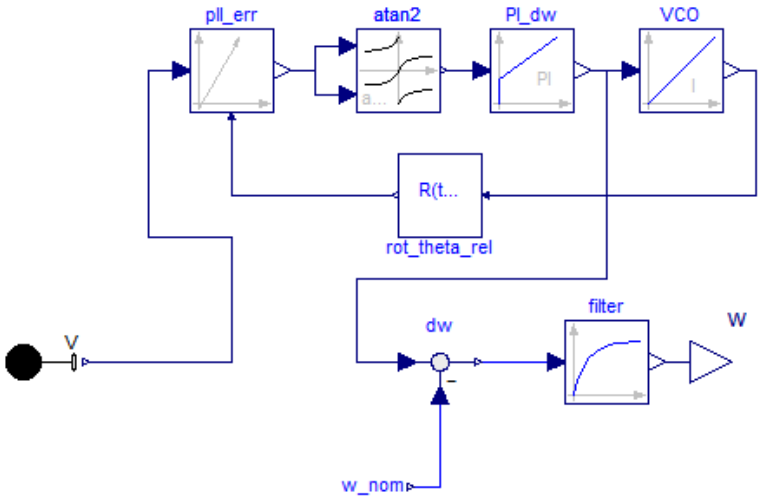

Figure 40: Phase locked loop (PLL) used for tracking local frequency based on the local dq-voltage.

3.4.2 Nonlinear load model

To embed the detailed ADN model in a grid simulation firstly requires alignment of the load flow solutions between the transmission grid solution power flow solution and that used by ADN model during generation. The transmission grid power solution will change depending on what scenarios are studied whereas the ADN power flow solution changes depending on the penetration level. The key here is to align the boundary conditions for load buses that are typically constraints on active and reactive power – loads are modelled as so called PQ-buses and fix the active and reactive power consumption to values P_0 and Q_0 at the initialization of the simulation. The procedure will be described in the following section.

The wrapper model in Figure 39 uses the original model defined for linear model generation shown in Figure 26 and thus contains a full order nonlinear representation of the grid. First, the voltage and frequency v and ω are extracted from the host simulation tool using appropriate voltage and frequency measurement blocks. In the example here, the voltage magnitude is extracted from the d and q components of the PCC voltage.

$$v = \sqrt{v_d^2 + v_q^2} \tag{17}$$

Furthermore, in grid simulations, frequency is typically not uniform between the different nodes in the grid when the network is in a transient state, and therefore the local frequency needs to be tracked based on the PCC voltage. This function is provided by the phase locked loop shown in Figure 40 which is similar to those used in converter control system, but tuned with a fast enough bandwidth of about 50 Hz in order not to affect the voltage and frequency dynamics in the grid simulation, that can be assumed to be in a frequency range below 10 Hz.

Therefore the voltage and frequency perturbation signals need to be constructed as

$$\Delta v = v - v_0 \tag{18}$$

$$\Delta \omega = \omega - \omega_0 \tag{19}$$

Here v is the time varying voltage in the host simulation environment and v_0 its initial value as given by the load flow solution. Analogously, ω is the time varying local frequency at the bus where the load model is connected and ω_0 its initial value.

These perturbation signals are then fed into the full nonlinear model using the wrapper model shown in Figure 26. The nonlinear grid model then produces the corresponding perturbations in terms of active and reactive power loads Δ_p^{model} and Δ_q^{model}. These are then scaled to match the boundary conditions in the host simulation P_0 and Q_0 and the pre-distrubance condition in the ADN model used for generating the load model. For example, the ADN considered in this report has an initial active and reactive power load, denoted P_0^{model} and Q_0^{model}, that also depends on the penetration level [24]. The resulting perturbation are then fed through the grid simulation using the relations

$$p = P_0 + \Delta p^{model} \frac{P_0}{P_0^{model}} \tag{20}$$

$$q = Q_0 + \Delta q^{model} \frac{Q_0}{Q_0^{model}} \tag{21}$$

3.4.3 Linear Load Model

The linear load model is implemented through the block diagram shown in Figure 41 and uses the same conventions for input and output signals as the nonlinear load model described in the previous section. The sole difference is that the grid is represented through a linear state space block where either the full or reduced linear models derived in Section 3.2.2 can be plugged in.

3.4.4 Load model validation: Two Area Test System

The validation of the reduced order ADN model in RMS simulation is based on modified version of the two are test system from [20]. The main modifications are:

- The 900 MVA generator at node 1 has been replaced with two units of 675 and 225 MVA, respectively.
- The inertia constants of all generators have been scaled down to 20 % of their original respective to simulate a low-inertia system.
- The generators employ a simple first order governor control system with droop constant 20 (pu power/pu frequency) and a time constant of 3 seconds.

The same scenario is simulated in RMS mode with the full nonlinear load model as well as the reduced linear equivalent. The 225 MVA generator generator G5 is diconnected at simulation time 1 s. This represents a generation loss of 6.25 % in terms capacity rating as well as actual production. The generator trip results in a rapid frequency drop that persists until the power balance is restored by joint effort of generator governors and the grid forming converters in the ADN.

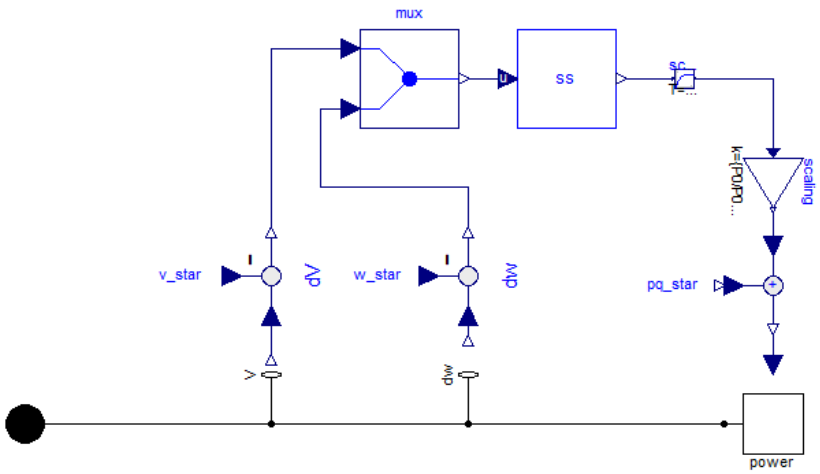

Figure 41: Wrapper model used for embedding aggregate distribution grid models in large-scale RMS simulation.

The simulation results are evaluated in terms of the system average frequency defined by the average rotational speed of the remaining generators in the system

$$\omega_{avg} = \frac{\omega_{G1} + \omega_{G2} + \omega_{G3} + \omega_{G4}}{4} \tag{22}$$

3.4.4.1 Nonlinear load model

Figure 42 shows the response of the rotational speed of generator 1 following the generator trip with varying grid supporting converter penetration levels. As expected the nadir frequency is increasingly improved thanks to the active power support as the penetration level increases. In the extreme cases of 5 % and 100 % the corresponding frequency drops corresponds to 230 and 137 mHz, respectively. This corresponds to and improvement of 40 %. With an in the short-term more realistic penetration level of say 40%, the improvement is about 30 %, which illustrates the diminishing returns in terms of nadir frequency improvements as the penetration level increases.

Figure 43 shows the voltage at Bus 9 following a trip of the generator 5 at 5 second under varying grid supporting converter penetration levels. A severe voltage drop is experienced in the middle of the long transmission line in the low penetration scenarios due to lack of reactive power following the generator trip. In the high penetration scenarios this effect is almost completely mitigated, demonstrating the effectiveness of supporting also the voltage through DERs in the distribution grid.

3.4.4.2 Linear load model

Figure 44 and Figure 45 show the system average frequency and mid point voltage in the same scenario simulated with the reduced order aggregate model. The results are near identical to those obtained with the detailed model. The accuracy will be investigated closer in the next section.

3.4.4.3 Comparison of linear and nonlinear model

The results are consistent with the findings in Section 3.2.2 where the load model was analysed in isolation. Figure 46 shows the nadir frequencies and voltages obtained with the detailed and reduced order linear model under varying penetration level. The reduced order model consistently predicts a slightly lower nadir frequency than the simulations with the detailed model, however the difference is small in terms of the total drop. As also could be predicted based on the results in Section 3.2.2 this difference increases with the penetration level, however it remains small with a maximum error of 3 mHz at a penetration level of 100 %.

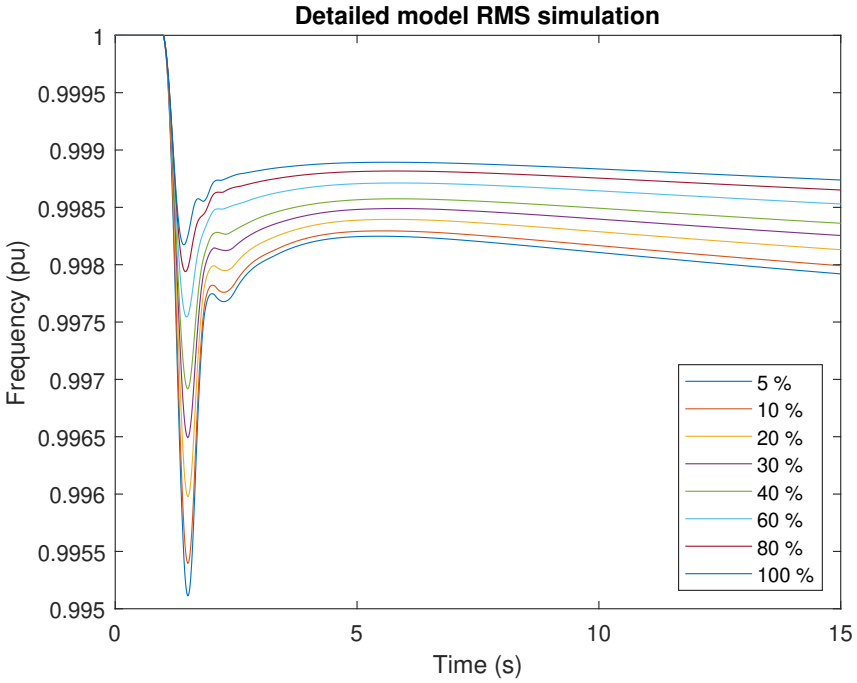

Figure 42: System average frequency following tripping of generator 5 using the detailed ADN model.

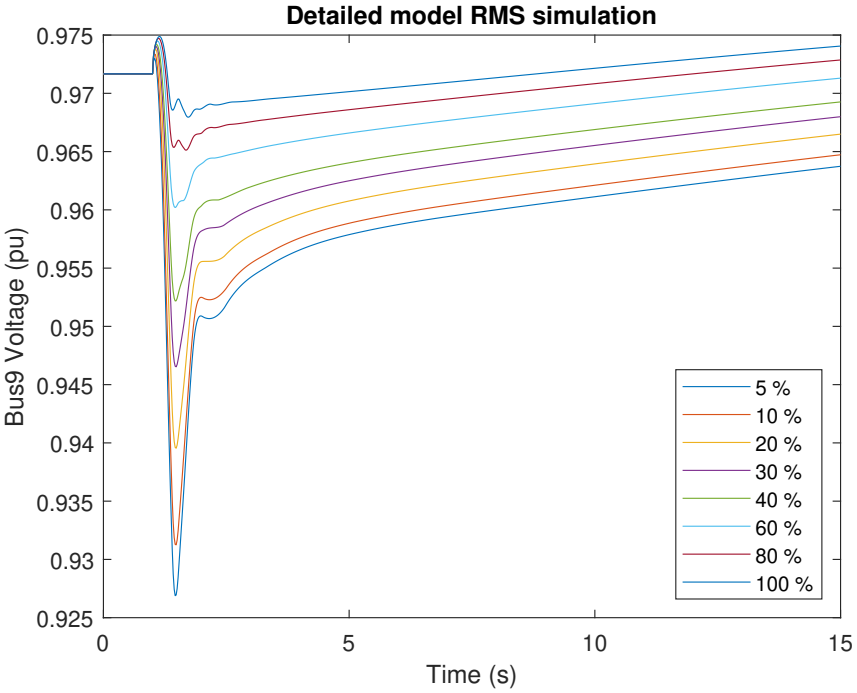

Figure 43: Response of Bus 9 voltage following tripping of generator 5 using the detailed ADN model.

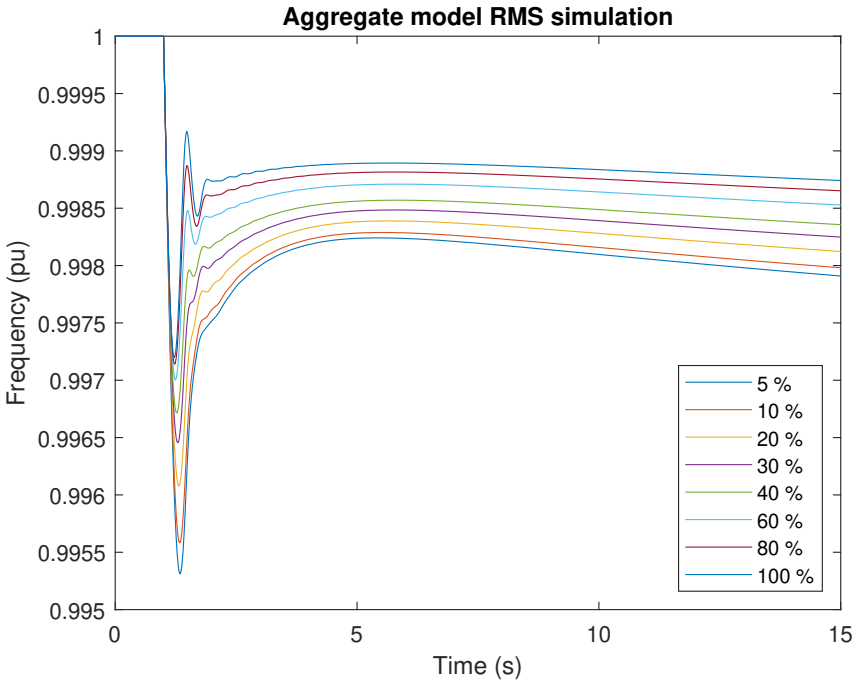

Figure 44: Response of Generator 1 rotational speed following tripping of generator 5 using the reduced order linear ADN model.

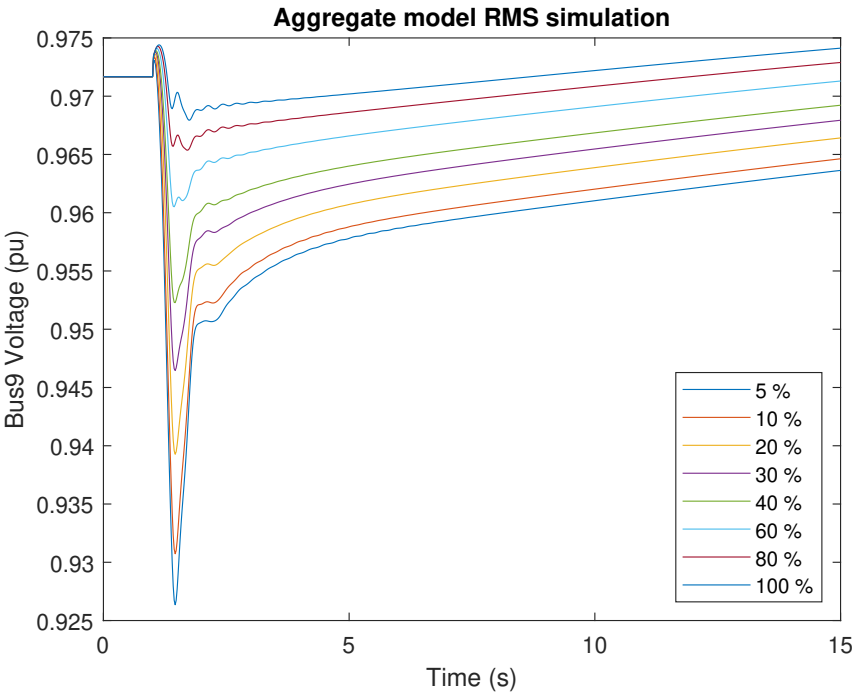

Figure 45: Response of Bus 9 voltage following tripping of generator 5 using the reduced order linear ADN model.

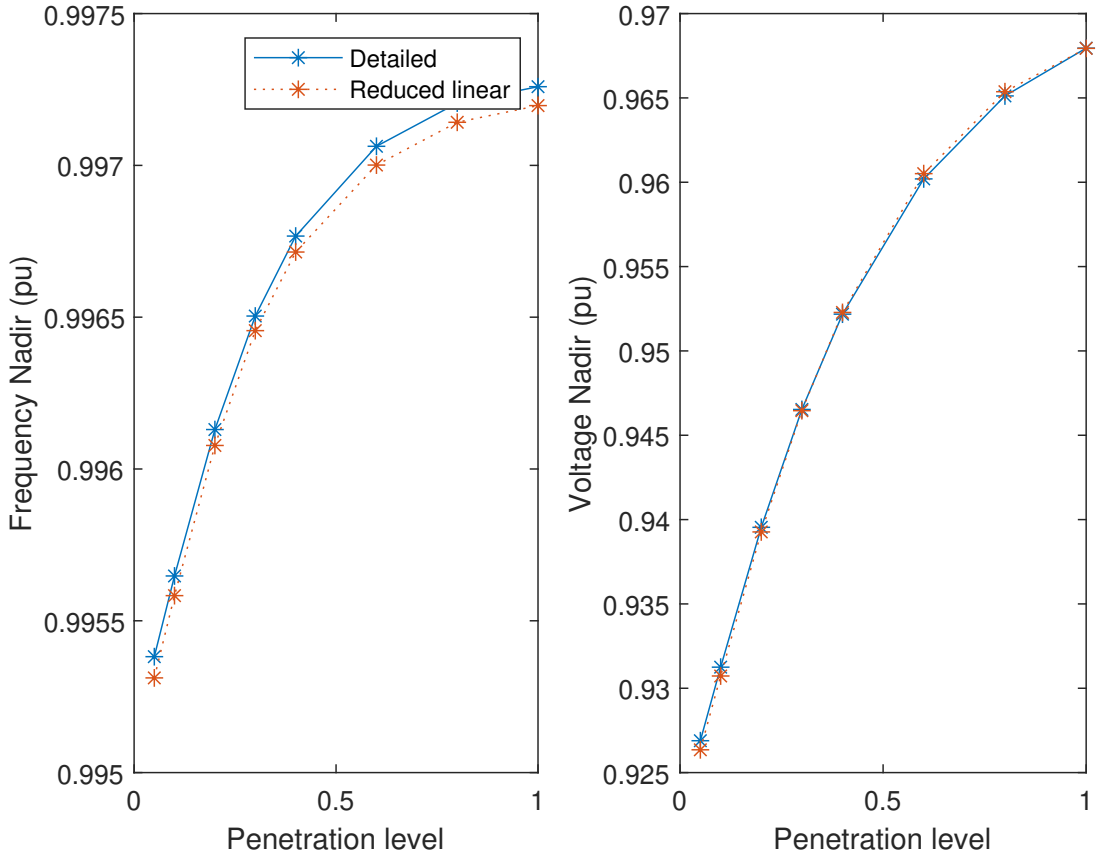

Figure 46: Nadir frequencies and voltages obtained with the detailed and reduced order linear model under varying penetration level.

3.4.5 Key results and connection to other tasks

This section has described the software implementation of the full order nonlinear and linear ADN models in the ConverterStab toolbox used for generation of the aggregate models. The procedure is based on embedding of a detailed grid model in wrapper models with predefined inputs and outputs that are then linearized to yield a linear representation. Furthermore well-known model reduction methods applicable to linear systems are used to reduce the orginal model with order over of several 100s to an order of 4 that is convenient for large-scale deployment in transmission grid simulation.

The accuracy of the reduced order linear models has been investigated for a frequency range of several hundred mHz and found adequate. Furthermore, the embedding of the reduced order model was demonstrated in a small test network and the response was compared to that of the orginal full order nonlinear model. Under worst-case conditions of a penetration level of 100 % the reduced model can be used to predict the nadir frequency following a generation loss of 6.25 % within an accuracy of 3 mHz. The reduced order models serves as basis for the scenario study on ENTSO-E network that is reported in the WP3 report.

4 Transmission grid investigation (WP3)

4.1 Introduction

4.1.1 Objective

This work package investigates the aggregated dynamic impact of distributed generation on the transmission grid. It concludes the project's overall objective, which is an integrated assessment of the future global dynamic power system performance with a substantial part of the generation harvested from the distribution grids.

WP1 focused on the converter and distribution grid modeling and control. WP2 introduced appropriate aggregation methods to capture the dynamic characteristic of active distribution networks. To obtain quantitative insights and derive policy recommendations regarding challenges and opportunities arising with a growing DER penetration, it is important to carry out performance assessments of the DER's impact on the global power system stability. To this end, WP3 now focuses on combining the models developed in WP1 and WP2 with a simulation of a detailed ENTSO-E transmission grid model. In particular, WP3 investigates the question, how the grid support functionality today provided by large synchronous machines can be replaced with distributed grid support at lower voltage levels, and interpret the conclusions from the Swiss perspective.

4.1.2 Approach

The overall approach to WP3 and the interface to external data and input from other tasks is depicted in Figure 47.

Two main **external data sets** are used in WP3:

- The first input is the continental **ENTSO-E dynamic transmission grid model**. The model was provided by ENTSO-E in the Powerfactory format and has been imported, validated and extended for the FLEXDYN simulator, as described in Section 4.3.
- The second input is the LTI load models generated in WP2. For each DER-VSM penetration scenario (in total 8 scenarios with penetrations varying between 5% and 100%), the state space matrices and the initial power values of the reference distribution grid are communicated. The incorporation of the LTI models and their control integration in the transmission grid simulation is further described in Section 4.4.

Within WP3, the analysis is carried out in 5 main steps, documented in the following sections.

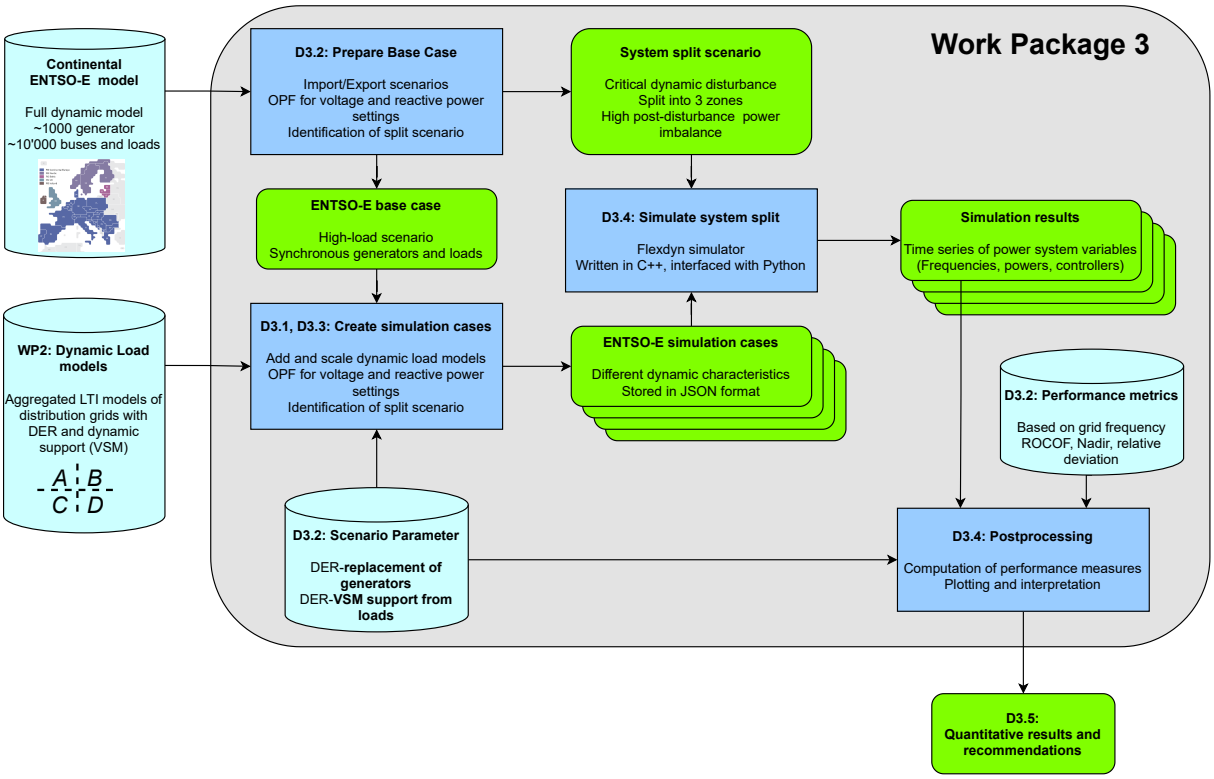

Figure 47: Structure of the task flow for the integrated transmission grid investigations, combining dynamic load models (from WP2), a dynamic model of the ENTSO-E grid (from ENTSO-E) and critical dynamic disturbance scenarios to gain quantitative insights regarding the impact of DERs replacing synchronous machines.

4.2 Software interface

This section describes the software interface used to combine dynamic load models, a dynamic model of the ENTSO-E grid and disturbance scenarios to perform the integrated transmission grid investigations.

4.2.1 Problem description

The simulation-based investigations in this work package pose two challenges to the simulation environment:

- The simulator must be efficient, running thousands of components and interactions.
- The simulator must be flexible to handle new components, in particular the dynamic load models developed in WP2, on a large scale.

The simulation environment FLEXDYN is used to address these challenges. It has been previously developed and applied to large power system models, but extended in important ways during the project.

4.2.2 Software structure

The overall modular structure of the FLEXDYN simulator is depicted in Figure 48. The key module "FLEXDYN"-Simulation has been implemented in C++, performing the dynamic initialization, event handling and time integration. New components are included as symbolic models, automatically differentiated and compiled to executable C-code.

Within the project, the interface of the simulator, covering all other modules in Figure 48 was developed in the programming language Python, using the text-based JSON-format for data exchange. Software components newly implemented during the project include:

- Systematic replacement and addition of components, making use of previous load flow solutions. This functionality is essential to modify the generations and loads in the model to be replaced by CER- and DER-models.
- Reinitialization of load flow scenarios. The initial settings of Voltage and Reactive powers can not be used over a wide range of scenario parameters. An OPF is executed to determine voltage settings, that lead to a successful initialization of the dynamic model.
- Automated parameter sweeps to perform scenario investigations.
- Postprocessing of the simulation results, plotting.

The validation of the simulation environment is shown in WP1 for a VSM converter simulation, compared in the Dymola-based distribution grid simulation tool and FLEXDYN. As illustration, see Figure 49 for comparison of the two simulation tools.

4.2.3 Key results and connection to other tasks

The FLEXDYN simulation tool is essential to carry large-scale power system simulations to investigate the aggregated transmission grid impact of active distribution networks. Other simulation tools lack the performance or flexibility required for the investigations of this project.

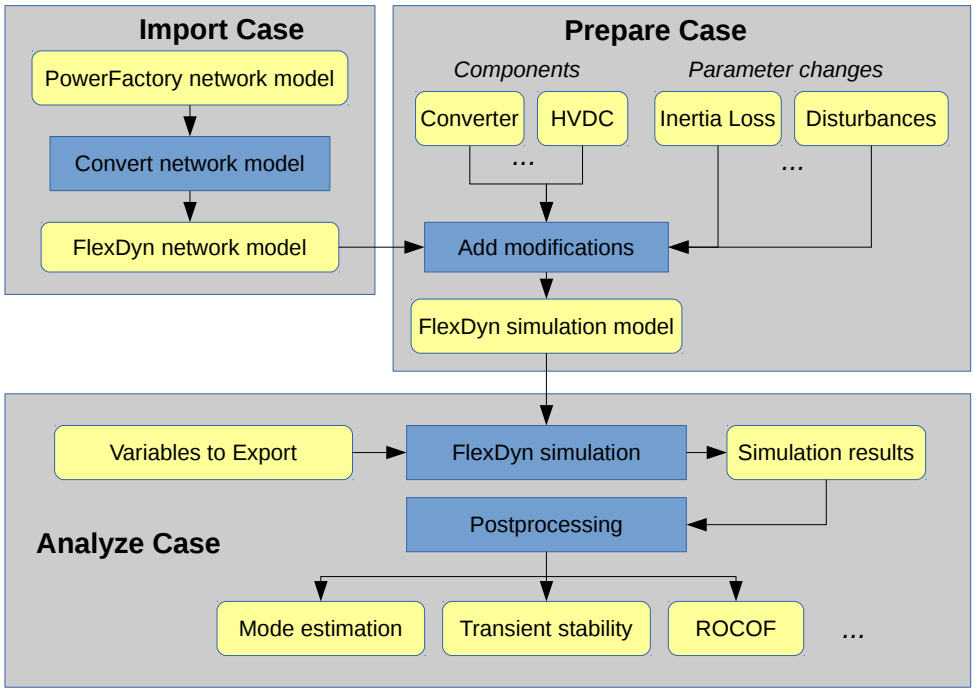

Figure 48: Structure of the FLEXDYN simulation framework.

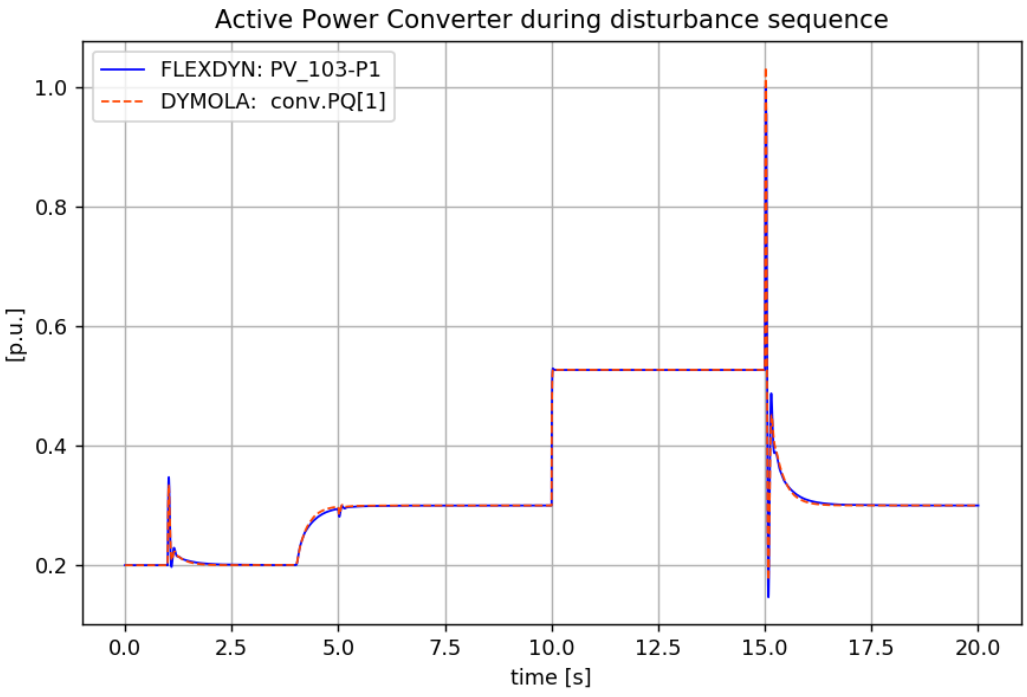

Figure 49: Active-power-Response of a VSM-Converter during a disturbance sequence of frequency and voltage steps. Validation of the FLEXDYN simulation results (used for the transmission grid investigations, blue) with the superimposed DYMOLA simulation results (used distribution grid aggregation, red).

4.3 Scenarios and performance metrics

4.3.1 Problem description

The quantitative assessment of the transmission grid impact from active distribution networks requires benchmark scenarios, under which the different networks are tested. This section describes the dynamic ENTSO-E transmission grid model used for this study. Furthermore, the relevant scenarios for grid developments (e.g. reduction of synchronous generation) and disturbances are presented.

To compare the aggregated performance on the level of the transmission grid, dynamic performance measure need to be selected. This section proposes and illustrates different time-domain measures, mostly based on the grid frequency.

4.3.2 ENTSO-E model and disturbance scenario

4.3.2.1 ENTSO-E model description The dynamic reference model used for the transmission grid investigations is the ENTSO-E initial dynamic model, published by ENTSO-E. It was provided in the PowerFactory fileformat and consists of around:

- 24'000 Buses
- 30'000 line elements (overhead, cable, transformer)
- 7'000 Loads and 5'000 static generators (impedance models)
- 1'000 synchronous generators (dynamic 6th order machine model, Governor, AVR and PSS)

For efficient and flexible simulation, the model was ported to the FLEXDYN simulator (described in Section 4.2). Within the recently completed project SCCER-FURIES (joint work with Swissgrid) [12], the accuracy of the model import and the plausibility of the simulation results have been validated. The model snapshot captures a high-load case with a total load of about 458 GW over the ENTSO-E area.

For the simulation, two model parameters have been modified independently:

1. **CER-static replacement of synchronous generators:**
   To model the impact of inertia reduction, all synchronous generators in the system are proportionally reduced by a certain percentage. This affects the inertia, the production and the power rating of the individual generators, as well as their contribution through droop control, AVR and power system damping. The generator power is replaced by centralized static generators, using on impedance models. Their injected power changes during transients with the local grid voltage level, but otherwise has no dynamic grid support.
2. **DER-VSM penetration of loads:**
   In the base scenario, the 12'000 loads of the ENTSO-E model, mostly representing aggregated distribution grids are represented by impedance model. For the simulation, they are replaced by the dynamic load models developed in WP2, that contain a contribution from grid forming converters, operating with sufficient headroom for dynamic grid support. The ratio between the grid forming converters rated power and the load demand is a model parameter, referred to as DER-VSM penetration. As outlined in Section 4.4, different DER-VSM penetrations correspond to different load characteristic of the underlying distribution grids.

4.3.2.2 ENTSO-E disturbance The full ENTSO-E dynamic model is quite robust to small disturbances. Individual outages of generators, lines or loads may trigger some inter-area oscillations but are not critical scenarios endangering the security of the system. During the SCCER-FURIES project, a review of different disturbance scenarios through simulation as well as discussions with Swissgrid has

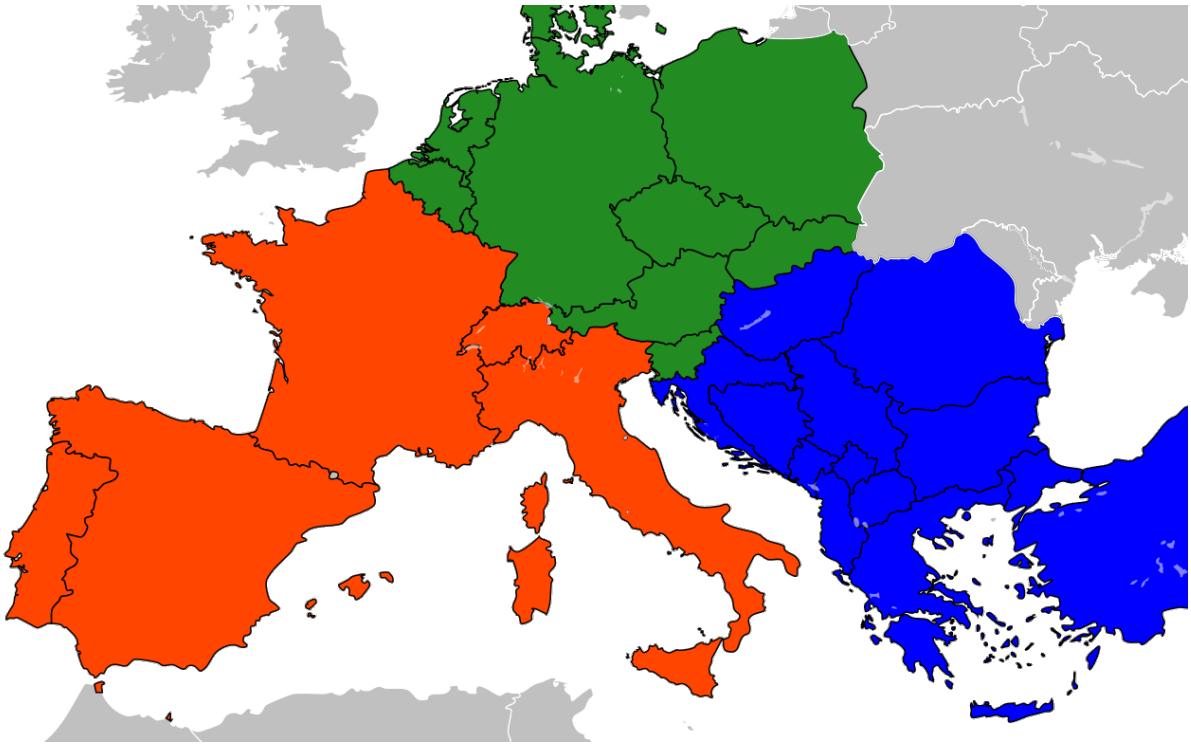

Figure 50: Investigated system split of the ENTSO-E network in 3 zones, motivated by [9].

identified a system split as the most crucial risk scenario, triggering dynamic instability and subsequent black-outs. After a split into multiple asynchronous zones, the power imbalance within each zone may be quite large, on the order of several GWs. Additionally, a split excites strong oscillations within each zone, since usually some inter-zonal lines are importing and others are exporting before the split.

The system split scenario that serves as reference case for the project is motivated by an actual system split that has occurred in 2006 [9]. The countries in each zone are illustrated in Figure 50. As the ENTSO-E data only includes the country information of each node, a graph analysis is performed to identify the transmission lines that need to be opened to achieve the separation. Small isolated bus groups remain connected to the closest large grid area. The simulation does not model the cascade of outages, but opens all lines at once.

The distribution of the initial load power is shown for each zone in Figure 51. Each of the more than 7'000 loads is subsequently replaced by a dynamic load model, whose power injection changes during the disturbance depending on the load location, in particular due to the voltage deviation.

4.3.3 Performance metrics

The quantitative assessment is based on time-domain simulations, generating trajectories for all power system variables.

The key indication for power system "health" is the frequency on the global level and the voltage on a local level. Active distribution networks support the stability of both.

On the transmission grid level, where the assessment is carried out, frequency-related performance measures are used. As an intermediate step, the mean frequency $\mu(t)$ and the relative frequency

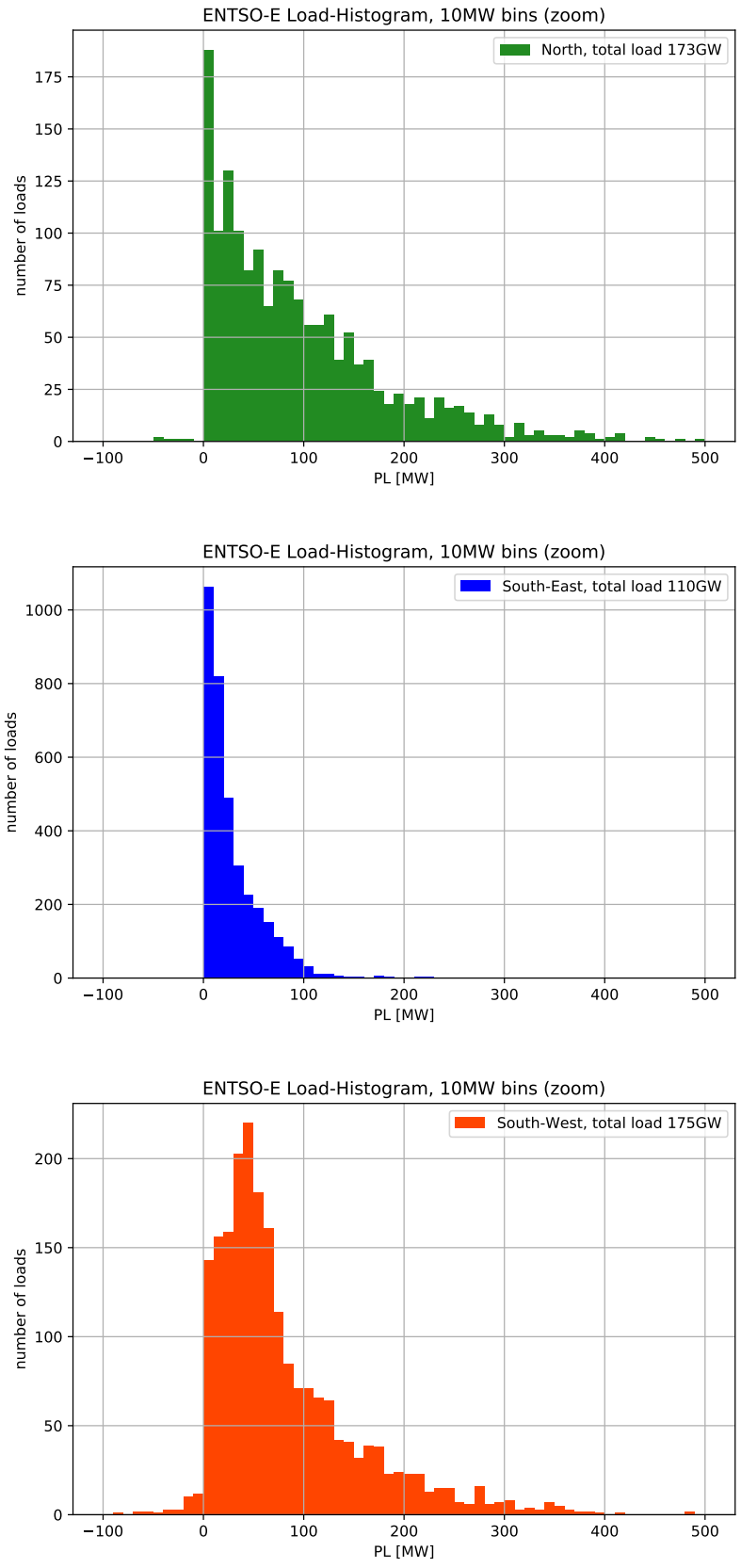

Figure 51: Distribution of the 7'000 loads in the 3 zones. Each load is replaced by an aggregated dynamic distribution grid model with the same steady state power.

deviation $\sigma(t)$ of each area are computed as:

$$\mu(t) = \frac{1}{N}\sum_{i}^{N}\omega_i(t) \tag{23}$$

$$\sigma(t) = \sqrt{\frac{1}{N}\sum_{i}^{N}(\omega_i(t) - \mu(t))^2} \tag{24}$$

The actual performance measures are defined as follows

- **Final frequency** μ_∞:
  The final frequency, defined as
  $$\mu_\infty = \lim_{t\to\infty}\mu(t) \tag{25}$$
  and computed as the value at the end of the simulation (i.e. after 50 seconds), is an indicator of power imbalance after the disturbance, creating a frequency offset. The power imbalance is compensated by the droop control of the synchronous machines and the converters.

- **Nadir frequency** $\hat{\mu}$:
  The nadir frequency, defined as
  $$\hat{\mu} = \max_t(\mu(t)) \quad \text{if} \quad \mu_\infty > 50\text{Hz} \tag{26}$$
  $$\hat{\mu} = \min_t(\mu(t)) \quad \text{if} \quad \mu_\infty < 50\text{Hz} \tag{27}$$
  is the frequency peak before the final frequency is reached. The nadir that is too far from the nominal frequency can cause a cascade of outages due to the protection of individual generation units and grid areas.

- **Peak frequency deviation** $\hat{\sigma}$:
  The peak of the relative frequency deviation σ, defined as
  $$\hat{\sigma} = \max_t(\sigma(t)) \tag{28}$$
  measures the "spread" between the frequencies of the generation units. High values indicate strong oscillations between the generation units.

- **Rate-of-change-of-frequency (ROCOF)** R_μ:
  If the system frequency accelerates too fast, a cascade of outages can occur due to the protection of individual generation units and grid areas. The reported ROCOF is computed using each area's average frequency μ over a time-window of 2 seconds after the disturbance:
  $$R_\mu = \frac{\mu(2\text{sec}) - 50\text{Hz}}{2\text{sec}} \tag{29}$$

The performance measures are illustrated for a sample simulation result of the ENTSO-E system split. The frequencies of all areas are shown in Figure 52.

The zoom in Figure 53 shows the strong oscillations in the first seconds after the system split. The same figure also shows the mean frequency μ and the relative frequency deviation σ, forming an envelope. Plotted seperately, Figure 54 shows the full trajectory of μ and σ. While μ serves to identify the final value μ_∞, the peak $\hat{\mu}$, and the ROCOF R_μ, the peak deviation $\hat{\sigma}$ is identified from σ.

Further potential performance measures relate to the settling time as well as other system variables (e.g. line powers and bus voltage deviations).

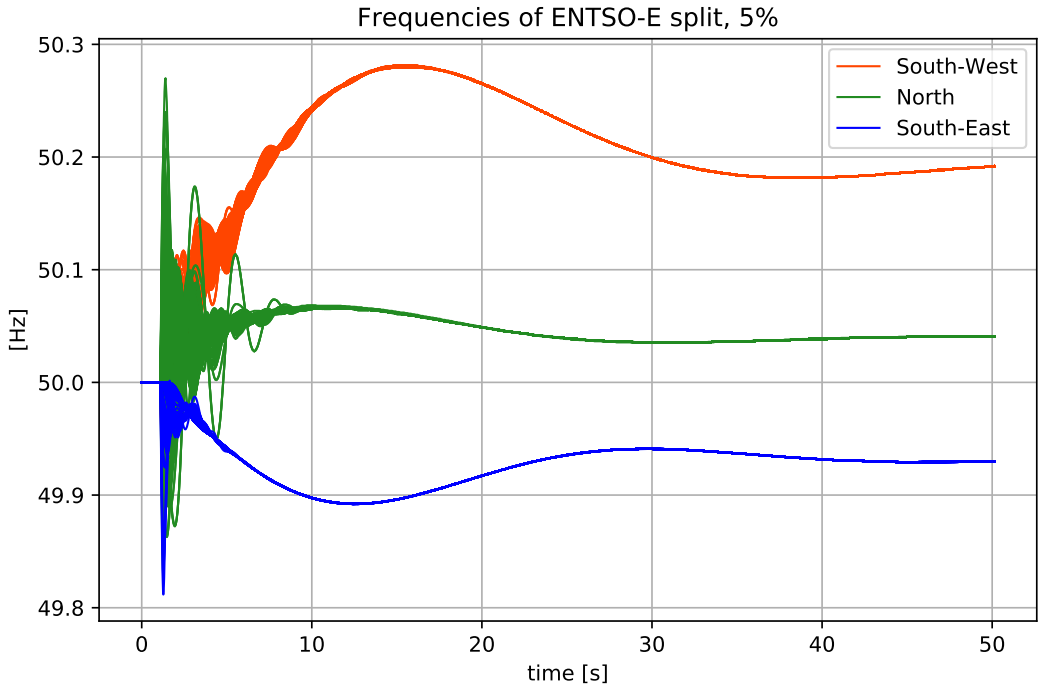

Figure 52: Typical frequency behaviour during ENTSO-E system split into 3 zones.

4.3.4 Key results and connection to other tasks

The key outcomes of this section are as follows:

- Specification of the ENTSO-E model and basic assumptions
- Specification of the two opposing scenario parameter (CER-static replacement of generators and the DER-VSM penetration of loads). The former is challenging grid stability, the latter is supporting grid stability.
- Specification of performance measures used to carry out the quantitative performance assessment.

They are a key input to the comparative assessement, documented in Section 4.5.

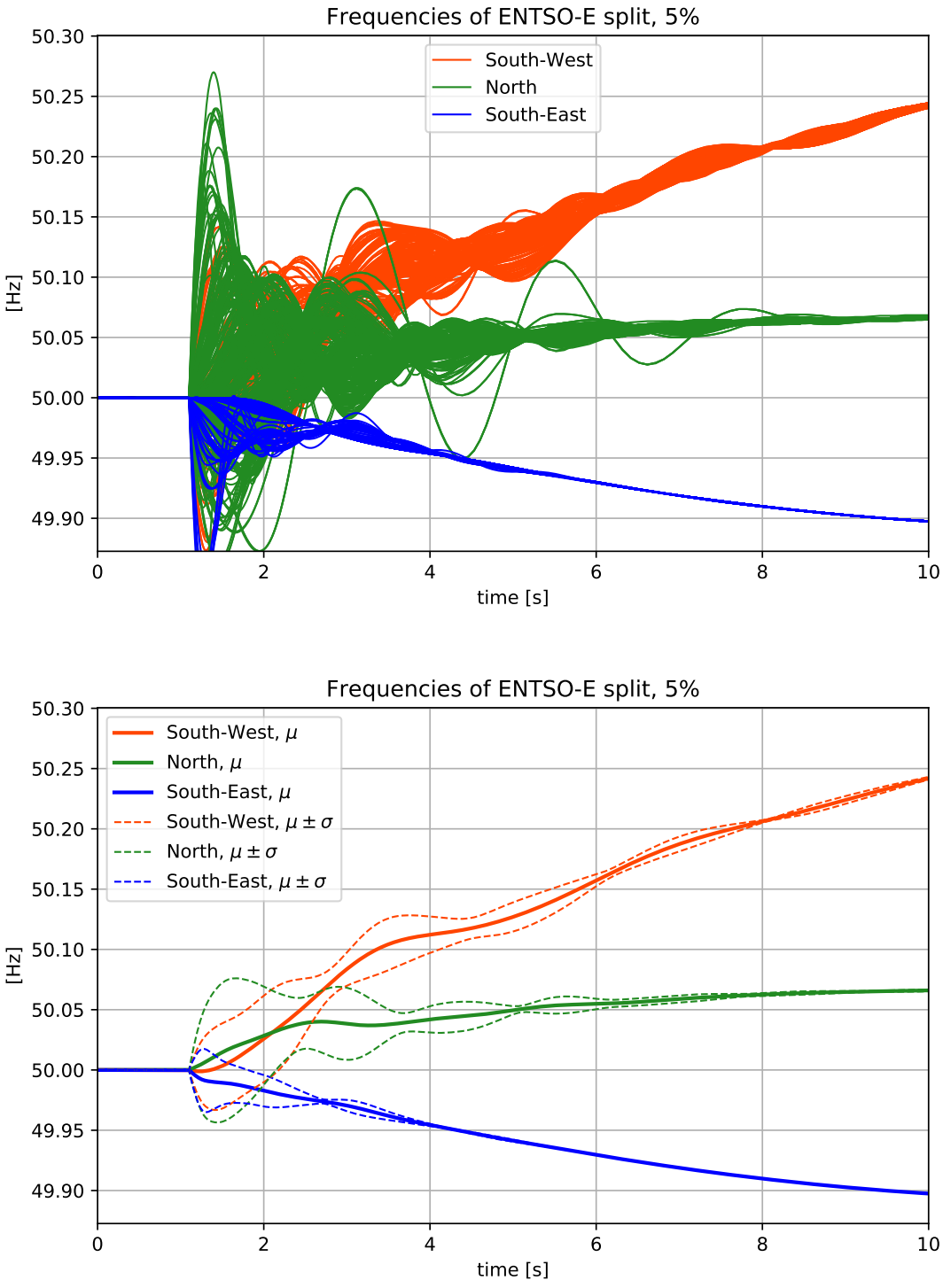

Figure 53: Typical frequency behaviour during ENTSO-E system split into 3 zones (top, zoom). Corresponding mean value μ with positive/negative standard deviation σ of frequencies in each zone.

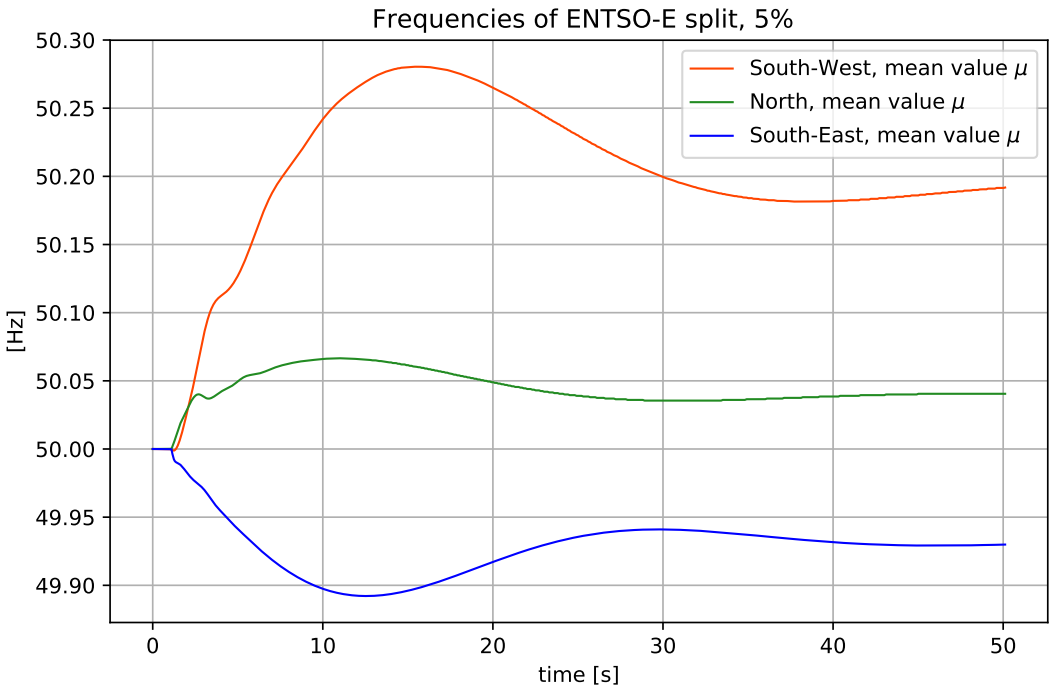

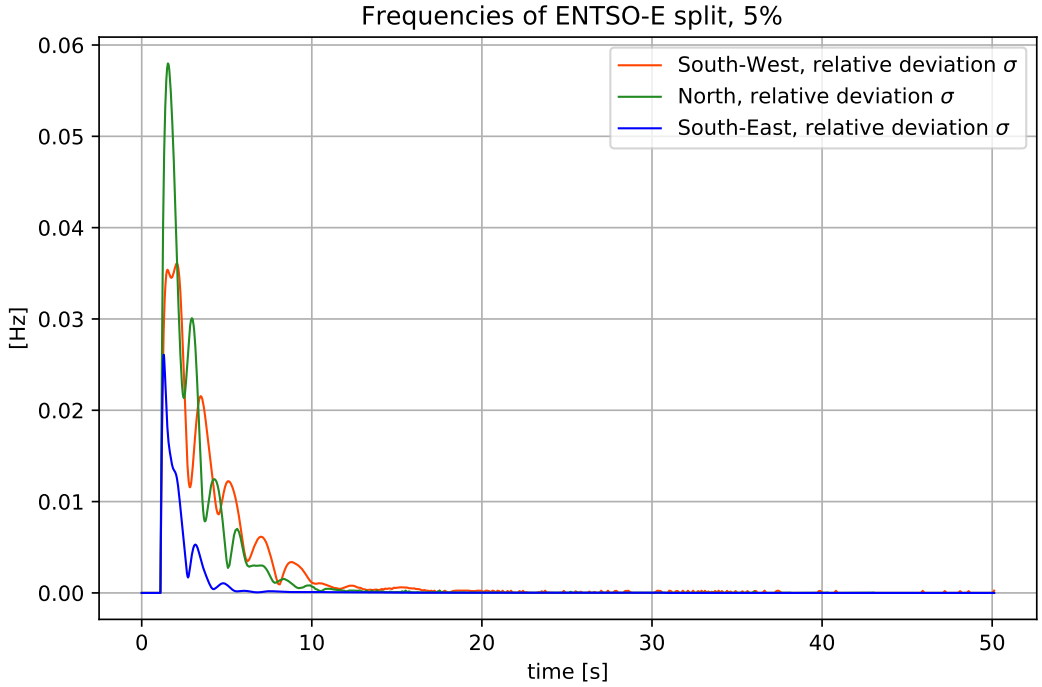

Figure 54: Typical frequency behaviour during ENTSO-E system split into 3 zones. Mean value μ and standard deviation σ of frequencies in each zone.

4.4 Grid control implementation for conventional generators and DER

4.4.1 Problem description

The transmission grid investigations in WP3 cover a range of scenarios and development paths, including today's situation with most grid control performed by synchronous generators up to a future scenario with a substantial share of synchronous generation removed and replaced by converter-based generation in distribution grids, that is either grid-forming or grid-following.

The following subsections introduce the sources of grid-control functionality in the modified ENTSO-E model and outline the parameter variations performed to investigate typical grid-control constellations encountered during the energy transition.

4.4.2 Grid control with synchronous generators (static and dynamic)

About 1'000 sources in the ENTSO-E transmission grid model are synchronous machines, providing a multitude of grid control functionality during transients:

- The synchronous machines in the simulation use a 6th order dynamic model. This includes a model of the **damper windings**, that provide grid control by damping out oscillations caused by sudden changes of the rotor load.
- The **inertia** of the synchronous machine determines how quickly the rotor (and thereby the generator frequency) accelerates during power (and torque) mismatches of the synchronous machine. High inertia values lead to slower acceleration. The reduction of system inertia due to the replacement of synchronous machines with converter-based generation is a main topic of the discussions concerning dynamic risks of the energy transition, also coined as *low inertia problem*.
- The **governor control** (or droop control) of the synchronous machines provide grid control by adjusting the mechanical power of the generator during frequency imbalances. The headroom for droop control is procured throughout the ENTSO-E system as primary frequency reserve.
- The **Automatic Voltage Regulator** (AVR) adjusts the excitation voltage of the generator, as reaction to changes of the local voltage level. This essentially provides grid control by reacting to voltage changes caused by disturbances or changes in reactive power demand.
- Finally, the **Power System Stabilizer** (PSS) modulates the excitation voltage of the generator, in order to damp frequency oscillations. PSS are often subject to individual tuning throughout the ENTSO-E network and play a key role for the damping of inter-area oscillations.

All models for synchronous machine components and controllers use standard models from the ENTSO-E Common Grid Model Exchange Standard (CGMES) Library. The control functionalities are reduced when synchronous generators are replaced with grid-following converters, as taking place during the energy transition In the WP3 simulations, this is captured by the scenario parameter determining the CER-static replacement of synchronous machines.

4.4.3 Grid control with static generators and loads

The ENTSO-E dynamic model has a large number of loads and generation unit modeled using static models without dynamic states. In principle static injections can be modeled as constant power, constant current or constant impedance sources (or a mixture thereof). All static sources in the ENTSO-E simulation use a constant impedance model. These models have good numerical properties, but also have a grid supporting functionality during transients. The power of the constant impedance model during

dynamic simulations follows the relation

$$P(t) = \frac{V(t)^2}{V_0^2} P_0 \tag{30}$$

$$Q(t) = \frac{V(t)^2}{V_0^2} Q_0 \tag{31}$$

with P_0 and Q_0 denoting the power at nominal voltage level V_0. Note that the constant impedance model reacts to changes in the local voltage $V(t)$ during transients. During a voltage drop, e.g. during a fault, the power consumed by a load (with $P_0 > 0$) or the power produced by a static generator (with $P_0 < 0$) is also reduced with the square of the voltage change.

The constant impedance model is commonly accepted and widely used to model loads and static generation units for large-scale transmission grid investigations. The main reason is the numerical efficiency (no dynamic states), that is important if thousands of units are simulated in parallel.

However, investigations in the project SCCER-FURIES have shown, that the impedance models tends to underestimate the frequency impact when used for the modeling of grid-following PV-converter units replacing synchronous generation units. Using a small-scale test system (the Kundur two-area system) over a wide range of load flow scenarios showed that the nadir frequency increases more than twice as much when a detailed grid-following converter model is used (a current-controlled capacitor model). The detailed grid-following converters more like a constant power source (instead of a constant impedance source). They have thus a harsher response during transients, in particular during voltage deviations.

The investigations in WP3 are carried out with a constant impedance model, for both the static loads and the static generation units. This includes the additional grid-following static generators implied by the scenario parameter for CER-static replacement of synchronous machines. The results can therefore be expected to be too optimistic regarding the change in frequency during the system split. However, they still allow the relative comparison of the effectiveness of additional grid support from the distribution grids. Ongoing investigations concern the use of current-controlled capacitor models for large fleets of grid-following converters in the detailed ENTSO-E transmission grid simulation.

4.4.4 Grid control with grid-forming converters

The load models developed in WP1 and WP2 capture the aggregated dynamic behaviour of distribution grids. The full models are based on the CIGRE-MV-Benchmark grid, modified to incorporate different shares of grid-forming converters based on the Virtual Synchronous Machine (VSM) control approach. After linearization and model reduction, the LTI models used for the transmission system analysis have 4 states, 2 inputs (frequency deviation and voltage deviation) and 2 outputs (change in active power and change in reactive power). The interface between WP2 and WP3 to communicate the model is very simple. Only 36 floating point numbers need to be transmitted to encode the state space matrices (commonly denoted as A, B, C, D). Additionally, the initial values for active power (P_0) and reactive power (Q_0) are communicated and used to scale the output of the LTI models to the actual size of the transmission grid loads they are representing. During simulation of the ENTSO-E grid, each of the more than 7'000 loads are equipped with an individual dynamic LTI model.

To implement the grid-control through the LTI model of the aggregated distribution grids, the two input parameters have to be locally estimated. Both the voltage and the frequency deviation are estimated based on the filtered bus voltage at the load bus. The voltage uses the magnitude, the frequency uses a Phase-Locked-Loop (PLL), determining a rotating dq-frame where the q-component of the local grid voltage becomes 0. Since the FLEXDYN simulator uses itself a rotating dq-frame for efficient simulation of the system-wide AC-quantities (voltages and currents), permanent frequency offsets would not be noticed. Therefore, the PLL also incorporates a system-wide quantity corresponding to the center-of-inertia frequency, a weighted average of all generator frequencies. Note that this usage of a global frequency is only an implementation issue of the simulator. In practice, a global frequency estimate is not required.

The grid control contributions of the distribution grid model with grid forming converters are scaled according to the size of the distribution grid. This means that a 200 MW load in the ENTSO-E model essentially behaves like 5 CIGRE-MV-networks in parallel (each of which has a net load of about 50 MW). This means, that also the power composition of the CIGRE network is replicated across the ENTSO-E network. The power composition of the CIGRE network is depicted in Figure 55, for different levels of DER-VSM penetration. It can be seen, that the Load power (yellow) remains constant for all penetration levels. However, the power injected by grid-forming converters (green, negative values indicate production) increases, as well as the losses and the power from grid-following converters. The penetration level p is shown along the horizontal axis and is defined as

$$p = \frac{P_{\text{capacity, grid-forming}}}{P_{\text{load}}} \quad . \tag{32}$$

Note that the converters operate at only 50% capacity, so the active power injected by the converters in steady state operation is $P_{\text{grid-forming}} = 0.5 \cdot P_{\text{capacity, grid-forming}}$.

As a result, the **net power injection** (blue line in Figure 55) is reduced for increasing DER-VSM penetration levels. Consequently, higher DER-VSM penetration levels require a larger scaling factor to be applied when incorporated with the ENTSO-E network model. This is illustrated in Figure 56 for ENTSO-E loads between 100 and 500 MW. The resulting effective load composition of the ENTSO-E load is illustrated for a 200 MW load in Figure 57. It can be seen that the increasing DER-VSM penetration has mainly two effects:

1. An **increase of grid-forming converter generation**, corresponding to new converters with sufficient headroom for power flexibility (from battery storages or PV-converters operating at less than full capacity).
2. An **increase of electric load demand**, corresponding to further electrification in the distribution grid, for example heat pumps and EV-charging stations.

Both of these trends (increase of electrical loads and increase of grid-forming converters) could also be studied independently. In the project, they are coupled and jointly varied through a single scenario parameter (p, the DER-VSM penetration of loads) due to the following reasons:

- Both trends are likely to take place simultaneously. One is motivated by consumers, causing the electrification of new loads. The other is motivated by regulators or the TSOs, who have to incorporate some sort of dynamic support contribution from DERs, since the replacement of synchronous machines also reduces their contribution to grid control.
- Coupling both trends reduces the complexity of the distribution grid representation, requiring less parameter sweeps and easing the presentation.

4.4.5 Parameter ranges for dynamic grid support

The scenarios investigated in the WP3 simulations study the dependence of the dynamic performance measures with regard to two parameters:

- DER-VSM support from dynamic loads, denoted by $p_{\text{DER-VSM}}$ and sampled between 5% and 100%
- CER-static replacement of synchronous generators, denoted by $p_{\text{CER-static}}$ and sampled between 0% and 60%

The two parameters are directly affecting the contribution of the different grid control devices specified in the previous sub-sections:

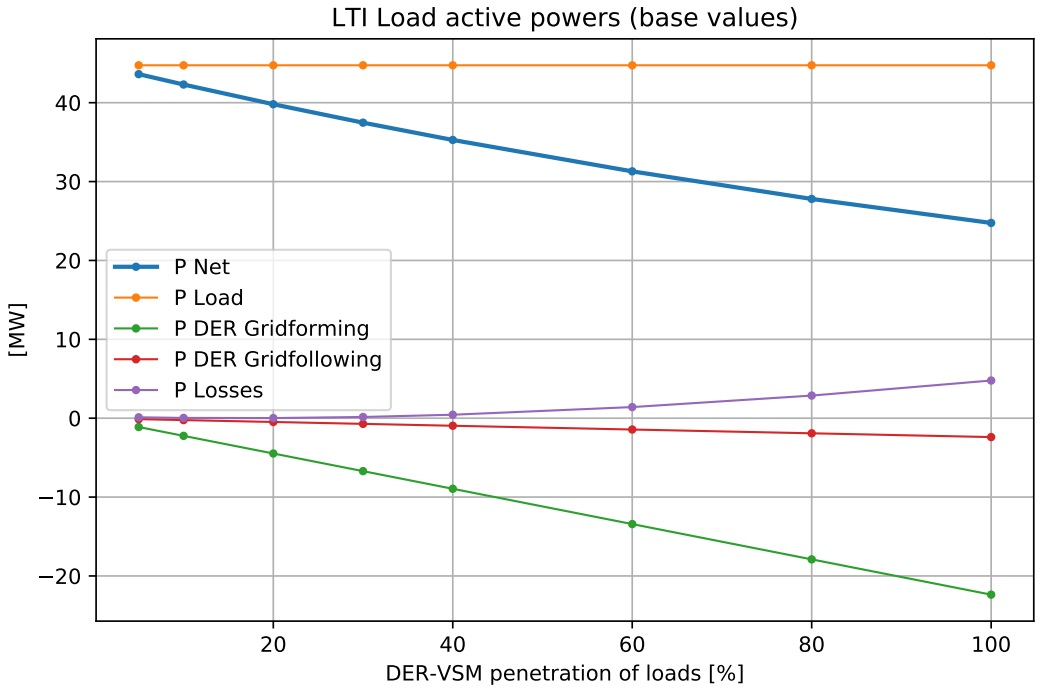

Figure 55: Nominal CIGRE distribution grid load composition for different penetrations of DER-VSM grid support.

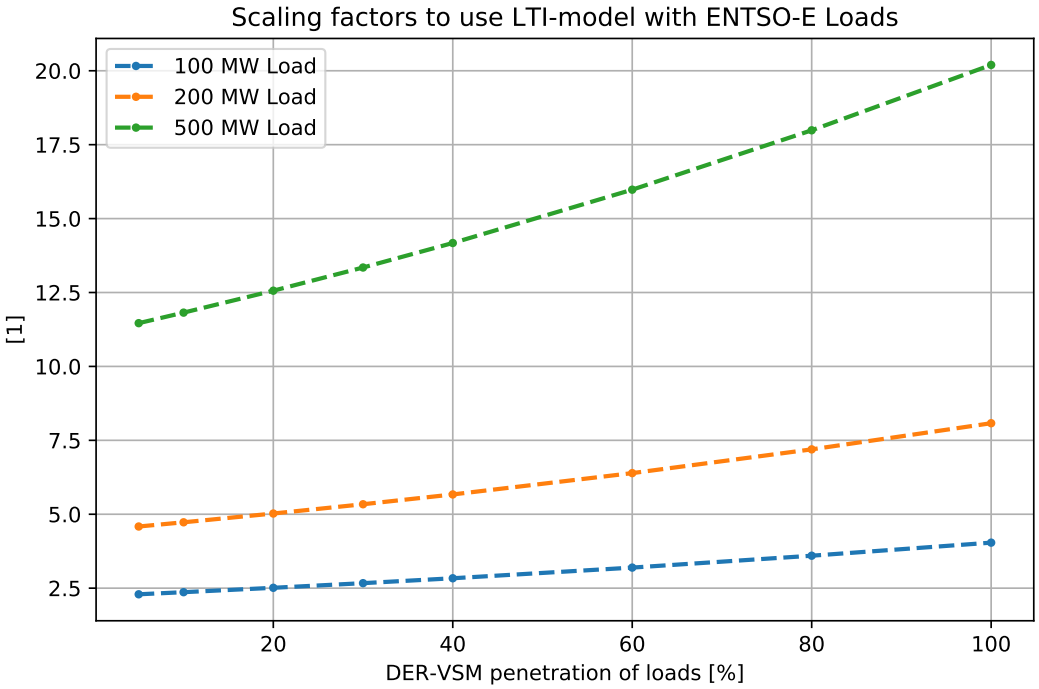

Figure 56: Scaling factor applied to transform the aggregated CIGRE distribution grid model to the ENTSO-E loads, for different load values and different DER-VSM penetration levels.

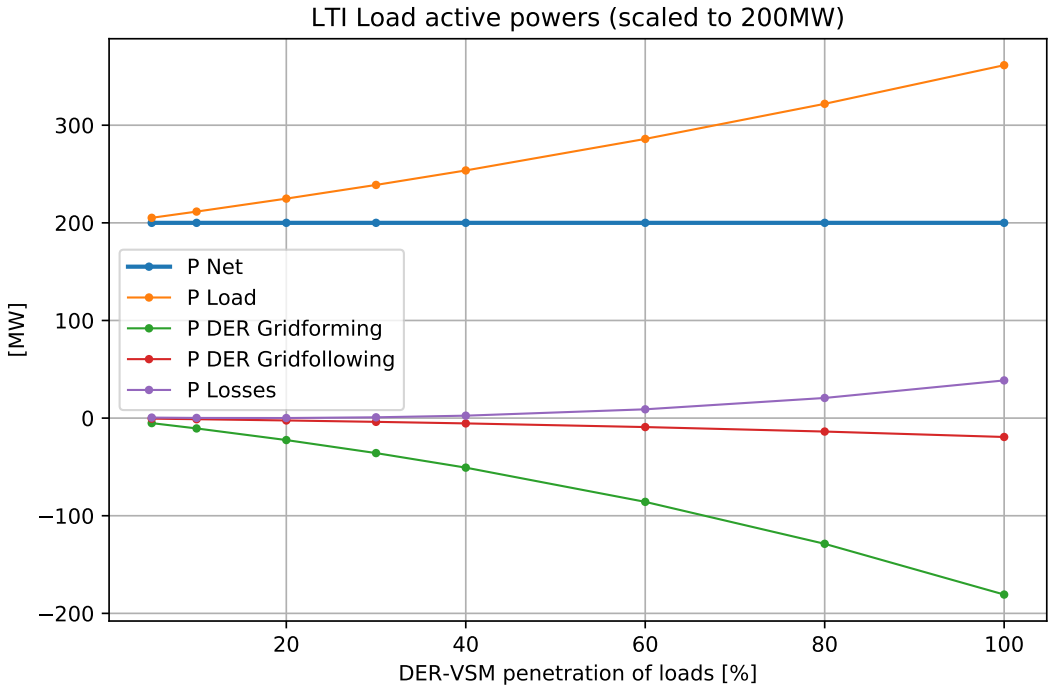

Figure 57: Nominal load composition for 200MW transmission grid load and different penetrations of DER-VSM grid support.

- Grid control with synchronous generators (static and dynamic):
  The base case is $p_{\text{CER-static}} = 0\%$, with all synchronous generators. A value $p_{\text{CER-static}} > 0\%$ indicates by how much the MVA-rating of each generator is reduced (and consequently also the injected powers and grid control capability).
- Grid control with static generators and loads:
  The base case is $p_{\text{CER-static}} = 0\%$ and $p_{\text{DER-VSM}} = 0\%$ with a certain number of static generation units (representing existing converter-based injections) and the 458 GW of static loads in the overall ENTSO-E system, both modeled through impedance models. A value $p_{\text{CER-static}} > 0\%$ indicates how much additional static generation is added to the system, as a percentage of the initial installed generation capacity from synchronous machines.

  A value $p_{\text{DER-VSM}} > 0\%$ indicates that some static load were added simultaneously with some grid-forming DER generation, cancelling each other and resulting in the same net load. The relation between $p_{\text{DER-VSM}}$ and the change in load and DER production is shown in Figure 57.
- Grid control with grid-forming converters:
  As discussed in the previous point, grid-forming converters are added for values $p_{\text{DER-VSM}} > 0\%$. The dynamic LTI model of the aggregated distribution grid captures the simultaneous impact of the increased load and the increased grid control functionality.

4.4.6 Key results and connection to other tasks

The key outcomes of this section are as follows:

- Scaling procedure to incorporate LTI load models
- Discussion of grid control functionality and its dependence on the investigated parameter ranges

The varying grid control functionality determines the relevant scenarios for development paths during the Energy Transition, that are investigated and compared with the subsequent grid simulations.

4.5 Comparative assessment

4.5.1 Problem description

The disturbance scenario, performance measures and grid-control scenarios described in D3.2 and D3.3 are used to create simulation cases, executed by the FLEXDYN simulator. The simulation results are used for the computation of the performance measures, that are presented and discussed in this section.

4.5.2 Variation of DER-VSM penetration

The result of the typical frequency trajectories in the three zones is depicted in Figure 58, for a share of grid-forming converters of $p_{\text{DER-VSM}} = 5\%$.

The mean frequency μ was computed for all areas and the process repeated for increasing values of $p_{\text{DER-VSM}}$, indicating higher shares of grid-forming converters in the distribution grids. Thereby, all synchronous machines remain fully active, only the dynamic characteristic of the loads in the system is modified.

Figure 59 shows the mean frequency trajectories for the Northern region of the ENTSO-E system. The nadir and the final value of the frequency is brought closer to 50 Hz with each step of $p_{\text{DER-VSM}}$, eventually reaching a trajectory with almost no overshoot (also denoted as overdamped). One can clearly make out an effect of diminishing returns, indicating that the first few percent of grid-forming converters in the distribution grids are the most important.

While the results in the other two regions in Figure 60 and 61 differ in magnitude, they still confirm the behaviour of increased frequency compensation. Note that a value of $p_{\text{DER-VSM}} = 100\%$ means that the grid-forming converter capacity in the distribution grids matches the initial load values. Since the converters operate only at 50% of the rated power and the loads were increased as well, production from synchronous machines and static generators is still required.

Figure 62 compares the nadir $\hat{\mu}$ and final frequency μ_∞ from Figure 59 to 61 in a single plot. The effect of diminishing returns for adding grid-forming converters becomes evident in this plot with the flattening out of the curves towards the right.

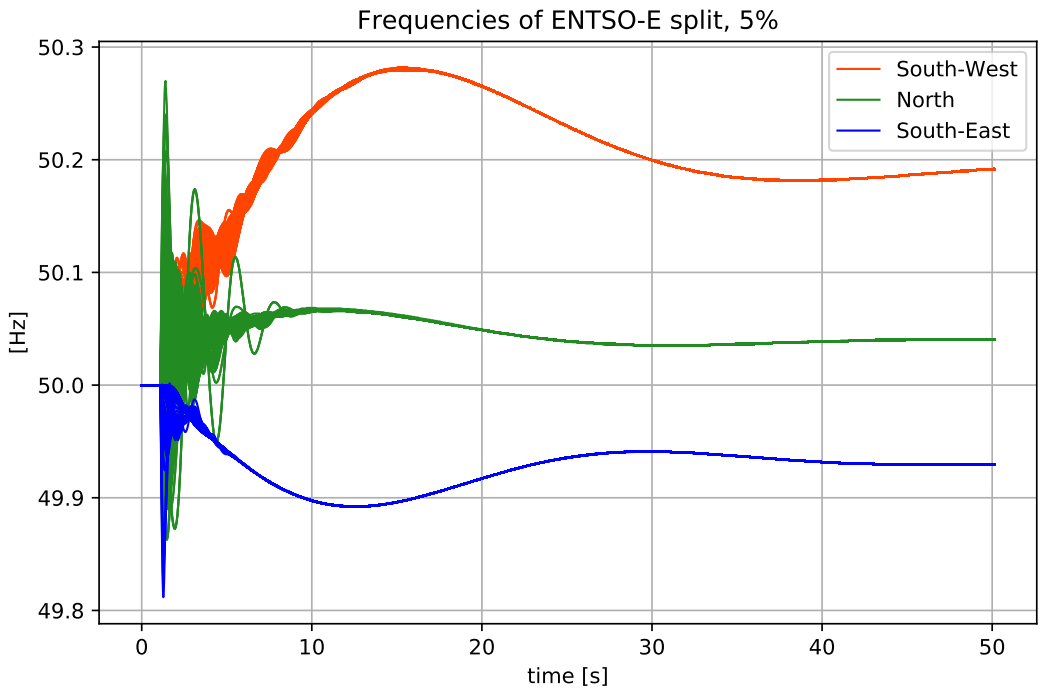

Figure 58: Typical frequency behaviour during ENTSO-E system split into three regions (colors).

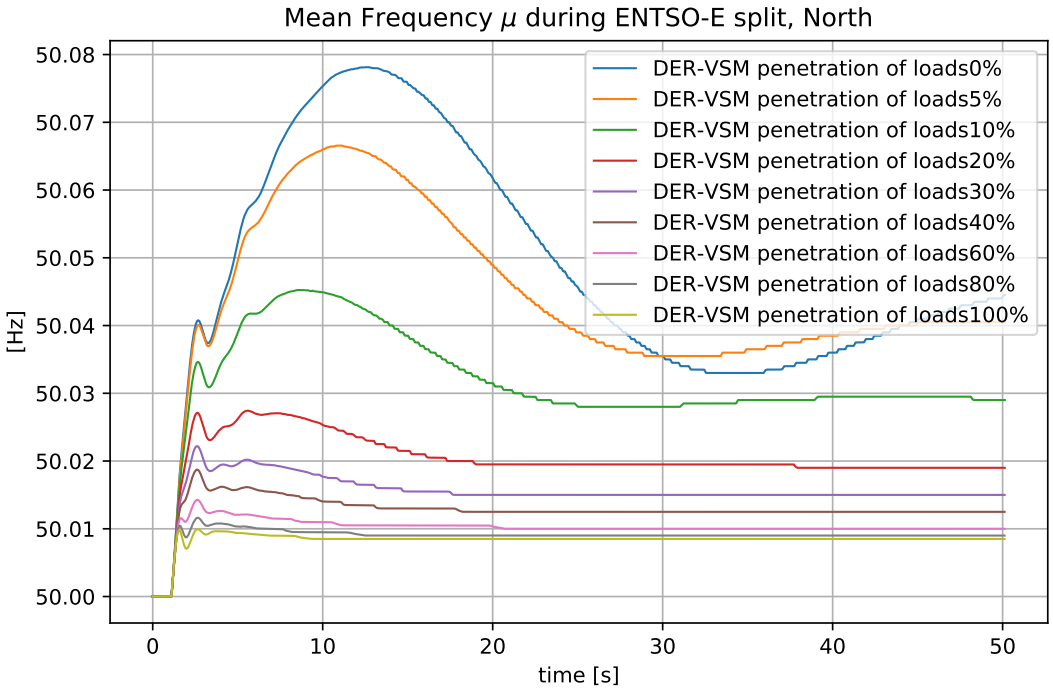

Figure 59: Mean frequency trajectories $\mu(t)$, computed for the Northern region of the ENTSO-E grid.

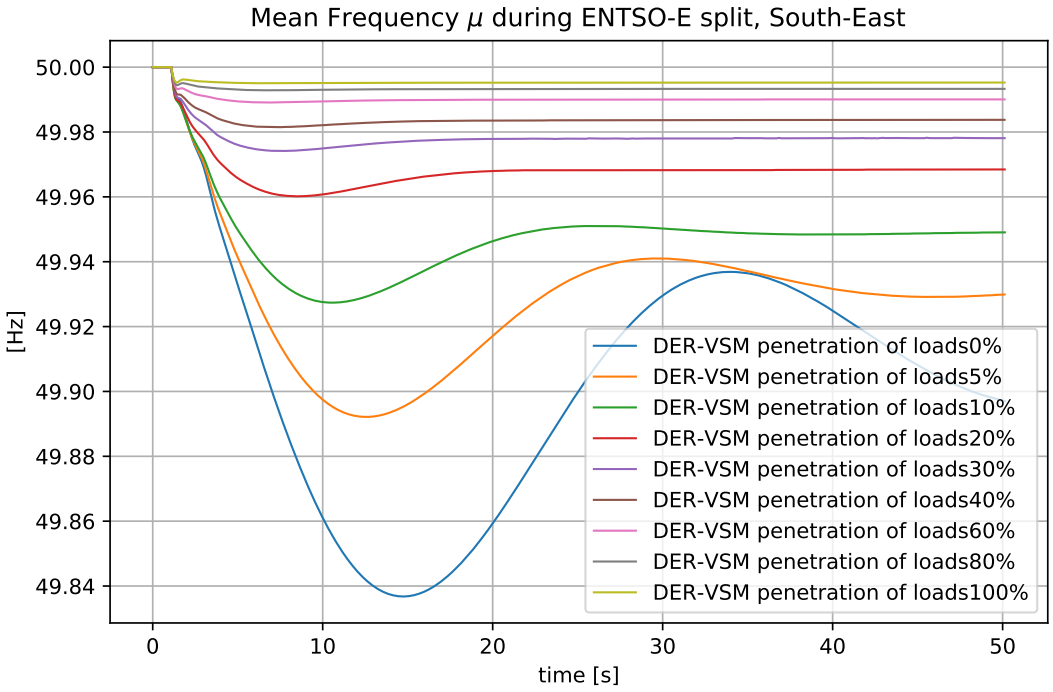

Figure 60: Mean frequency trajectories $\mu(t)$, computed for the South-Eastern region of the ENTSO-E grid.

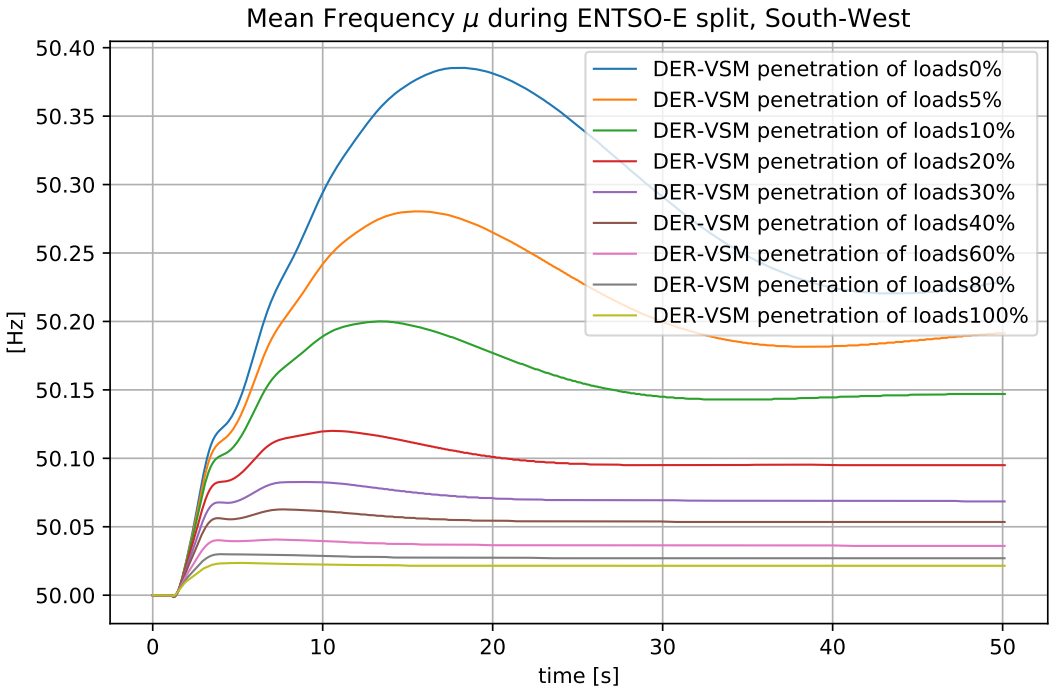

Figure 61: Mean frequency trajectories $\mu(t)$, computed for the South-Western region of the ENTSO-E grid.

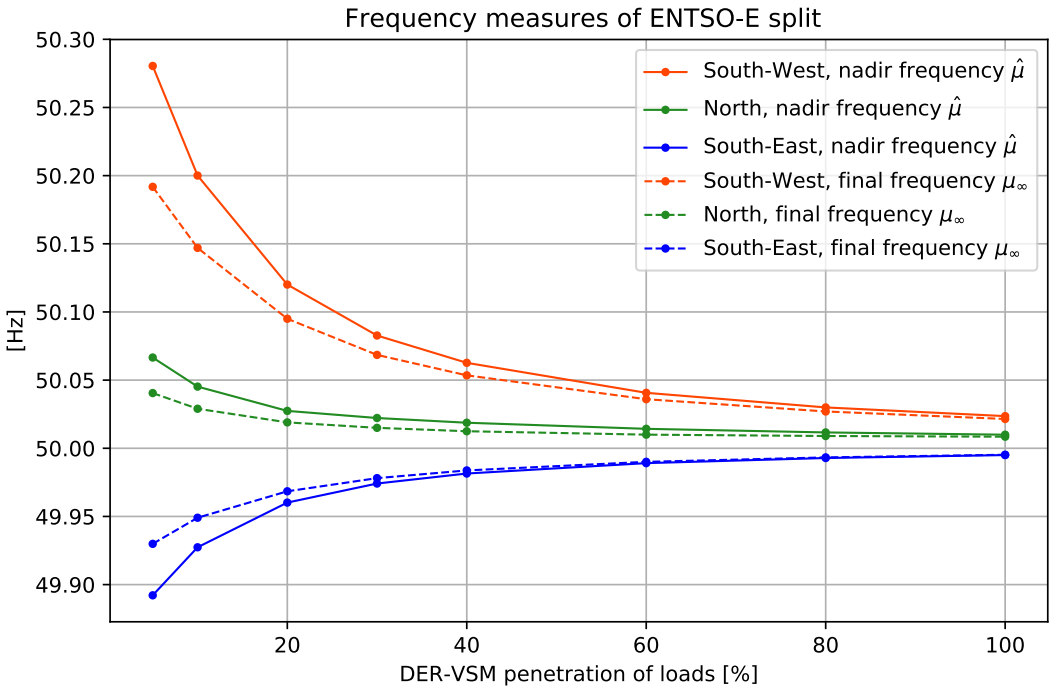

Figure 62: Nadir frequency $\hat{\mu}$ and final frequency μ_∞ for different shares of grid-forming converters $p_{\text{DER-VSM}}$ and three regions (colors).

4.5.3 Joint variation of CER-static replacement and DER-VSM penetration

The previous section showed the frequency trajectories for the base case with all synchronous machines fully active, combined with varying shares of DER-VSM penetrations.

The simulations of the full range of DER-VSM penetrations was repeated for cases with decreasing shares of synchronous generation, replaced by static generators, as indicated by $p_{\text{CER-static}}$. The results shown in this section correspond to three different values $p_{\text{CER-static}}$ =0%, 30% and 60%.

In total, there are 4 different parameters that are varied between the simulations:

1. Total rated power of synchronous generators
2. Total power of loads (active and reactive)
3. Total rated power of converters at transmission grid level without grid support (CER-static)
4. Total rated power of converters at distribution grid level with grid support (DER-VSM)

The cases of converters at transmission grid level with grid support (CER-VSM) and converters at distribution grid level without grid support (DER-static) are not varied. However, the main difference lies between the case with and without grid support (static and VSM) since all converters are distributed over the entire power system.

Due to the power balance requirement, the sum of all variations must equal zero (accounting for losses), leaving 3 possible independent degrees of freedom for variation. Additionally, another constraint on the system load parameter is introduced for the parameter variation, motivated by the illustration of different development paths. The two following sections present two possible scenarios for the parameter variation with the system load constraint. In the first case, the load grows proportionally with the share of distribution generation with support (DER-VSM) and the reduction of synchronous machines is compensated by static generation (CER-static). In the second case, the load is constant, and the reduction of synchronous machines is compensated by both CER-static and DER-VSM in different proportions.

4.5.3.1 Scenario with load growing proportional with DER-VSM

Figure 63 shows the average frequency's final value and nadir. It can be seen, that the parameter $p_{\text{DER-VSM}}$ has a much stronger impact on the nadir than the parameter $p_{\text{CER-static}}$ In fact, beyond a $p_{\text{DER-VSM}}$ share of 20%, there is almost no difference by varying $p_{\text{CER-static}}$. This means that the grid-forming converters in the distribution grids have effectively taken over all the grid control from the synchronous machines, it does not matter when even 60% of the are replaced with static generators. Of course 20% of a total load of 458GW are more than 90GW of grid-forming converters. However, such numbers will become accessible if the energy transition takes place, since

- Most battery storages are used for other purposes than dynamic grid support. They need to provide such dynamic services only during a short time period.
- Not only battery storages can provide this service, but also PV-converter operating not at full capacity, but with some headroom. This will also become a common situation, since overcapacities of PV-production may become common during mid-day to cover more hours of the morning and the evening demand.

Inspecting the nadir in the lower plot of Figure 63 of the South-West (orange) yields another interpretation when comparing the case with full synchronous generation (bold orange) and the case with 60% reduction of synchronous generation (dashed orange): Even when **more than half of the synchronous generation** would be removed, causing a 300mHz increase in Nadir, one can recover the performance by **adding 10% to the DER-VSM penetration** of the loads. For Switzerland with a hypothetical load of 10 GW, this would correspond to 1 GW of converters with grid support.

The two percentage values can not be directly compared, since one is expressed relative to the synchronous machines (there are also other static generators in the system), one is expressed relative to the total load. A direct comparison of the effectiveness of static converters vs. converters with grid support is presented in the next section. Furthermore, the synchronous machines are operated in the current setting of the droop constants. Higher values would be possible, but require also a much higher procurement of frequency reserves.

However, the results show that the compensation of a global replacement of synchronous machines with CERs is possible, if a small share of the converters is equipped with grid-forming control schemes.

Note, that for moderate penetration levels of converter-based generation sources (either centralised or distributed), the grid-control functionality can also be achieved using grid-following control approaches with additional frequency control loops. However, for increasing penetration levels of converter-based generation sources, if only grid-following control is used, the grid stability is at risk. The stability limit depends mostly on two sources:

- The strength of the transmission grid connecting to the converter (characterized by the Short-Circuit-Ratio).
- The structure and load-flow situation of the local distribution grid, including other local generation sources.

At some point the stability limit is reached, requiring grid-forming converter control. Additionally, grid-forming converters improve some dynamic performance metrics not tackled by grid-following systems, such as ROCOF.

The upper plot of Figure 64 shows the same comparison for the ROCOF (computed over 2 seconds). The plot confirms the trend, that DER-VSM penetration improves the ROCOF, but the slope is flatter and the effect of diminishing returns not as pronounced. This means, grid-forming DERs can not fully reduce the 2 second ROCOF. In fact, inspection of Figure 59 shows, that a ROCOF computed over a smaller time window than 2 seconds, say 500ms, stays almost the same. This shows that the initial ROCOF is not affected very much through the grid-forming converters.

The three previous figure showed performance measures computed form the mean frequency μ in each area. Finally, the lower plot of Figure 64 shows $\hat{\sigma}$, the peak frequency deviation, denoting a measure how well the frequencies in each area stay together. If the peak relative frequency deviation $\hat{\sigma}$ becomes too high, cascades of outages may occur, potentially causing black-outs or further separating the areas. The trend of the performance measure is very flat, only high DER-VSM penetrations can significantly reduce the peak relative deviation. Note that the DER-VSM converter a spread of the entire regions with the same tuning irrespective of the location. This contrasts with the common tuning approach for PSS, which is very much area dependent to control specific inter-area oscillations. A more sophisticated individual tuning approach may dampen specific oscillations to further reduce the relative frequency oscillations and keep the system together.

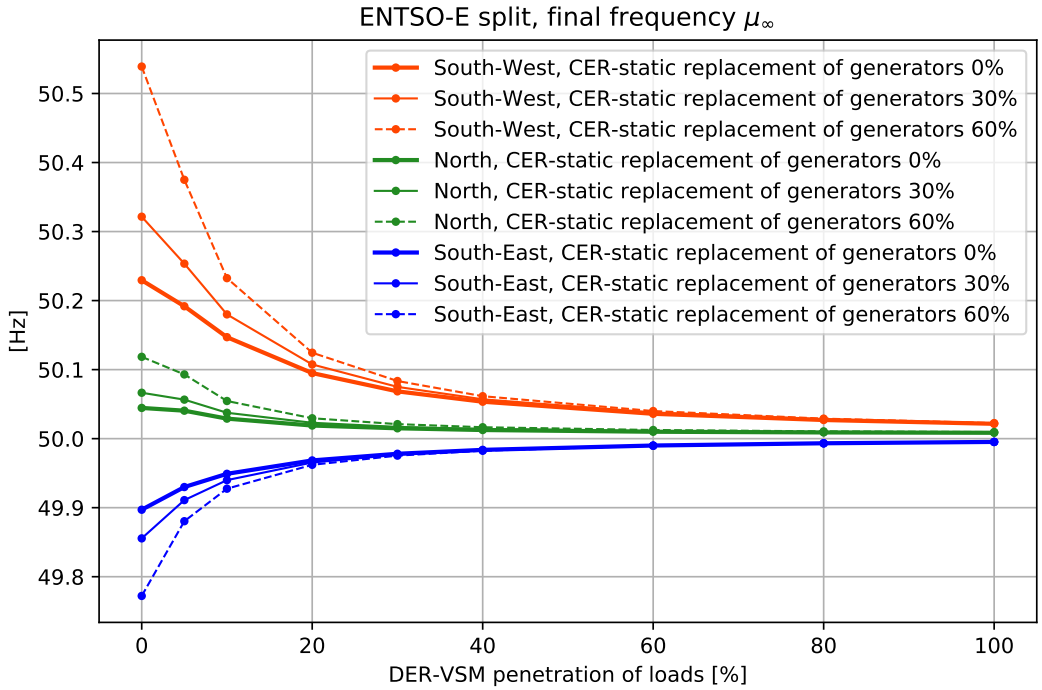

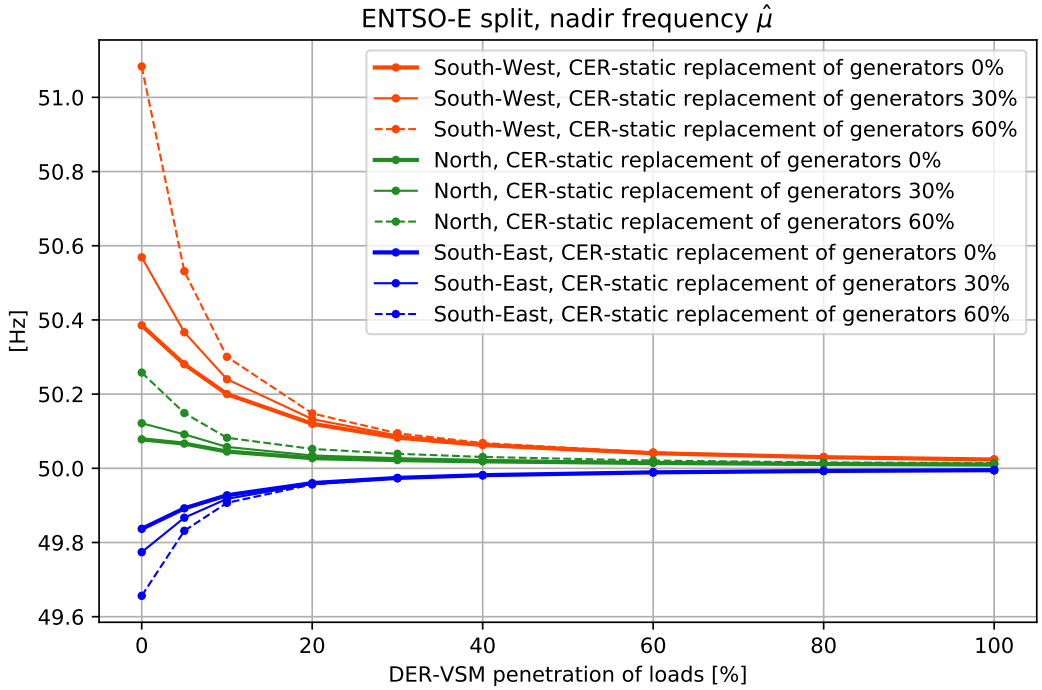

Figure 63: Final frequency μ_∞ and frequency nadir $\hat{\mu}$ for different shares of grid-forming converters $p_{\text{DER-VSM}}$ (horizontal axis), three shares of synchronous generation replaced by static generation $p_{\text{CER-static}}$ (bold, thin, dashed line) and three regions (colors).

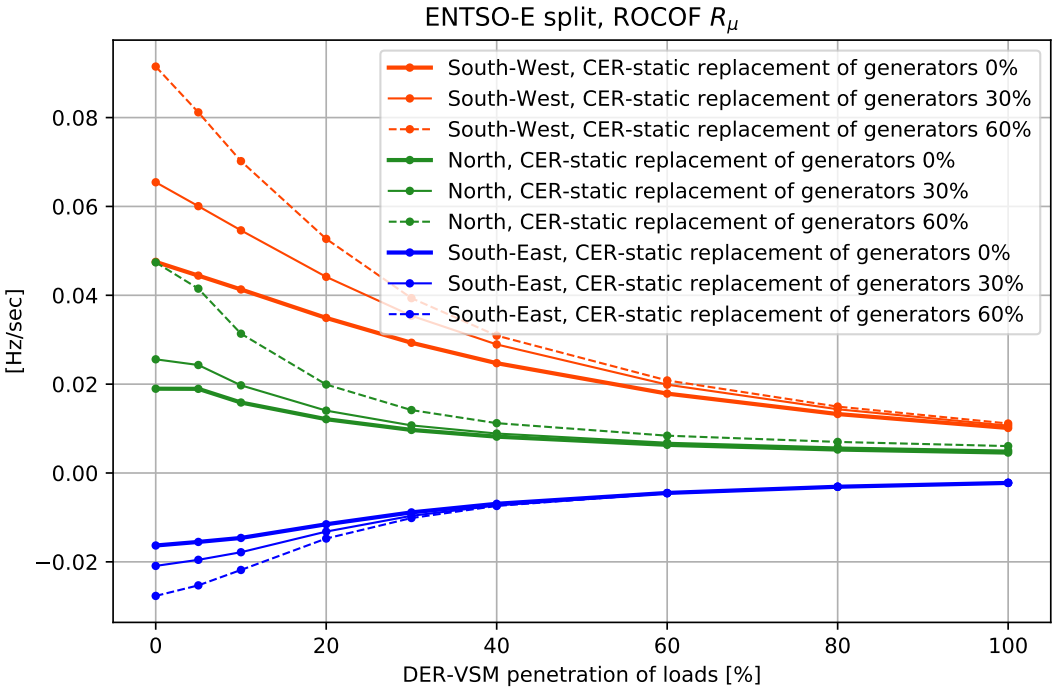

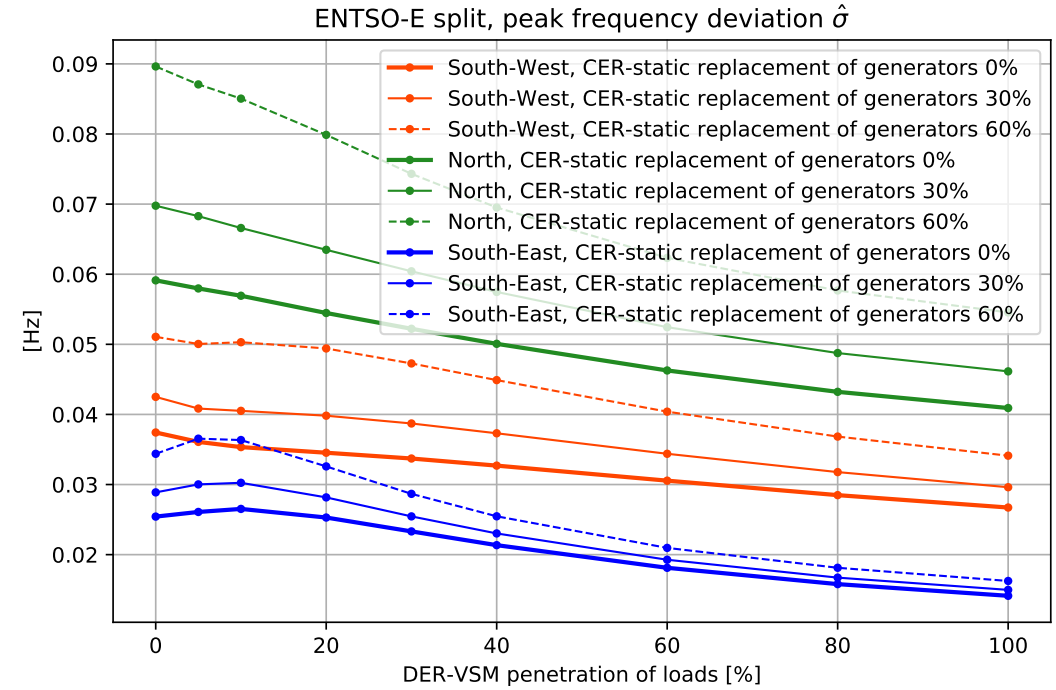

Figure 64: Frequency ROCOF R_μ (computed over 2 seconds) and peak relative frequency deviation $\hat{\sigma}$ for different shares of grid-forming converters $p_{\text{DER-VSM}}$ (horizontal axis), three shares of synchronous generation replaced by static generation $p_{\text{CER-static}}$ (bold, thin, dashed line) and three regions (colors).

4.5.3.2 Scenario with constant load

In the second presentation, the load is constant, and the reduction of synchronous machines is compensated by both CER-static and DER-VSM in different proportions. Since CER-static and the system loads both use a constant impedance model, it is possible to post-process the sampled results of the previous section to obtain the results for the constant load assumption.

Figure 65 shows the final value and the nadir of the frequency in each region. The bold horizontal line denotes the base case, with no reduction of synchronous machines. The other two lines (thin and dashed) present the case with 30% or 60% of synchronous machines replaced by converters. The horizontal axis denotes different distributions between the two converter types, static converters (CER-static) and grid-forming converters with grid support (DER-VSM), used for the replacement. It can be seen, that for low shares of grid forming converters (left of the horizontal axis), the performance gets worse. The nadir of the system frequency exceeds 51 Hz or can drop below 49.8 Hz. This range of nadir values could, in combination with critical local ROCOF values, already start under-frequency-load-shedding (UFLS) measures in certain parts of the network [10]. Also note, that the performance is potentially worse for higher inter-area power exchanges before the system split and more accurate dynamic models of the static converters. However, the results confirm the findings of the previous section: when about 5-10% of the new converters are equipped with grid support, the nadir performance can be recovered.

Figure 66 shows that the ROCOF requires a share of 20-30% of new converters to be equipped with grid-support in order to recover the performance. Even more is required to recover the relative frequency deviation. However, note that this could be improved with a dedicated tuning, since the optimal damping of relative oscillations was not considered for the tuning of the converter control. Again, the average ROCOF value computed over 2 seconds is in the range of a most 0.1 Hz, does not seem critical regarding protection settings or load shedding. However, ROCOF values of individual generator units and computed over shorter intervals (e.g. 200ms) were observed to be much higher, in the range or above 1 Hz/s. Similarly, these values further increase with higher power imbalances before the system split.

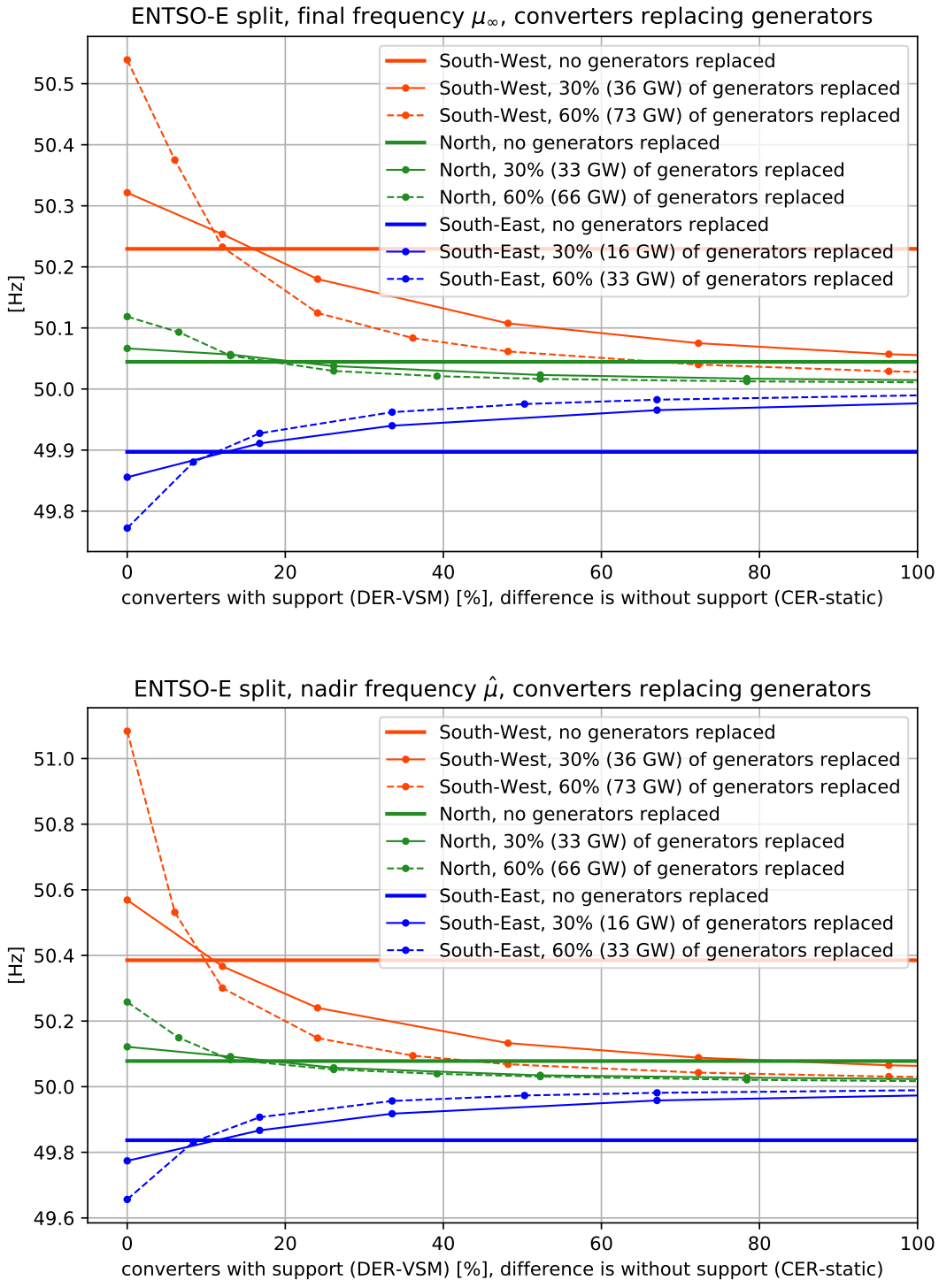

Figure 65: Final frequency μ_∞ (top) and frequency nadir $\hat{\mu}$ (bottom) for three shares of synchronous generation replaced by new converters (bold, thin, dashed line) and three regions (colors). The horizontal axis denotes different distributions between static converters (CER-static) and grid-forming converters with grid support (DER-VSM). On the left of the horizontal axis (0%) all new converters are static, on the right (100%) all new converters have grid support.

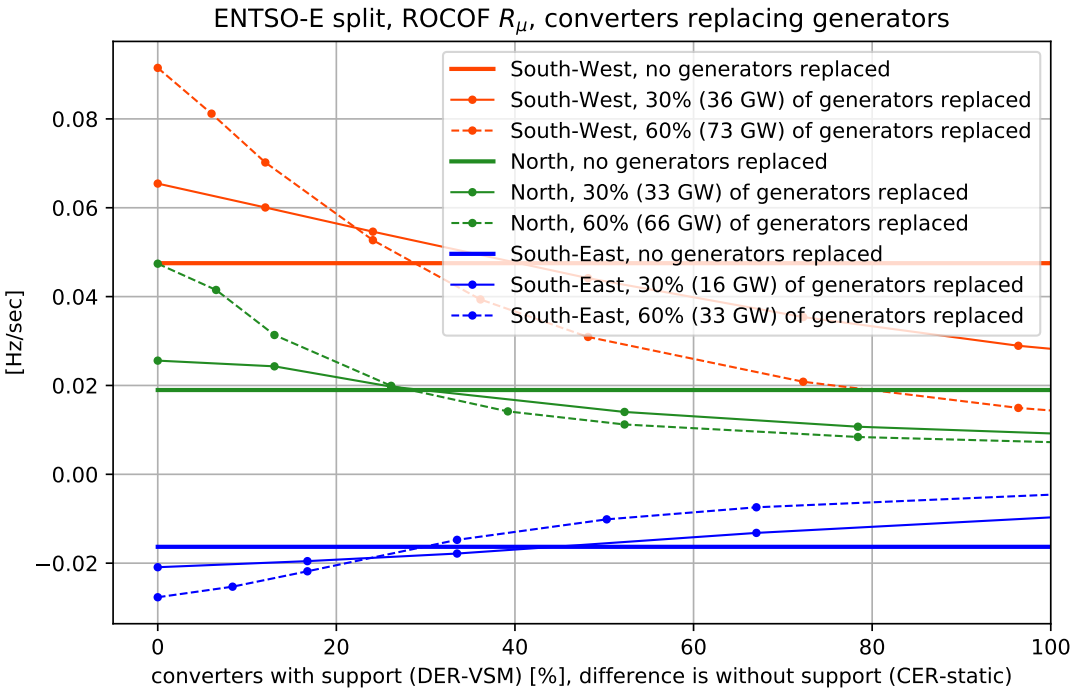

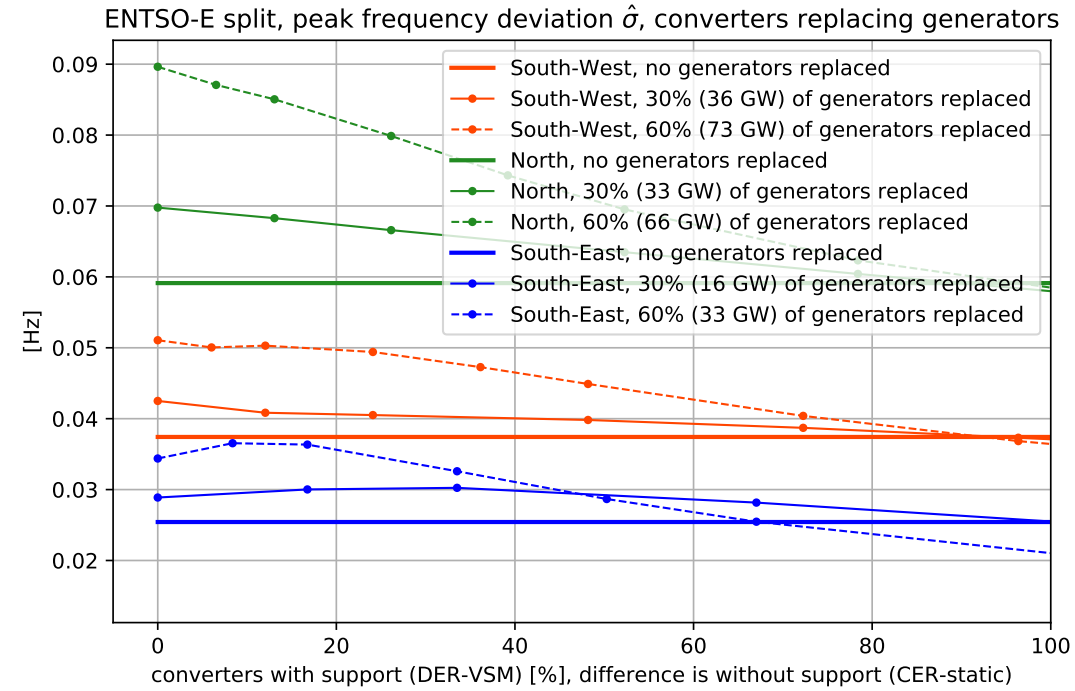

Figure 66: Frequency ROCOF R_μ (top, computed over 2 seconds) and peak relative frequency deviation $\hat{\sigma}$ (bottom) for three shares of synchronous generation replaced by new converters (bold, thin, dashed line) and three regions (colors). The horizontal axis denotes different distributions between static converters (CER-static) and grid-forming converters with grid support (DER-VSM). On the left of the horizontal axis (0%) all new converters are static, on the right (100%) all new converters have grid support.

4.5.4 Key results and connection to other tasks

The key outcomes of this section are as follows:

- A critical ENTSO-E disturbance scenario is simulated using different converter types (grid level, with or without support) replacing synchronous machines.
- An aggregated presentation of the performance measures is presented to see how the reduction of synchronous machines impacts performance.
- The results are interpreted and discussed to identify the support requirements for converters on the global ENTSO-E level.

The insights gained from the ENTSO-E simulations serve as input to Section 5, providing a synthesis and recommendations for Switzerland.

5 Evaluation of Swiss role

5.1 Problem description

So far, the project has developed general methods, models and quantitative assessments that can be applied for any distribution grid (converter modeling), can be applied to any power system (converter aggregation) or provide insights on the general ENTSO-E level (WP3 simulations).

It is of interest to Swiss policy makers, Swissgrid and DSOs, how these finding affect Switzerland as part of the ENTSO-E CESA grid and which actions need to be taken to make the Swiss power system resilient to dynamic challenges of the energy transition. This section first presents the findings of WP3 in view of the Swiss perspective and then continues to propose a Swiss strategy to tackle the challenges and opportunities identified in the ACSICON project.

5.2 Conclusions for Switzerland

We recap the most important project findings of WP3 as well as related investigations in WP1 and WP2, with particular insights from the Swiss perspective.

- In practice, the usage of existing and newly built converters connected to storages or PV-sources is very attractive. All hardware components are installed anyhow for different use-cases (production, price arbitrage, self-consumption, peak-shaving, charging of EVs...) and the grid-forming DER-VSM support is only a change to the control-structure. No further measurements are required that are not performed anyhow for conventional grid-following converters. This means, the existing converter infrastructure could be upgraded through the software interface to use a grid-following control approach. Grid-control actions during strong disturbances are very limited in duration and will not affect the main operation of the converter units. Since the aforementioned use-cases are a strong ongoing development at the center of Swiss ES2050, the **deployment of grid-forming DER support in Switzerland comes at little additional effort** compared to other solutions, like dedicated FACTS or synchronous condensers. Additional frequency support could also be contributed from the remaining synchronous machines in the system. Note that this would imply to keep machines running at part load purely for reserve reasons.
- Figure 63 shows the frequency nadir during the system split for three different levels of synchronous machines replaced by converter-based generation without grid support (today with 0%, 30% and 60%). These percentages represent discrete **points along a development path of the energy transition**. In order to **preserve the initial frequency nadir** of about 50.4 Hz in the Southwest (which includes Switzerland) when 30% of the synchronous machines are replaced, it can be seen that about 5% of the peak load should be provided by DER with grid support. For 60% of synchronous machines replaced, the recommended share of DER with grid support increases to 8% of the peak load. If less grid support than the recommended share is provided by the DER, a loss in performance is to be expected, e.g. an increase in nadir or ROCOF. The case of **no DER grid support** shows that the **loss of performance accelerates** as more synchronous machines are disconnected. In Figure 63, the Nadir in the South-West grows only from 50.4 to 50.6 Hz when 30% of the synchronous machines are disconnected, but can reach **critical values above 51 Hz** for the case of 60%. Note that two trends further reinforce the loss of performance. A reduction in synchronous machines and inertia can occur temporarily (e.g. during times with a low system load but high PV-production), even though the production from synchronous machines is much higher when seen from the annual energy balance. Furthermore, the impact on the Nadir becomes stronger for higher initial power imbalances, either due to larger power exchange between the zones or cascading outages into multiple islands (observed in more detailed studies of the ENTSO-E system [12]).
- For the **short-term perspective** and to **initiate the development to dynamic grid support from**

DERs, a share of converters with grid-support of 1% of the installed peak load is proposed. This value would compensate the loss in dynamic performance if about 6% of the synchronous machines were replaced by converters without grid support (estimated through simple interpolation of the Nadir in Figure 63, one fifth of 30%). Depending on the replacement of synchronous machines, the DER support of 1% of the peak load can **improve the Nadir of the tested scenarios up to 100 mHz**. For Switzerland, this would mean a **mid-term goal of 100MW grid-forming converters in Switzerland** (assuming 10GW of peak load), that could be procured using a regulation-based or a market-based approach. The effectiveness of this approach is strongly influenced by the frequency support actions taken on the ENTSO-E level. The coordinated ENTSO-E efforts dominate the impact on the dynamic performance. It is not possible for a single country to maintain the frequency performance alone.

- For the long-term perspective, WP3 has identified a DER-VSM penetration of 5% - 10% of the installed peak load as a suitable amount to maintain today's level of system stability during strong transients. For Switzerland, this would mean a **mid-term goal of 500MW to 1GW grid-forming converters in Switzerland** (assuming 10GW of peak load), in a future where more than 50% of the synchronous generation has been removed from the overall ENTSO-E grid.

- The **additional costs of a grid-forming converter** compared to a grid-following converter need to be determined for the specific project. However, to obtain a rough estimate of the additional cost for end-consumers using grid-forming converters, a brief market analysis has been performed. Two converters from the same manufacturer and vendor, the same size (power rating), comparable quality and similar interface functions, are compared: The *SMA Sunny Tripower 8.0* (grid following) and the *SMA Sunny Island 8.0H* (grid-forming, can be used for islanding) have very similar high efficiency and performance parameters [31, 30]. The main difference between the two 8 kW converters is the grid-forming capability, leading to a price increase of about 70% [2]. While the grid-forming converter is specifically designed for off-grid applications, the technical capabilities are the same as those for grid-forming frequency and voltage support. For larger installations with higher power rating, economies of scale can be expected, for both the absolute converter costs and the price difference. In any case, the price difference only affects the converter costs (typically accounting for 20% or less of the project costs) and not the costs for battery cells or photo-voltaic modules, which are assumed to be installed anyhow for use cases like production, self-consumption or peak-shaving. In conclusion, the grid-forming capability will increase the installation costs of a typical use case for RES less than 10-15%. Note that some grid support can in principle also be obtained with *grid-following* converters, for which the price increase can expected to be smaller.

- For the desired effect on the transmission grid level, the grid-forming converters can be placed anywhere in the distribution grid, in a decentralized manner of partly centralized close to the transformer. For practicality reasons the DER-VSM support should initially come preferably from **Swiss utility-size converter units** (order of 1MW), several of which are currently installed in Switzerland and used for some of the aforementioned use-cases (e.g. price arbitrage or conventional grid-following frequency reserve). This way, tuning, operation, and the performance during dynamic transients can be closely monitored before a wider rollout also including smaller units is taking place.

- For moderate penetration levels of converter-based generation sources, the grid-control functionality can also be achieved using grid-following control approaches with additional frequency control loops. An example from Switzerland is the EKZ battery in Volketswil, used in the primary reserve market. However, for increasing penetration levels of converter-based generation sources, if only grid-following control is used, the grid stability is at risk, depending on the local transmission grid strength and distribution grid configuration. In Switzerland, this could become an issue for **rural grids with a weak transmission grid connection** and high local PV-production.

[2] Costs obtained at www.europe-solarstore.com, on May 31st 2021: SMA Sunny Tripower 8.0 (1519 EUR) and SMA Sunny Island 8.0H (2559 EUR), a price difference of 68%. The relative price difference can be confirmed with several other online vendors, e.g. www.shop-muenchner-solarmarkt.de.

- The DER-VSM converter needs to operate with sufficient headroom, for example by batteries used for peak-shaving or self-consumption. The flexibility could also be provided from PV-converters operating at part-load. This becomes more realistic in view of the envisioned creation of a substantial over-capacity of PV-generation in Switzerland (requiring storage or curtailment during some times of the day to use more energy in the evening or morning). Furthermore, the required **headroom can also be shared between PV-converters and storages** depending on the time of the day.
- They can be **integrated with the network tariffs** accrued at grid voltage level 1, accounted for by Swissgrid and distributed to end-consumers by rolling over the network levels. It is to be expected that the DER-VSM support overlaps with today's frequency containment reserve. DER-VSM support could also be combined with today's market based procurement, only **changing the reserve prequalification procedure** to account for the grid-forming performance.
- Switzerland is at a **central location of the ENTSO-E grid**. This means it could potentially **"export" DER-VSM support** to other countries. It could also provide **DER-VSM support specifically tuned to its location in the ENTSO-E grid**. This aspect has not been considered in the WP3 investigations, where all DER-VSM units were equally distributed across the loads and used the same tuning. However, a wide range of literature and experience exists on the tuning of conventional grid control devices, such as PSS and FACTS. Of course, both of these aspects ("export DER-VSM support" and the "dedicated tuning") need a close coordination with ENTSO-E and the other European TSOs.
- An important opportunity for Swiss-based DER-VSM support would also be the installation of an **HVDC-terminal in Switzerland**, as was recently investigated in projects on hybrid AC/DC links in Switzerland. Such a terminal is essentially a large-scale converter, that can support the power sytem stability very effectively. Previous studies have shown that 2-3 HVDC links can replace the entire damping currently performed by the European PSS of the synchronous machines [11].
- While the dynamic challenges of the energy transition to the power system security is recognised by all ENTSO-E and all TSOs, and grid-forming converters and their control approaches are studied academically and developed in industry, they are not yet deployed on a large scale. Pioneering DER-VSM deployment is an opportunity for Switzerland to be **truly innovative and contribute a new service to the future European power system security**.

5.3 Recommendations

Based on the previous insights of the WP3 findings from the Swiss perspective, a potential strategy has been developed. It allows the stakeholders of the Swiss energy sector, to initiate and carry out the recommended DER-VSM deployment.

The proposed strategy is depicted in Figure 67 and operates in three phases:

- **Phase 1** studies the results of ACSICON and related projects and collects additional expertise from Academia, the TSO, and component manufacturers. The goal is to refine the proposed strategy for a stepwise integration of grid-forming converters.
- **Phase 2** performs the first two steps of the DER-VSM deployment, reaching about 10MW capacity.
  - A demonstrator of a utility size DER-VSM converter (e.g. combined with a battery) shows the overall feasibility of the intended DER-VSM deployment.
  - A small rollout of multiple DER-VSM converters (if possible also utility size) follows up.

  Both steps are closely monitored, the lessons reviewed and for the second step also coordinated with the findings of other TSOs in the ENTSO-E grid.
- Finally, **Phase 3** deploys the DER-VSM support on a larger scale. Here, a decision is taken whether the procurement shall occur through regulatory requirements, e.g. all DER above x MW

are required and compensated to install grid-forming converter control schemes, or whether a market-based procurement is preferred. Both approach have their pros and cons. Other frequency reserve products are all procured in a market-based fashion, but DER-VSM support also tackles the low-inertia aspect, that is currently intrinsically provided by synchronous machines. Of course this decision should also be coordinated with other ENTSO-E members. The intermediate deployment goal (1% of the peak load, about 100MW) can be updated according to the needs and replacement of synchronous generators.

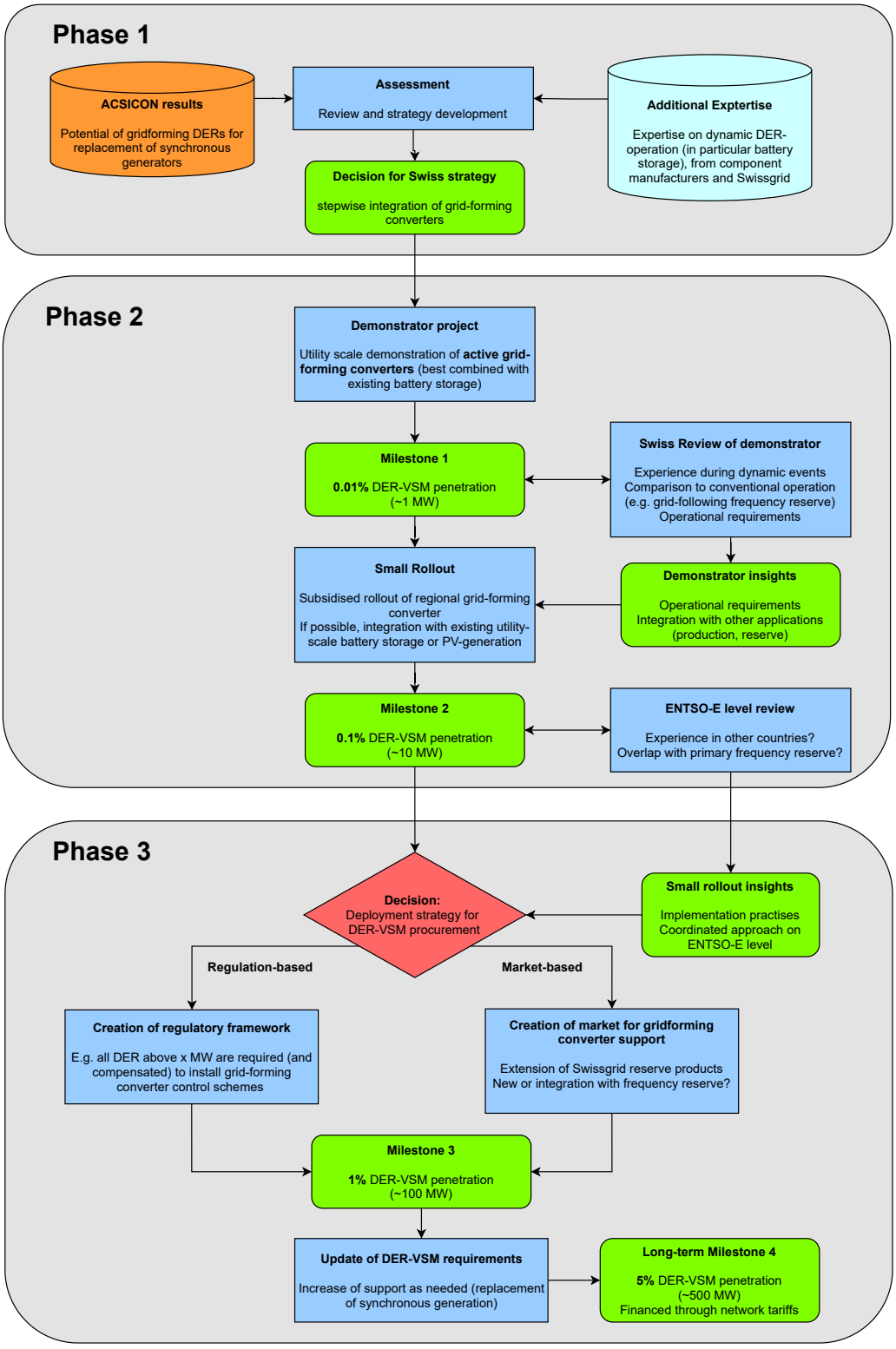

Figure 67: Proposed strategy for Swiss deployment of grid-forming converters to counter dynamic challenges of the ES2050 and the European energy transition.

6 Conclusion

This chapter summarizes the project conclusions, summarizes the key added values for different stakeholders of the electricity sector and provides an outlook on future work.

6.1 General conclusions

Workpackage 1 of the project developed the dynamic distribution grid models used for the subsequent investigations in a holistic manner:

- First the emerging need for grid supporting converters was identified and representative converter control structures discussed:
  - Electricity is expected to be the fastest growing energy carrier over the next decades.
  - A significant share of the growth will come in the form of distributed renewables, embedded in the distribution grid.
  - The power systems currently relies on having a sufficient amount of synchronous machine based generation for sufficient equivalent inertia to respond to frequency changes, frequency control capability to correct short term frequency deviations and short-circuit strength to keep the operational voltage stable and provide sufficient fault current to activate protection systems in case of fault.
  - In many countries, the shift towards renewable energy results in decommissioning of synchronous machine based generation.
  - A significant share of the DERs will be non-dispatchable from the point of transmission grid operator. Thus, it is necessary to rely on local control to ensure that frequency and voltage support is provided.
  - There are principal difference between grid-forming and grid following converter control architectures. The provision of voltage and frequency requires a change in philosophy, as most DER today rely on grid following control architectures.
  - Use of grid forming or grid supporting control architectures allow converter based DERs to contribute frequency and voltage support services to the grid, as well as operate stably also in very weak grids.
- Two reference converter control architectures for grid-following and grid-forming control architectures were presented, to be used in the modelling of a benchmark distribution grid. The defined converter control architecture are generic, but also representative of commercial as well as academic control implementations. The models for distribution grid components, and in particular grid-following and grid-forming converters were validated in both the simulation tools (DYMOLA and FLEXDYN) of the two project partners. They produce very similar results, which ensures that the findings from all work packages are consistent, irrespective of which simulation was used. Furthermore, a procedure for scenario creation through scaling of the DERs has been presented and applied to the benchmark grid. Simulation experiments on the detailed model of the CIGRE benchmark system under varying levels of DER penetration has demonstrated the effectiveness of the distributed frequency support. This detailed model with parameterization of DER penetration level and representative control schemes will be used in WP2 as basis for the derivation of simplified aggregated models of the distribution grid.
- A tutorial then summarized the harmonic stability assessment for converter control system tuning based on modal analysis that has also appeared in [23]. Modal analysis was then applied to adapt the tuning of the DERs to the CIGRE grid yielding a robust set of parameters with which the DERs can operate reliably, both in grid connected and islanded mode. This parameter set has been used in the simulation in Section 2.3.6 as well as the linear aggregation studies documented in [14].

Workpackage 2 investigated aggregation procedures to model the dynamic behavior of distribution grids on the transmission grid level in an aggregated manner:

- A linear aggregation procedure was developed to be used to generate low order equivalents of ADNs to be used as load models in large-scale RMS simulations. The procedure has been tested on the CIGRE benchmark ADN under penetration levels ranging from 5-100 %. The main limitation of the linear model, is that it is linearized and thus ignores capacity constraints of DERs unless they were already activated at the operating point of linearization. Thus, the model makes the implicit assumption that sufficient headroom is available in each DER.
- Both the full order nonlinear and reduced order linear models have been implemented in the ConverterStab toolbox [22]. Furthermore, the embedding of the reduced order model was demonstrated in a small test network and the response was compared to that of the original full order nonlinear model. Under worst-case conditions of a penetration level of 100 % the reduced model can be used to predict the nadir frequency following a generation loss of 6.25 % within an accuracy of 3 mHz. The reduced order models serves as basis for the scenario study on ENTSO-E network that is reported in the WP3 report.
- Investigations with the detailed nonlinear converter models with the CIGRE grid connected to small transmission system were carried out to identify the limits of the linear model representation. Two key findings are as follows:
  - The linear aggregation model performance is very similar to the nonlinear aggregation even for high loadings of the converter system. Only when less than 10% headroom is available, the internal converter constraints become critical.
  - A nonlinear aggregation of the distribution grid can also be performed, using on model of a converters with grid support, one model of a converter without grid support, and one aggregated load with a rating equal to the sum of all elements in the distribution grid. This approach keeps the headroom constraint, but loses the information on local distribution grid stability. It is also still much more complex for numerical simulation than the simple linear aggregated model.

Workpackage 3 studied the dynamic challenges and opportunities of the energy transition on a global ENTSO-E transmission grid level:

- The focus was on distributed converter-based generation with and without grid-supporting functionality, aggregated at the transmission grid level.
- The investigations have shown that the dynamic distribution grid models developed in WP2 can be efficiently used in the large transmission grid investigations, to gain insights regarding the new grid control capability. Extensive simulations of a detailed ENTSO-E transmission grid model during a large disturbance (system split) investigated their potential to compensate the deterioration of dynamic performance when synchronous generation is replaced by static centralized generation units in the grid.
- It has been found, that if a small share of the converter new converters (5%-10%) is equipped with grid-forming capabilities (such as the VSM control scheme), the dynamic performance can be maintained at today's level, even if more than 50% of the synchronous generation is otherwise replaced by static (grid-following) converters. The effect is particularly strong for the frequency nadir and low levels of grid-forming DER penetration, with diminishing returns for higher levels of grid-forming DER. For ROCOF and relative frequency deviation the effect is still present, but less pronounced.
- Without support measures from converters, the nadir of the system frequency in the simulations can exceed 51 Hz or can drop below 49.8 Hz. This range of nadir values could, in combination with critical local ROCOF values, already start under-frequency-load-shedding (UFLS) measures

in certain parts of the network [10]. Also note, that the performance is potentially worse for higher inter-area power exchanges before the system split more detailed dynamic models of static converters than the impedance models used in this study.

- The results also confirm the frequency support capability of the active distribution networks studied in WP1, on the transmission grid level.
- Energy storage solutions for medium voltage employing fully fledged grid forming control solutions are already commercially available, e.g. in the form of the e-mesh^{TM} PowerStore^{TM} from Hitachi ABB Power Grids [17]. This has been deployed in various microgrid environments and is capable of on and off grid operation. A simplified form of grid forming control is also applied in various HVDC projects for offshore wind connection, where the offshore HVDC terminal is used to energize and operate the offshore collector grid to which the wind turbines are connected [16].

Finally, a roadmap has been proposed for Switzerland:

- The findings propose a step-wise introduction of grid-forming DERs, preferably first using existing utility size batteries.
- The efforts should be closely monitored and coordinated with other TSOs in ENTSO-E.
- A penetration level of grid-forming DERs in Switzerland of up to about 1% (100 MW) will represent an important Swiss pioneering contribution towards the future dynamic security of the ENTSO-E power grid.

6.2 Project value for stakeholders

The ACSICON project created value for multiple stakeholders of the Swiss and European electricity sector, both in the form of general insights for future policy development as well as setting the basis for further investigations in academia and industry (TSOs, DSOs, component manufacturers):

- For the general policy development, the project created a roadmap for dynamic stability requirements during the energy transition, based on a quantitative analysis of the ENTSO-E system.
- For both industry and academia, the aggregated distribution grid models developed in WP2 and applied in WP3 will be published for further investigations. This is particularly interesting for TSOs to gain quantitative insights of the DER-contributions to voltage and frequency support.
- On a similar note, the project key findings will be disseminated not only through publications but also in a dedicated workshop for ENTSO-E TSOs.
- For component manufacturers, insights in grid related requirements for converters point to future directions of developments.
- For the project partner ETHZ-FEN, the extension of the FlexDyn simulator enables future investigations to gain quantitative insights of the transmission grid behavior with active distribution networks. Furthermore, the FlexDyn simulator can now be used to study the **global power system security**, combining transmission grid and distribution grid models of realistic sizes.
- For the project partner HAPG, the knowledge building surrounding grid-forming converter control supports both future business development for storage and medium-voltage-converters, as well as the usage of the research results for future product developments.

6.3 Outlook and future work

Several open questions and areas for future investigation have been identified:

- Regarding the converter modeling, the **optimal parameterization** of the grid-forming converters (e.g. inertia constant, headroom) can be further refined for the surround distribution grids and their operating condition. Ideally, and adaptable mechanism to provide optimal support of damping and ROCOF should be developed, estimating and accounting for the current grid state and the location of the converter within the grid.
- Furthermore, the **difference between grid-forming and grid-following** converter technologies needs further investigations. This investigation is independent of the amount of grid support, that can be carried out with both technologies. Grid-forming converters are important in particular in weak parts of the power grid, both on the distribution and the transmission grid level (not only in islanding situations). However, the exact stability limit without grid-forming control needs to be better identified.
- For the distribution grid aggregation, More **variation of the distribution grid structures** would be useful, since the entire project has used the CIGRE-MV benchmark grid.
- Furthermore it would be good to develop **simple aggregated models with headroom constraints**. Currently, the investigations assume a 50% headroom in the distribution grid.
- For the transmission grid investigations, three main directions for improvement have been identified:
  - It would be useful to incorporate a better representation of static converter models in the large-scale simulation, that have currently been represented with impedance models due to complexity reasons.
  - The investigation can be expanded to a larger range of **scenario variations**, including other load flow conditions of the ENTSO-E network with larger transit flows, as well as the independent variation of grid support on the transmission grid level.
  - Further additional scenarios include the contribution of grid support from the remaining synchronous machines in the system. Note that this would imply to keep machines running at part load purely for reserve reasons.
  - The pricing mechanisms for additional dynamic grid support measures from converters have not been investigated. For the developed Swiss roadmap, two main directions were identified - either a market based procurement or a regulation based requirement. The most price efficient approach is not clear and needs to be coordinated on the ENTSO-E level.

References

[1] J. D. Ainsworth. Harmonic instability between controlled static convertors and a.c. networks. *Proceedings of the Institution of Electrical Engineers*, 114(7):949–957, July 1967.

[2] CENELEC. Railway applications - fixed installations and rolling stock - technical criteria for the coordination between power supply and rolling stock to achieve interoperability - part 2: stability and harmonics. prEN 50388-2: Draft Standard for review, August 2017.

[3] Migrate consortium. Migrate deliverable 1.1: Report on systemic issues. *https://www.h2020-migrate.eu/_Resources/Persistent/9bf78fc978e534f6393afb1f8510db86e56a1177/MIGRATE_D1.1_final_TenneT.pdf*, 2016.

[4] Kai Strunz (Convener). Benchmark systems for network integration of renewable and distributed energy resources. Tech. Report 575, CIGRE, 2013.

[5] Salvatore D'Arco, Jon Are Suul, and Olav B Fosso. A virtual synchronous machine implementation for distributed control of power converters in smartgrids. *Electric Power Systems Research*, 122:180–197, 2015.

[6] Turhan Demiray. *Simulation of Power System Dynamics using Dynamic Phasor Models*. PhD thesis, ETH Zurich, Zürich, 2008.

[7] DNV GL. Energy transition outlook. Technical report, DNV GL, 2020.

[8] H. Dong, S. Yuan, Z. Han, X. Ding, S. Ma, and X. Han. A comprehensive strategy for power quality improvement of multi-inverter-based microgrid with mixed loads. *IEEE Access*, 6:30903–30916, 2018.

[9] ENTSO-E. Final Report System Disturbance on 4 November 2006. *https://www.entsoe.eu/fileadmin/user_upload/_library/publications/ce/ otherreports/Final-Report-20070130.pdf* , 2007.

[10] ENTSO-E. Policy 5: Emergency Operations. *RG CE Plenary Meeting 16 of September of 2015* , 2015.

[11] A. Fuchs, M. Imhof, T. Demiray, and M. Morari. Stabilization of Large Power Systems Using VSC-HVDC and Model Predictive Control. *IEEE Transactions on Power Delivery*, 29(1):480–488, 2014.

[12] Alexander Fuchs. Dynamic Transmission System Emulator for Stability Assessment (Presentation slides and Video). *SCCER-FURIES Annual Conference, https://www.epfl.ch/research/domains/sccer-furies/outreach/events/2020-annual-conference/*, 2020.

[13] Alexander Fuchs, Turhan Demiray, Felix Rafael Segundo, and Petr Korba. Evaluation of the ENTSO-E Initial Dynamic Model of Continental Europe Subject to Parameter Variations. *Submitted to IEEE PSCC 2018.*, 2017.

[14] Alexander Fuchs and Mats Larsson. ACSICON - dynamic distribution grid aggregation. Technical report, Research Center for Energy Networks, ETZ Zürich and Hitachi ABB Power Grids, 2021.

[15] M.J. Gibbard, P. Pourbeik, and D.J. Vowles. *Small-signal stability, control and dynamic performance of power systems*. University of Adelaide Press, 2015. http://dx.doi.org/10.20851/small-signal.

[16] Hitachi ABB Power Grids. Offshore Wind connections. *https://www.hitachiabb-powergrids.com/ch/de/offering/product-and-system/hvdc/offshore-wind-connections* , 2021.

[17] Hitachi ABB Power Grids. e-mesh™ PowerStore™. *https://www.hitachiabb-powergrids.com/offering/product-and-system/energystorage/powerstore* , 2021.

[18] Mathworks Inc.

[19] Hassan K. Khalil. *Nonlinear Systems*. Taylor and Francis Ltd, 1991.

[20] Prabha Kundur. *Power System Stability and Control*. McGraw Hill, 1993.

[21] M. Larsson. Harmonic Resonance and Control Interoperability Analysis for HVDC Connected Wind Farms. *Invited panel talk*, August 2017.

[22] Mats Larsson. ConverterStab–a toolbox for harmonic stability analysis for networked power converters. Technical Report 2016/CHCRC/C/TR/1044, Corporate Research, ABB Switzerland Ltd., 2016.

[23] Mats Larsson. *Electricity Supply Systems of the Future*, chapter DC Systems and Power Electronics, page 243. CIGRE Green Books. Springer, 2020.

[24] Mats Larsson and Alexander Fuchs. ACSICON - dynamic modelling of distribution grids. Technical report, Hitachi ABB Power Grids and Research Center for Energy Networks, ETZ Zürich, 2021.

[25] C. Li. Unstable operation of photovoltaic inverter from field experiences. *IEEE Transactions on Power Delivery*, 33(2):1013–1015, April 2018.

[26] X Liu, A Forsyth, H Piquet, S Girinon, X Roboam, N Roux, A Griffo, J Wang, S Bozhko, P Wheeler, M Margail, J Mavier, and L Prisse. Power quality and stability issues in more-electric aircraft electrical power systems. In *host publication*, 9 2009.

[27] Christine Haag Martin Aeberhard, Rene Vollenwyder and Benedikt Aeberhardt. Resonanzproblematik im SBB energienetz. Technical Report SD12010BAVV1, SBB, Schweiz, 2010.

[28] A. Ouroua, L. Domaschk, and J. H. Beno. Electric ship power system integration analyses through modeling and simulation. In *IEEE Electric Ship Technologies Symposium, 2005.*, pages 70–74, July 2005.

[29] B. Porter and R. Crossley. *Modal Control Theory and Applications*. Taylor and Francis Ltd, 1972.

[30] SMA. SMA Sunny Island 8.0H Datenblatt. *https://files.sma.de/downloads/SI44M-80H-13-DS-de-21.pdf*, 31.05.2021.

[31] SMA. SMA Sunny Tripower 8.0 Datenblatt. *https://files.sma.de/downloads/STP8-10-3AV-40-DS-de-20.pdf*, 31.05.2021.

[32] Martin Stämpfle. Mathematical methods, January 2013. http://www.hs-esslingen.de/fileadmin/medien/mitarbeiter/koch/numerische_methoden_lecture_notes.pdf.

[33] VDE. Technische regeln für den anschluss von HGÜ-systemen und über HGÜ-systeme angeschlossene erzeugungsanlagen. Draft guideline VDE-AR-N 4131, August 2018.

[34] G. C. Verghese, I. J. Perez-Arriaga, and F. C. Schweppe. Selective modal analysis with applications to electric power systems, part ii: The dynamic stability problem. *IEEE Power Engineering Review*, PER-2(9):30–31, Sept 1982.

[35] Denis von Arx. Grid forming converter control for low inertia power grids. Master's thesis, ETH Zürich, 2018.

Node	Name	DER type	Pmax (kW)
3	PV3	Grid following	20
4	PV4	Grid following	20
5	PV5	Grid following	30
5	Bat5	Grid forming	600
5	FC5	Grid forming	33
6	PV6	Grid following	30
7	WT7	Grid forming	1500
8	PV8	Grid following	30
9	PV9	Grid following	30
9	CHPD9	Grid forming	2*310 [3]
9	CHPFC9	Grid forming	212
10	PV10	Grid following	40
10	Bat10	Grid forming	200
10	FC10	Grid forming	14
11	PV11	Grid following	10

Table 10: Types and ratings of DER units.

A Appendix

A.1 CIGRE Benchmark Adaptation for Model Reduction

The model reduction in Section 3.2.2 is performed using a simplified version of the CIGRE MV benchmark distribution grid model described in Section 2.3.5 where all DERs are modelled using either grid forming or grid following converter structures. That is, the diesel generator in the original CIGRE benchmark system has been replaced by a grid forming converter. In this phase of the work, the grid forming converter model was also improved and somewhat simplified compared to the version used in Section 2.4.3.2.

Figure 5 shows the single line diagram of the benchmark system with its grid supporting converter systems developed in Task 1.1. Table A.1 shows the types and rating of the various DER units. The grid model assumes a connection point to a 220 kV level transmission grid and includes modelling of the medium voltage grid at 20 kV. The low voltage grids are represented by impedance loads initialized based on power flow data of the original source [4]. There are two distribution feeders, one of which is modelled in detail including DER units as tabulated in Table A.1. This feeder is connected by several cable sections. The second feeder is modelled with two load buses connected via overhead lines. In the base case considered here, the sum of the load is around 44 MW and the total DER capacity about 3.4 MW. This results in a relatively low penetration level of DER of 8% in terms of the ratio between converter system rating and the total active power load. Future work during the project will modify this base case to study higher penetration levels.

A.1.1 Converter Main Circuit Modelling

The main circuit used for both the grid forming and grid following converter systems is shown in Figure 68. Each converter is modelled with a converter transformer in series with a converter system (top left). The converter system itself has a LC filter setup consisting of a filter capacitor and series reactance, thus when combined with the transformer it is an LCL filter setup. The representation of the DC side is different between the grid following and grid forming converters. The grid following converter model represents the DC side as a capacitor fed by a dc current source and corresponds to e.g. wind and solar PV converter system. The grid following converters require a stable DC link to provide grid support and is modelled using ideal dc voltage sources as shown in the figure. Furthermore the control system is supplied with measurement data both from the PCC on the MV side of the converter transformer and

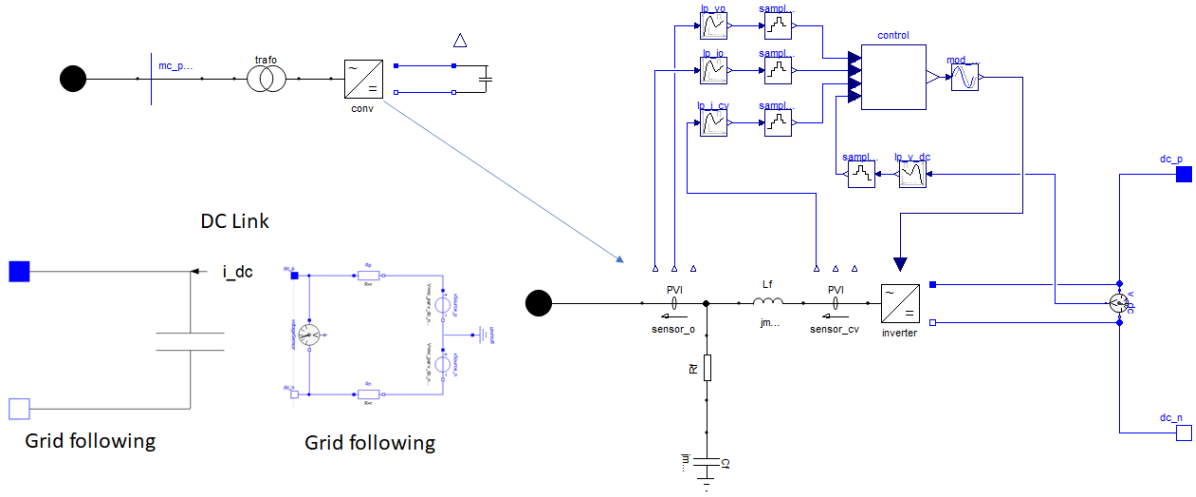

Figure 68: Main circuit of grid following and grid forming converters.

the converter filter bus on the LV side of the transformer. For the purpose of small signal modelling the sampling and modulation delay are represented by Pade approximations of the sampling and delay.

Main circuit parameters are given below.

```
record MainCircuitParameters
  "Grid following main circuit parameters, representative of wind turbine converter"
  extends Modelica.Icons.Record;
  outer ObjectStab3.Base.SimConfig config;
  parameter Real Sbase=config.Sbase "Rated power";
  parameter ObjectStab3.PSunits.Frequency f_sw=2950 "Switching frequency";
  parameter ObjectStab3.PSunits.Frequency f_samp=2*f_sw
    "Sampling frequency (Hz)";
  parameter ObjectStab3.PSunits.PerUnit k_mod=sqrt(3/2)
    "Modulation constant (Sine PWM)";
  parameter ObjectStab3.PSunits.PerUnit v_dc_nom=2 "Nominal dc voltage (pu)";
  parameter ObjectStab3.PSunits.PerUnit r_f=l_f/20 "Filter resistance";
  parameter ObjectStab3.PSunits.PerUnit l_f=0.105577572899468
    "Filter inductance inverter side (pu)";
  parameter ObjectStab3.PSunits.PerUnit r_cf=0.003 "Filter resistance";
  parameter ObjectStab3.PSunits.PerUnit c_f=0.075720433282689
    "Filter capacitance";
  parameter ObjectStab3.PSunits.PerUnit c_dc=0.00666540000000 "DC capacitor";
  parameter ObjectStab3.PSunits.PerUnit r_t=0.4/100/(9.2/8)
    "Trafo resistance";
  parameter ObjectStab3.PSunits.PerUnit l_t=10/100/(9.2/8) "Trafo inductance";
end MainCircuitParameters;
```

A.1.2 Converter Control System Modelling

The modelling of the example distribution grids foresee two different converter control systems. Firstly a typical following converter control signal that is similar to those found for example in wind and photovoltaic converters, and secondly a grid forming control system similar to those found for example in grid supporting battery energy storage systems. The two control system variants are described in the following sections.

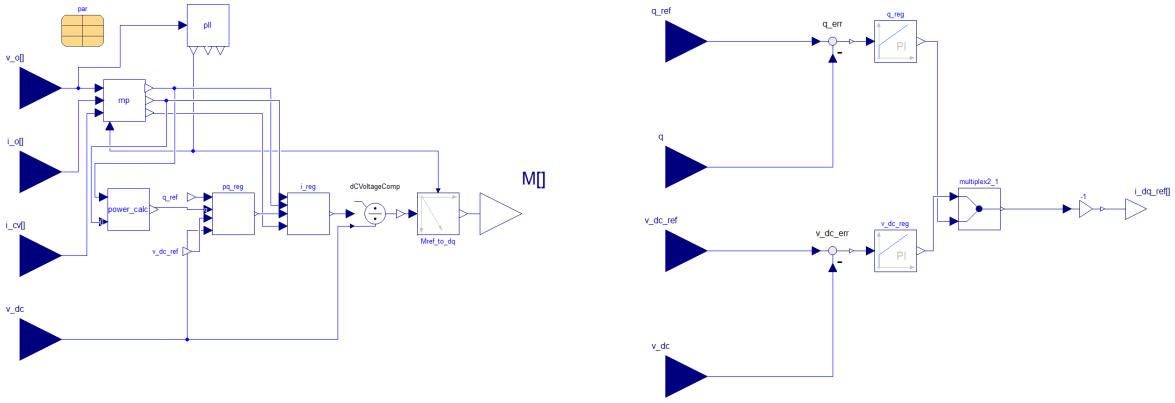

Figure 69: Overview of grid following control system. Main control structure (left), Active power and reactive power loops (right).

A.1.2.1 Grid Following Converters

The grid following converter models use a control structure shown in Figure 69. The overview is seen in the bottom left subfigure. The PLL is driven by measurement from the PCC bus. The current control is of a standard dq type with decoupling and voltage feedforward. Additionally an optional active damper is implemented based on an estimated of the capacitor current. Furthermore outer loops are implemented to control the reactive power at the PCC and the dc voltage controller constant in steady state.

Grid following controller parameters are given below.

```
record Parameters
  parameter PerUnit k_p_PLL = 0.25 "PLL proportional gain";
  parameter PerUnit k_i_PLL = 10 "PLL integral gain";
  parameter AngularVelocity omega_LP_PLL = 500 "PLL filter";
  parameter AngularVelocity w_s = 314.1592653589793
    "Rated angular frequency";
  parameter PerUnit k_pc = 1.2 "Current controller proportional gain";
  parameter PerUnit k_ic = 4.16 "Current controller integral gain";
  parameter PerUnit k_ffv = 1 "Current controller feedforward gain";
  parameter PerUnit k_decouple = 1 "Current controller decouple gain";
  parameter PerUnit v_cv_max = 1.2;
  parameter PerUnit i_cv_max = 1.2;
  parameter AngularVelocity omega_AD = 50 "Active damping filter";
  parameter PerUnit k_AD = 0.58 " Active damping gain (pu)";
  parameter PerUnit k_pdc = 0.5 "DC voltage controller proportional gain";
  parameter PerUnit k_idc = 2.16 "DC voltage controller  integral gain";
  parameter PerUnit k_pq = 0.35 "Q controller proportional gain";
  parameter PerUnit k_iq = 2.5 "Q controller integral gain";
  parameter PerUnit k_p_vac = 0.0001 "AC voltage controller proportional gain";
  parameter PerUnit k_i_vac = 100 "AC voltage controller integral gain";
end Parameters;
```

A.1.2.2 Grid Forming Converters

The grid following converter models use a control structure shown in Figure 70.The overview is seen in the bottom left subfigure. Also the grid forming control scheme includes a PLL, however this is not used for grid synchronization but rather for the implemented of the damping term in the inertia emulation. The grid forming controller also omits the current controller and directly receives its converter but reference from the reactive power loop providing the magnitude of the reference and the active power controller (inertia emulation) providing the angle. Thus the con-

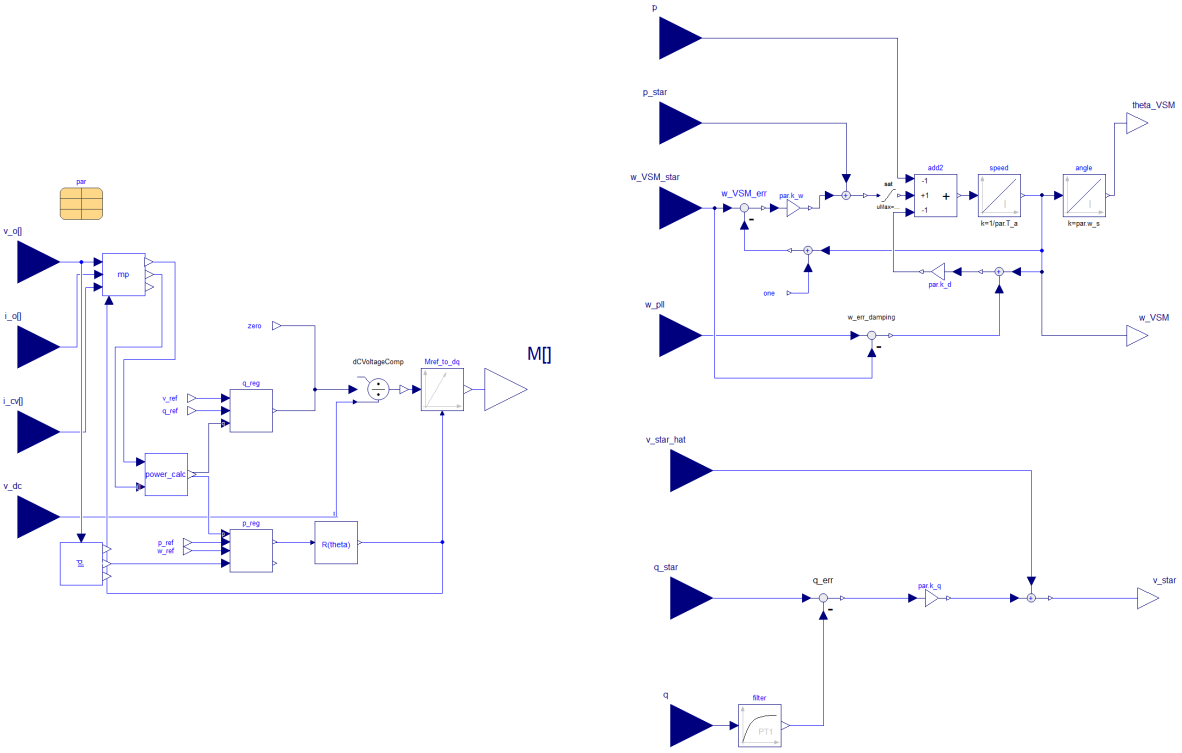

Figure 70: Overview of grid forming control system. Main control structure (left), Active power loop (top right), Reactive power loop (bottom right).

troller employed is a variation on the virtual synchronous machine (VSM) concept commonly used in the literature, e.g. [5]. The reactive power loop is implemented using a droop scheme where the voltage repference is compensated by a droop term proportional to the reactive power injection. This ensure stability of the voltage control when multiple grid forming converters are operating in parallel.

Grid forming controller parameters are given below.

```
parameter PerUnit k_p_PLL = 0.25 "PLL proportional gain";
parameter PerUnit k_i_PLL = 10 "PLL integral gain";
parameter AngularVelocity omega_LP_PLL = 500 "PLL filter";
parameter AngularVelocity w_s = 314.1592653589793
  "Rated angular frequency";
parameter PerUnit T_a = 2 "VSM Inertia constant";
parameter PerUnit k_d = 5 "VSM Damping coefficient";
parameter PerUnit k_w = 20 "Frequency droop gain";
parameter PerUnit k_q = 0.02 "Reactive power droop gain";
parameter AngularVelocity omega_f = 500 "Reactive power filter (rad/s)";
```